

ICOLD

**COMPUTATIONAL ASPECTS
OF ANALYSIS AND DESIGN OF DAMS**

**Tenth Benchmark Workshop on Numerical Analysis of
Dams**

Theme C “Stability of a dam abutment including seismic loading”

The problem statement shall consist of the static and seismic stability assessment of a three-dimensional multi-faceted rock "wedge" of an arch dam abutment. Firstly, dam-rock interface forces shall be evaluated from a finite element model and then, abutment stability assessments shall be performed using conventional (Londe Method) and/or finite element techniques.

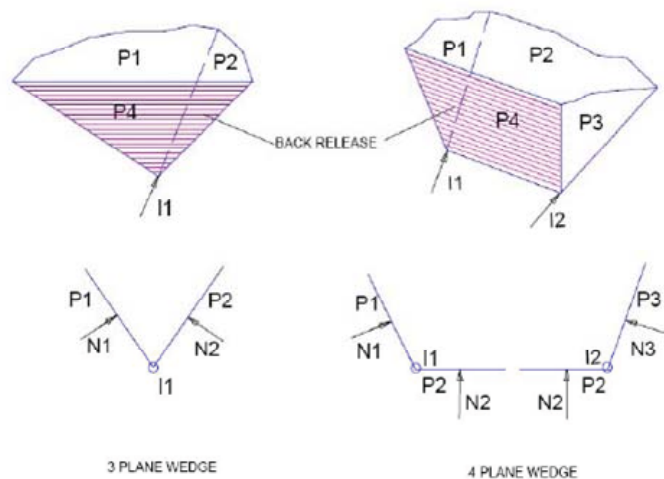
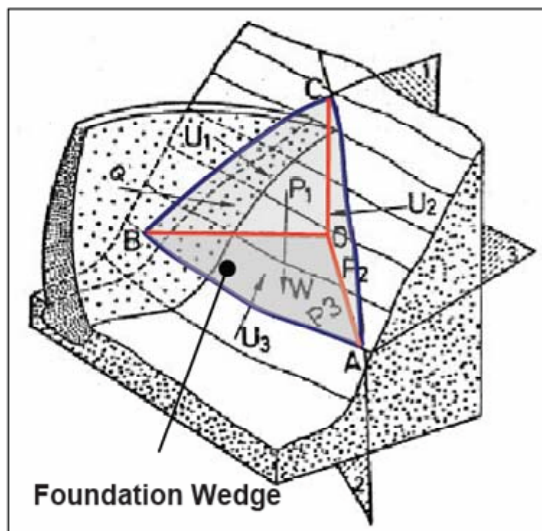




Table of contents

1	Acknowledgement	1
2	Executive Summary	1
3	Problem statement	2
3.1	Wedge Definition	3
3.1.1	Overview	3
3.1.2	Geological characteristics	3
4	Data Preparation	6
4.1	Dam and Foundation Bodies	6
4.2	Wedge Topographical and Geometric layout	6
4.3	Dam and Foundation Interface	7
4.4	Seismic data	7
5	Methodology	8
5.1	Modelling	8
5.2	Material parameters	8
5.3	Boundary conditions	8
5.4	Loading	8
5.5	Approach to the analyses	9
6	Results	9
7	References	9



1 Acknowledgement

The Theme C organiser would like to acknowledge and gratefully thank Dr. A. Baumer of OFIMA for his acceptance of allowing the Luzzone Dam to be used in the Benchmark.

2 Executive Summary

The proposed benchmark is aimed at abutment stability analyses of three-dimensional wedges typically encountered for the rock foundations of arch dams. The loading regime to be evaluated is firstly static (self-weight and hydrostatic pressure) and then seismic (three component acceleration-time histories applied in the orthogonal directions of the dam axis). The wedge geometry shall be delimited by three planes of which one shall be a back-plane and the other two by predominant geological formations in the rock structure.

The interest in such a benchmark is firstly to allow concrete traditionalists to review another aspect of arch dam stability and encourage geologically minded colleagues to reflect on the analytical problems encountered in arch dam engineering.

The first step of the analyses shall concentrate on the interface forces between the concrete dam and the foundation and how these forces are determined and then applied to the wedge for static and seismic loading.

Static loads shall then be applied to the wedge to ascertain the factors of safety under different geomechanical material properties. Sensitivity analyses are encouraged.

Seismic loading shall be applied in three orthogonal directions and similar safety analyses applied over the time history. The participant is asked to reflect on the design criteria which are suggested and the methods of analyses to evaluate the permanent post-earthquake resultant displacement. The *Newmark method* is proposed and the participants are encouraged to review underlying assumptions of the method related to multi-directional movement of a rigid block. Indeed, all aspects of this traditional method are open to discuss and review through the common problem statement to be investigated by the participants.

It is emphasised that the participant is positively encouraged to develop on the standard methods of abutment stability and to demonstrate how state-of-the-art computational aspects of analysis and design of dams can be applied to the problem. The methods of analyses are not restricted to finite elements; discrete rigid and deformable elements can also be applied for example.

The results from each of the participants shall be reviewed and compiled in a general report to allow both new and old "hands" to these types of problems to gain a rapid first experience from the benchmark.



3 Problem statement

The Luzzone double curvature arch dam located in the south eastern part of Switzerland has been selected for the benchmark, figure 2.1.

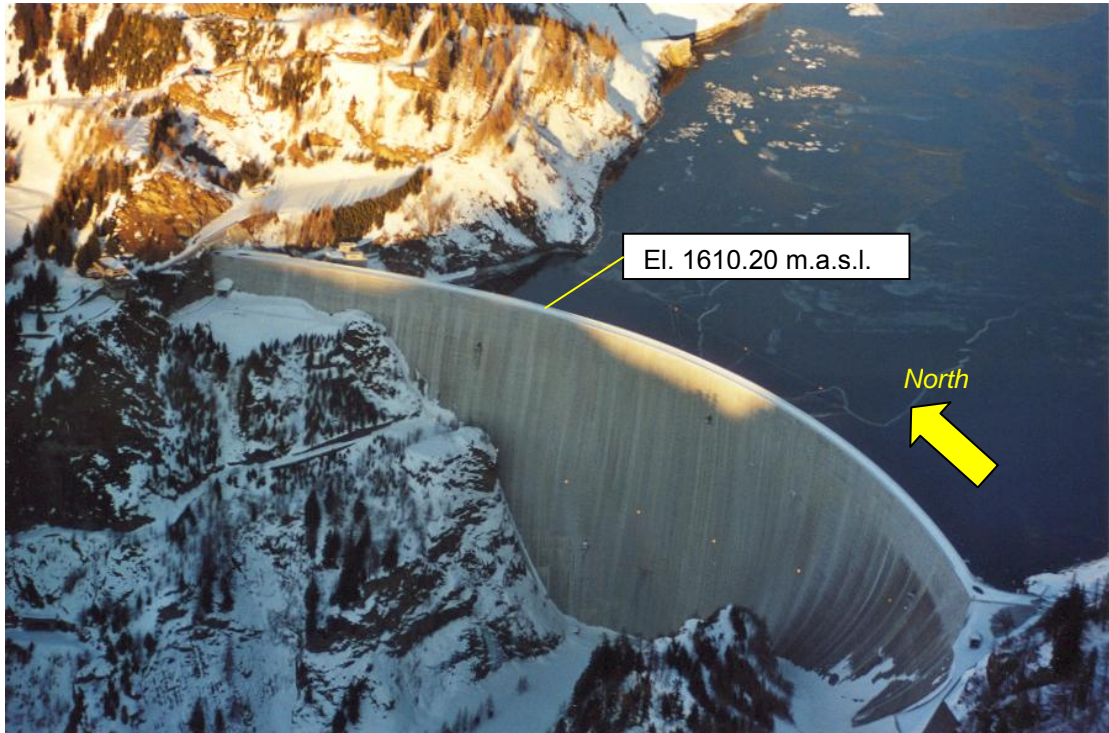


Figure 2.1 Luzzone Dam (Switzerland), $H = 225$ m.

The location and main characteristics of the structure are presented in **appendices 1** and **2**. The dam was built in the sixties and heightened in the ninetieths. The behaviour of the structure is sound and normal, but presents some interesting aspects for the dam engineering community.

The structure originally started its design life as a relatively classic arch dam parabolic layout until during the construction, a family of decompressed joint structures on the left bank opened and provoked an instability which had important consequences on the geometrical definition of the dam and the stability of the abutments. For the upper section of the dam, a geometric rotation was applied. The above figure reveals that the left bank has both an unusual upper elevation abutment and section closure for the 17 m heightening.

The problem statement consists of the static and seismic stability assessment of a three-dimensional multi-faceted rock "wedge" on the left bank of the Luzzone arch dam abutment. Dam-rock interface forces shall be evaluated from a finite element model and then, abutment stability assessments shall be performed using conventional (Londe Method) and/or finite element techniques.



3.1 Wedge Definition

3.1.1 Overview

The right bank geological features do not present kinematically feasible wedges and are therefore classified as verified. The left bank presents only two geological features (joints, J_1 and J_2) that are deemed as presenting a *realistic wedge* with the potential for sliding and therefore verifications are necessary.

Heightening studies verified the important of drainage and demonstrated that the factor of safety could be important by an order of 1.

3.1.2 Geological characteristics

The Luzzone valley extends in the North-east /South-west direction parallel to the geological features defined by a zone of sedimentary and metamorphic rocks which are located between the crystalline formations of the Saint-Gothard and the pennique layers.

The dam and the rock slopes immediately upstream for the first 500 m on the right bank are situated on the Sosto schist formations which have a dip of 25 to 35° towards the east forming a tectonic element which are separated from the other pennique features that extend towards the south.

The Sosto schists are composed of marble, limestone-silicate schists and micas and phyllite micas. The rock mass does not present any distinctive planes of schistosity and a general stratification is not visible.

The Sosto schists are in general slightly fractured. In the abutment areas of the dam, the upper surfaces of the rock contain decompressed diabase which is generally parallel to the slopes (J_1 system). Additionally, two tectonic diabase systems are visible; J_2 which is inclined towards the North-west and the second J_3 , towards the North-east.

The decompressed diabase rock formations are predominant on the left bank as is evident from the relatively large seepages observed on the left bank as compared to the right bank.

On the left bank above elevation 1500 m.a.s.l., the arch abutment is founded on a thick mass concrete wall and the downstream face of the rock apron is sub-vertical.

The schist rock formations of the apron are of a good quality and the weak schist was removed during the excavation stages of the dam foundation.

Two main diabase formations have been recorded by the Geologist, *Aperta* and *Chiuaa* which can lead to similar wedge sliding as observed during the excavation of the foundation (year of 1959).

The geomechanical properties of the rock formations are as presented below.



Material	Modulus (E) GPa	Poisson (ν)	Dry density ρ kg/m ³	Wedge Characteristics Wedge volume = 1.92 x 10 ⁶ m ³			Cohesion (c) MPa	Friction (φ) °	Dip (α) °	Dip dir'n (β) °	Damping (ζ) %
				(A _t) m ²	(A _w) m ²	Uplift %					
Mass Concrete	27.00	0.167	2'400	-	-	-	-	-	-	-	5
Diabase	25.00	0.200	2'600	-	-	-	Variable	40-42	-	-	5
J ₁	-	-	-	33'907	23'300	100	Variable	40-42	50-90	005-350	5
J ₂	-	-	-	10'811	7'200	100	Variable	40-42	50-76	280-295	5
J _h	-	-	-	28'650	28'650	100	Variable	40-42	-	360.00	5
J ₁ Benchmark	-	-	-	33'907	23'300	100	-	35.00	65.00	5.00	5
J ₂ Benchmark - crack	-	-	-	10'811	7'200	100	-	-	76.00	280.00	5
J _h Benchmark - 1510	-	-	-	28'650	28'650	100	-	35.00	-	360.00	5

Notes:

- Subscripts -
 s = static
 r = flexural strength (prismatic beam)
 d = dynamic
 t = total plane surface area
 w = wet plane surface area (below reservoir elevation)
 1 = plane 1
 2 = plane 2
 h = horizontal plane (elevation indicated)
- Foundation modulus refers to *deformation modulus* and for dynamic analyses taken as zero (*massless*)
 Concrete modulus refers to *modulus of elasticity*
 Damping is the percentage of *critical damping*
Wedge volume = 1.92 x 10⁶ m³

Table 2.1 Dam Mass Concrete and Rock Properties

Geometric arrangement of the wedge is presented below.

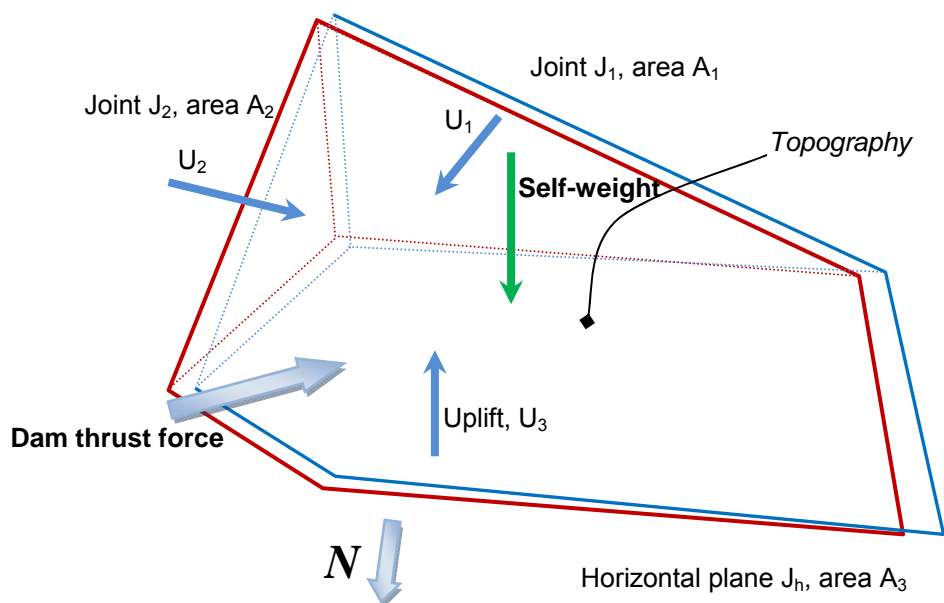


Figure 2.2 Three-dimensional wedge arrangement



The wedge presented in figure 2.2 is formed by a horizontal plane due to the inexistence of other joints that could produce a cinematically feasible wedge. The horizontal plane may vary in depth between elevations 1510 to 1570 m.a.s.l. Below 1510 m.a.s.l., the wedge volume is deemed to be too large to cause foundation instability.

For the Benchmark, the horizontal plane shall be considered only at elevation 1510 m.a.s.l.

Review of the geometric formations indicates that two wedge types could be defined. **Type A** shall be defined by two joint sets (J_1 and J_2) and a horizontal plane. **Type B** consists of only two planes (J_1 , vertical plane and the horizontal plane) whereby J_1 is defined by the maximum possible dip values of 90° . These wedge types are presented below.

*For the Benchmark, only the **Type A** wedge shall be analysed (three planes).*

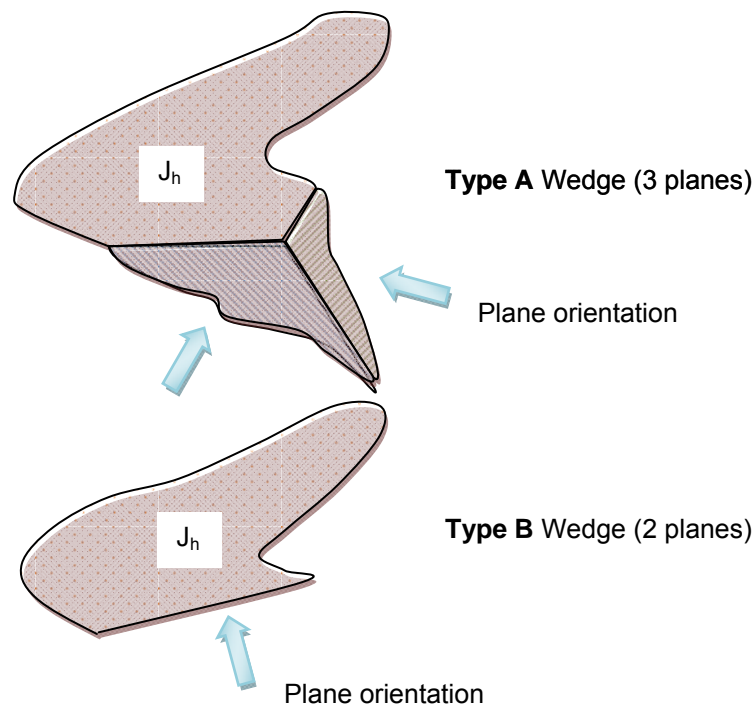


Figure 2.3 Wedge Types – A (3 planes) and B (2 planes)

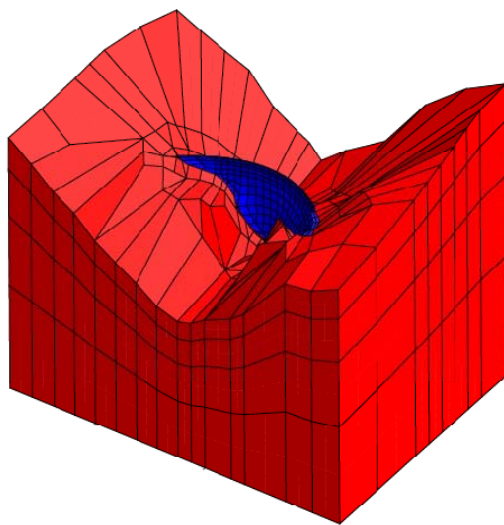


4 Data Preparation

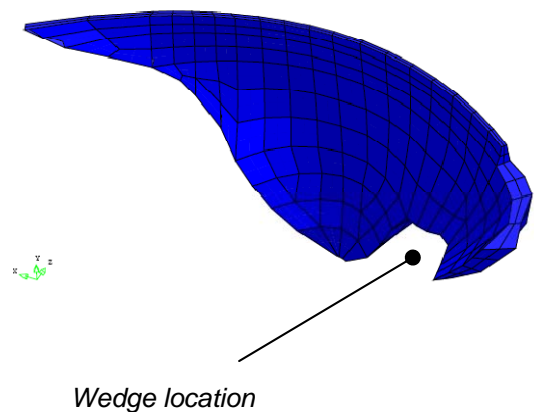
The participants of the benchmark Theme C are provided with the data listed in **Appendix 3**. (digital format). The information below gives an overview of the data.

4.1 Dam and Foundation Bodies

Geometrical and finite element model: Dam and foundation only (without reservoir).



Dam and Foundation Finite Element Mesh



Dam Finite Element Mesh

Figure 3.1 Dam and Foundation Finite Element Mesh

The main data is in text (ASCII) format with free formatting and can be found in *ThemeCModel.fga*. The model was originally generated using the DIANA software package for which more information can be found on the web (www.tnodiana.com).

The file has been structured in such a way to facilitate modelling, analyses and evaluation of results. The detailed description of the *ThemeCModel.fga* file is given in **Appendix 4**.

For information purposes only, **Appendix 5** provides the participants with three standard cross-sections.

4.2 Wedge Topographical and Geometric layout

The topographical and geological data for the selected wedge to be used in the benchmark are given in **appendix 12**. The volume of the wedge has been estimated as $1.92 \times 10^6 \text{ m}^3$. Depending on the method of analysis, the participant is free to model the wedge using finite elements and/or other types.



4.3 Dam and Foundation Interface

Special importance is given to the interface between the dam and the foundation which is named *INFACE*. The labelled geometrical points (*entity name*) are given in **Appendix 6** with global coordinate values (X, Y, Z).

Since only the left bank abutment wedge stability above elevation 1510 m.a.s.l. is relevant to the benchmark, **Appendix 7** presents the node numbers and global coordinates for this area.

For reference and evaluation purposes, the geometrical surface entity numbers for the left abutment are also provided in **Appendix 7**.

4.4 Seismic data

Three stochastically independent acceleration time-histories are provided as described in **Appendix 8**. The time step is 0.01 second, duration 30.71 seconds giving a total number of 3072 time steps. The peak ground accelerations in the cross valley, vertical and upstream-downstream directions are 0.12g, 0.93g and 0.93g respectively and **appendices 9, 10** and **11** present the graphs. The scaling factors applied to these values are given in the format in the *ThemeCModel.fga* data file. Hence, the following peak ground acceleration values shall be applied:

1. Downstream-upstream (Z - direction) : **+ 0.16g**
2. Vertically upwards (Y – Direction) : **+ 0.1067g**
3. Cross-valley direction L - R (X – Direction) : **+0.16g**

The vertical peak ground acceleration is two-third (0.6667) of the horizontal components.

The participant is free to convert the time histories into the frequency domain, but this is not recommended for stability analyses.



5 Methodology

5.1 Modelling

Based on the data provided and as described in the preceding chapter, the participant is asked to model the dam and foundation structure using finite elements and/or any other numerical modelling technique (for example discrete elements). The extent of the foundation has been defined to minimise constraint effects (static and dynamic loading) for different degrees of restraints (translations and rotations) and also to allow the selected volume of wedge in the foundation to be modelled using any method.

Sufficient data have been provided to numerically model the wedge in the case that a Londe type solution is not desired. The structure of the mesh using for example interface elements along sliding planes and solid elements etc. shall be the choice of the participant.

Once again, the participant is free to modify the mesh for example refinement, element types, etc.; however the geometry of the problem shall remain unchanged.

The dam body and foundation have been separated into five *construction stages* to allow a reasonable computation of the self-weight loading.

5.2 Material parameters

The material parameters for the mass concrete dam and the foundation (material zoning) are to be defined in accordance with table 2.1. Uniform properties (diabase) are assumed for the entire rock foundation for simplicity and the concrete dam shall be treated only as mass concrete (no facing and/or interface concrete).

The influence of softening elements along the upstream dam-rock interface can be defined freely if the participant desires to reduce the effects of stress discontinuities. Such elements are normally defined just in front and/or as part of, the grout curtain (first top layer of foundation elements).

The layout of the topography, major rock joints and determinant cross sections (used for volume calculations only) are given in **Appendix 12**.

5.3 Boundary conditions

The boundary conditions for the finite element model are defined in accordance with the model data file and selected such as to minimum their influence on the results for static and dynamic loading conditions.

5.4 Loading

The static loading (self-weight and full hydrostatic pressure = 1610.20 m.a.s.l.) shall be computed and applied as initial conditions for the dynamic loading. The latter can be evaluated using any method (modal, direct time integration etc.).



5.5 Approach to the analyses

The conceptual approach described by *Newmark* in reference [1] can be applied. The basic understanding is that permanent displacements are accumulated for the case when the *critical acceleration* has been exceeded. The double integration of the computed accelerations shall produce these displacements.

The manner in which the critical acceleration is computed and the fundamental reasoning behind *Newmark's Method*, are the essential subject for discussion. Hence, we are not only interested in obtaining numerical solutions, but also the participant's views on the subject.

Other methods of solving such stability problems are also encouraged.

6 Results

The participants shall produce results in the format given in **Appendix 13** and give their own evaluations/recommendations for future benchmarks based on the same Theme C.

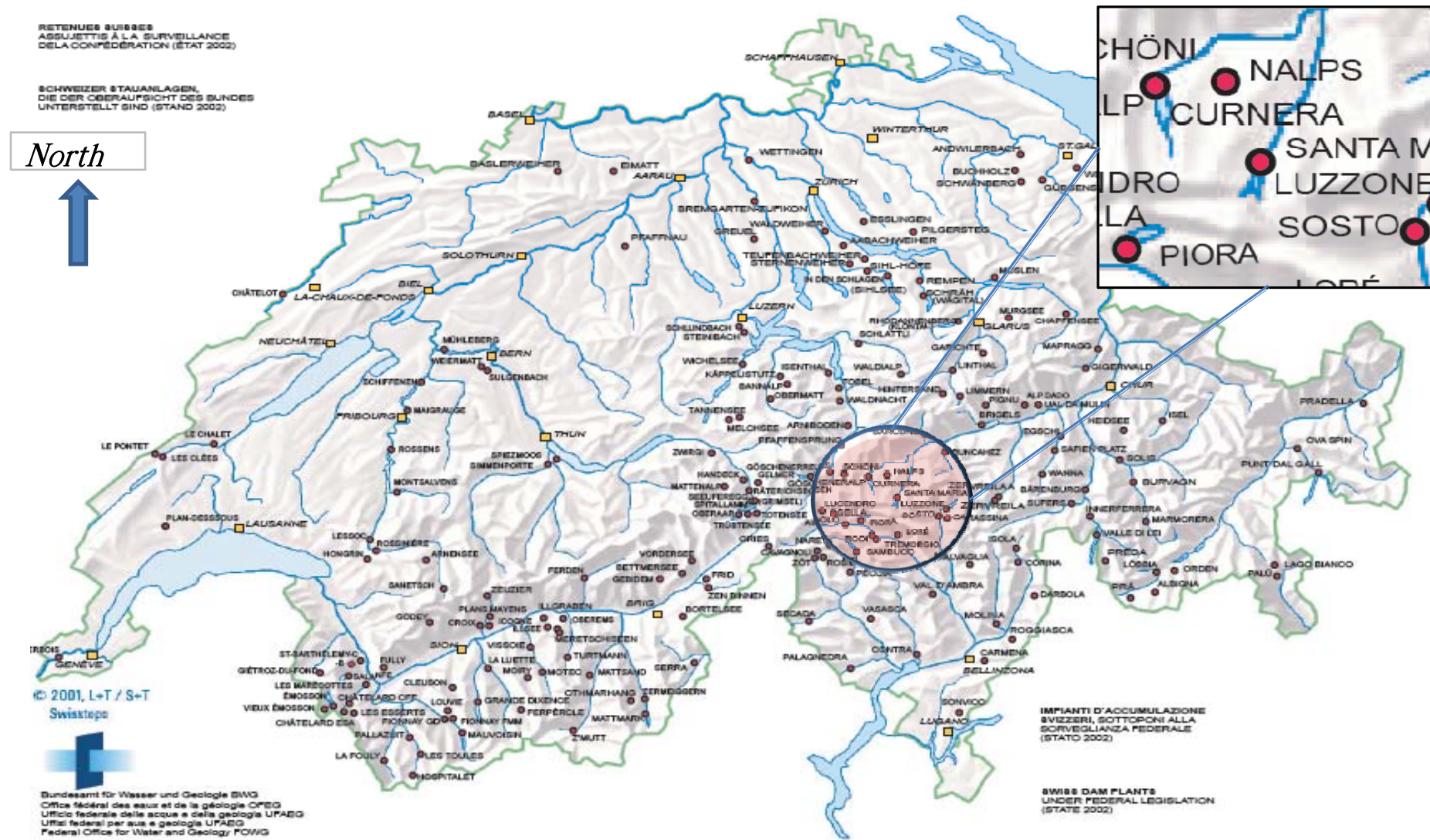
7 References

1. Prof. N. M. *Newmark*, "Effects of Earthquakes on Dams and Embankments", published in *Geotechnique*, "*Milestones in Engineering*", Vol. 15, N°. 2, pp.109 – 129, 1965.
2. P. *Londe*, "Une method d'analyse à trios dimensions de la stabilité d'une rive rocheuse"; Published in *Annales des Ponts et Chaussées*, Vol. 1, pp.37 – 60, 1965.

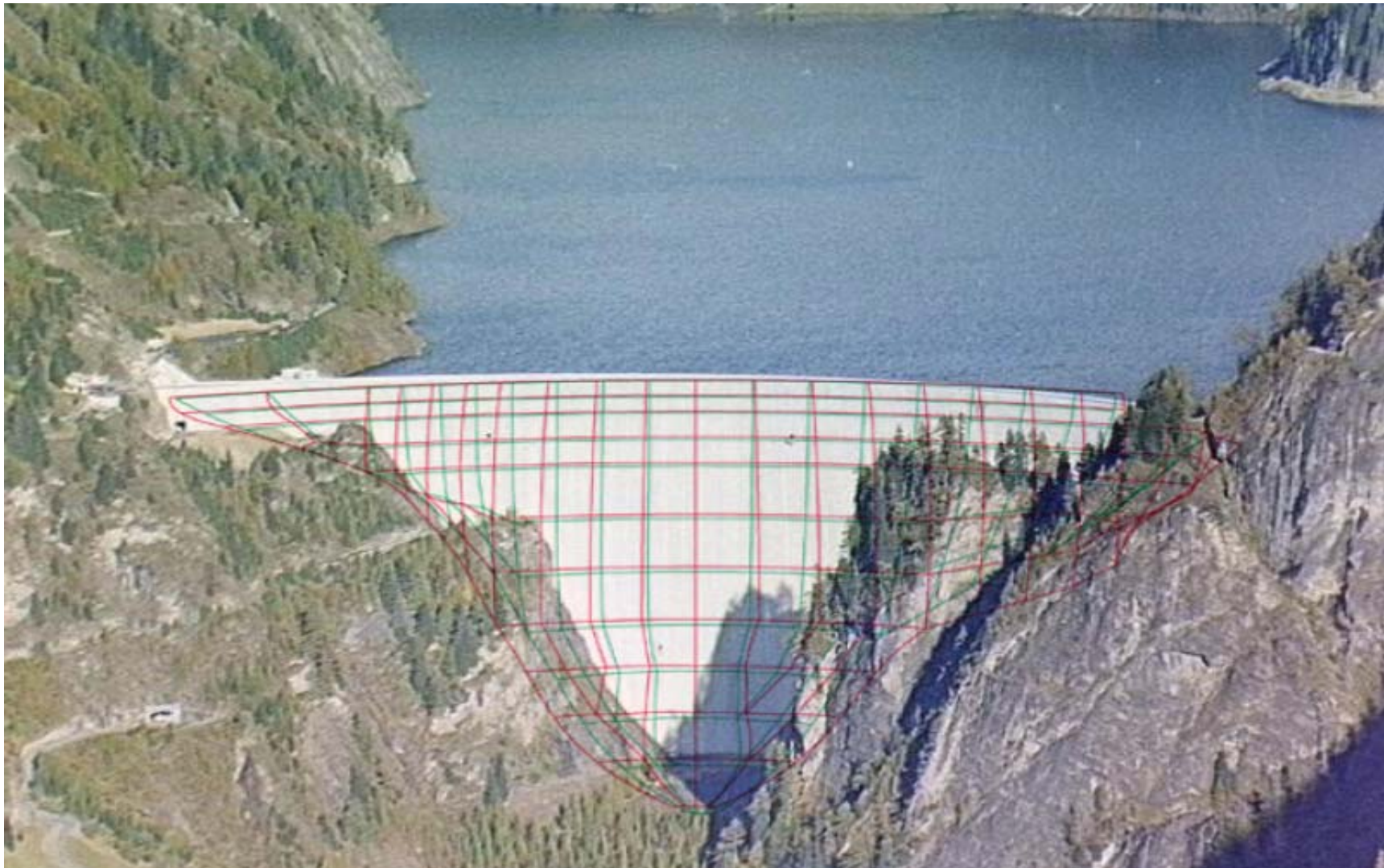
STUCKY Ltd

Dr. Russell Michael GUNN

Luzzone Arch Dam - Characteristics



Luzzone Arch Dam - Location - Reservoir, Dam and FE Mesh Overlay



Luzzone Dam - Characteristics

Description	Units	Old dam (< 1995)	New dam
Type		Double curvature arch dam	
Maximum above the foundation	m	208.00	225.00
Crest length	m	530.00	510.00
Maximum thickness (crown)	m		36.00
Freeboard	m	2.30	4.20
Elevation normal	m.a.s.l.	1'591.00	1'606.00
Normal operation elevations	m.a.s.l.	1'592.40	1'607.00
PMFreservoir elevation	m.a.s.l.		1'607.60
Maximum reservoir level including u/s block sliding	m.a.s.l.		1'610.20
Minimum operation elevation	m.a.s.l.		1'435.00
Elevation of the bottom outlet	m.a.s.l.		1'407.70
Parapet elevation	m.a.s.l.	1'593.30	1'610.20
Dam concrete volume	m ³	1.33 x 10 ⁶	1.40 x 10 ⁶
Grout curtain depth	m	165.00	165.00
Grout curtain surface area	m ²	74'100.00	77'320.00
Normal volume of the reservoir	m ³	88 x 10 ⁶	108 x 10 ⁶
Maximum volume of the reservoir	m ³	90 x 10 ⁶	112 x 10 ⁶
Live load volume	m ³	87 x 10 ⁶	107 x 10 ⁶
Reservoir basin area	km ²	1.27	1.44

App. 3 List of Supplied Data**List of Supplied Data (ASCII Text Format)**

Item	Name	Description
1	<i>ThemeCModel.fga</i>	Model data in ASCII format containing all geometrical, finite element, material property definitions (static and dynamic - Rayleigh damping), boundary conditions and loading.
2	<i>eqt1.tcv</i>	Acceleration-time history in direction 1 (Global X-direction)
3	<i>eqt2.tcv</i>	Acceleration-time history in direction 2 (Global Y-direction)
4	<i>eqt3.tcv</i>	Acceleration-time history in direction 3 (Global Z-direction)
5	<i>botsurf.dat</i>	Compressible fluid parameters: Speed of sound in water and reservoir bottom absorption (<i>Supplied for Information</i>)
6	<i>csound.dat</i>	Compressible fluid parameters: Speed of sound in water (<i>Supplied for Information</i>)
7	<i>farfield.dat</i>	Compressible fluid parameters: gravitational acceleration, far-field absorption (<i>Supplied for Information</i>)

Description of Geometry and Finite Element Model Data Structure and Formatting

Reference: ThemeCModel.fga
 Creation software: DIANA Version 9.2, 2008

File Number Lines	Command	Entity	Description
4 - 57	CONSTRUCT SET OPEN		Define sets for easy pre and post-processing
		SURF1	Excavated topographical surface
		SURF2	Water face
		SURF3	Air face
		SURF4	Bottom of topographical surface
		SURF5	Foundation limit boundary surface (4 sided box)
		SURF6	Foundation limit boundary surface (4 sided box)
		SURF7	Foundation limit boundary surface (4 sided box)
		SURF8	Foundation limit boundary surface (4 sided box)
		DAM	Dam body
		FOUND	Foundation body
		INFACE	Interface zone between dam and foundation
		CREST	Crest surfaces
		SURF2M	Water face post-processing - developed views!
		BORDS	Sum of external boundaries surf 4,5,6,7,8
		DAM1	Dam construction stage 1
		DAM2	Dam construction stage 2
		DAM3	Dam construction stage 3
		DAM4	Dam construction stage 4
		DAM5	Dam construction stage 5
		XSECT1	Crown cantilever x-section 1
		XSECT2	Left bank wing x-section 2
		XSECT3	Right bank wing x-section 3
		FLUSTR	Fluid-structure interface
		FLUID	Reservoir body
		FFSURF	Far-field surface

Description of Geometry and Finite Element Model Data Structure and Formatting

Reference: ThemeCModel.fga
 Creation software: DIANA Version 9.2, 2008

File Number Lines	Command	Entity	Description
		FRESURF	Reservoir free surface
		BOTSURF	Reservoir bottom surface
58 - 11901	GEOM POINT P1 X Y Z	Geometry point 1 defined by Cartesian co-ordinates X, Y, Z X Horizontal Direction - Crown to Right positive Y Elevation - Vertical direction upwards positive Z Horizontal Direction - Downstream - upstream positive	
11902 - 15980	CONSTRUCT SET APPEND	Append geometric part to set name	
15981 - 16001	PROP MAT NAME ELASTIC ISOTROP	Define material property NAME Elastic Isotropic values of E = 25 GPa and $\nu = 0.18$	
	PROP MAT NAME MASS DENSITY	Define material property NAME Mass density kg/m3	
	PROP MAT NAME DAMPING VISCOUS	Define material property NAME dynamic viscous Rayleigh parameters 0.6 and 0.01	
	PROP MAT NAME FLOW ISOTROP	Define material property NAME thermal conductivity 2.2222 and capacitance = 0	
	PROP MAT NAME THERCONC ISOTROP	Define material property NAME thermal expansion coefficient of 10^{-5}	
	PROP MAT WATER EXTERNAL EXTERNAL	Define material property NAME with external file NAME	
16002 - 22256	GEOM LINE STRAIGHT NAME Pname Pname	Define straight line between two points with line division (not important)	
22257 - 30749	CONSTRUCT SET APPEND	Append geometric part to set name	
30750 - 34869	GEOM SURF 4SIDES NAME L1 L2 L3 L4	Define a surface with 4 sides using lines $L_x - L_{x+4}$	
	GEOM SURF 3SIDES NAME L1 L2 L3	Define a surface with 3 sides using lines $L_x - L_{x+3}$	
34870 - 40269	CONSTRUCT SET APPEND	Append geometric part to set name	
40270 - 40994	GEOM BODY 6SUR NAME SF1, SF2, SF3 ... SF6	Define a body with 6 surfaces NAME, Surface names $SF_x - SF_{x+6}$	
	GEOM BODY 5SUR NAME SF1, SF2, SF3 ... SF5	Define a body with 5 surfaces NAME, Surface names $SF_x - SF_{x+5}$	
40995 - 41896	CONSTRUCT SET APPEND	Append geometric part to set name	

Description of Geometry and Finite Element Model Data Structure and Formatting

Reference: ThemeCModel.fga
 Creation software: DIANA Version 9.2, 2008

File Number Lines	Command	Entity	Description
41897 - 42300	MESHING TYPE NAME QU8		Define mesh type as 8-node quadrilateral surface element
	MESHING TYPE NAME TR6		Define mesh type as 6-node triangular surface element
42301 - 43025	MESHING TYPE NAME HE20		Define mesh type as brick element with 20 nodes
	MESHING TYPE NAME PE15		Define mesh type as wedge element with 15 nodes
43026 - 43932	PROP ATTACH NAME material NAME		Attach material property for entity NAME to material NAME
43933 - 43935	PROP BOUNDARY CONSTRAINT CO1 NAME X		Define boundary constraints for NAME with constraints X <u>Note</u> : X refers to constraints X,Y,Z translations and RX, RY and RZ rotations which can be accumulated such as 123456 means X Y Z RX RY RZ
43936 - 43970	CONSTRUCT TCURVE NAME LIST FILE NAME		Construct a time curve NAME from filename NAME
	CONSTRUCT TCURVE NAME TSHIFT <i>tsh</i>		TSHIFT shifts the LIST curve by adding <i>tsh</i> to all times
	CONSTRUCT TCURVE NAME ASHIFT <i>ash</i>		ASHIFT shifts a LIST curve by adding <i>ash</i> to all amplitudes
	CONSTRUCT TCURVE NAME TSCALE <i>tsc</i>		TSCALE scales a LIST curve by multiplying all ties by <i>tsc</i>
	CONSTRUCT TCURVE NAME ASCALE <i>asc</i>		ASCALE scales a LIST curve by multiplying all amplitudes by <i>asc</i>
	CONSTRUCT TCURVE NAME TSTART value		TSTART overrides the start time of a LIST curve by TSTART
	CONSTRUCT TCURVE NAME TSTOP value		TSTOP overrides the end time of a LIST curve by TSTOP
43971 - 43995	CONSTRUCT SCURVE NAME GLOBAL Y LIST = EL 1 value EL 2 value		Construct a space curve NAME using GLOBAL Y LIST = Start elevation, value Stop elevation, value
	PROP INITIAL INIPOT NAME SET value		Define initial property NAME for temperature load, value
	PROP LOAD GRAVITY NAME 1 SET = -9.8100 2		Define gravitational load NAME to set NAME, value, direction
	PROP LOAD PRESSURE NAME 2 SURF2M = 2.16801E+06 0		Define hydrostatic pressure
	PROP ATTACH NAME HYDC1		Attach space curve HYDC1 to NAME
	PROP LOAD BASE EQ1 3 ALL = 1.000 1		Define base load excitation EQ1 as loadcase 3, all parts, value = 1, direction X = 1, Y = 2, Z = 3

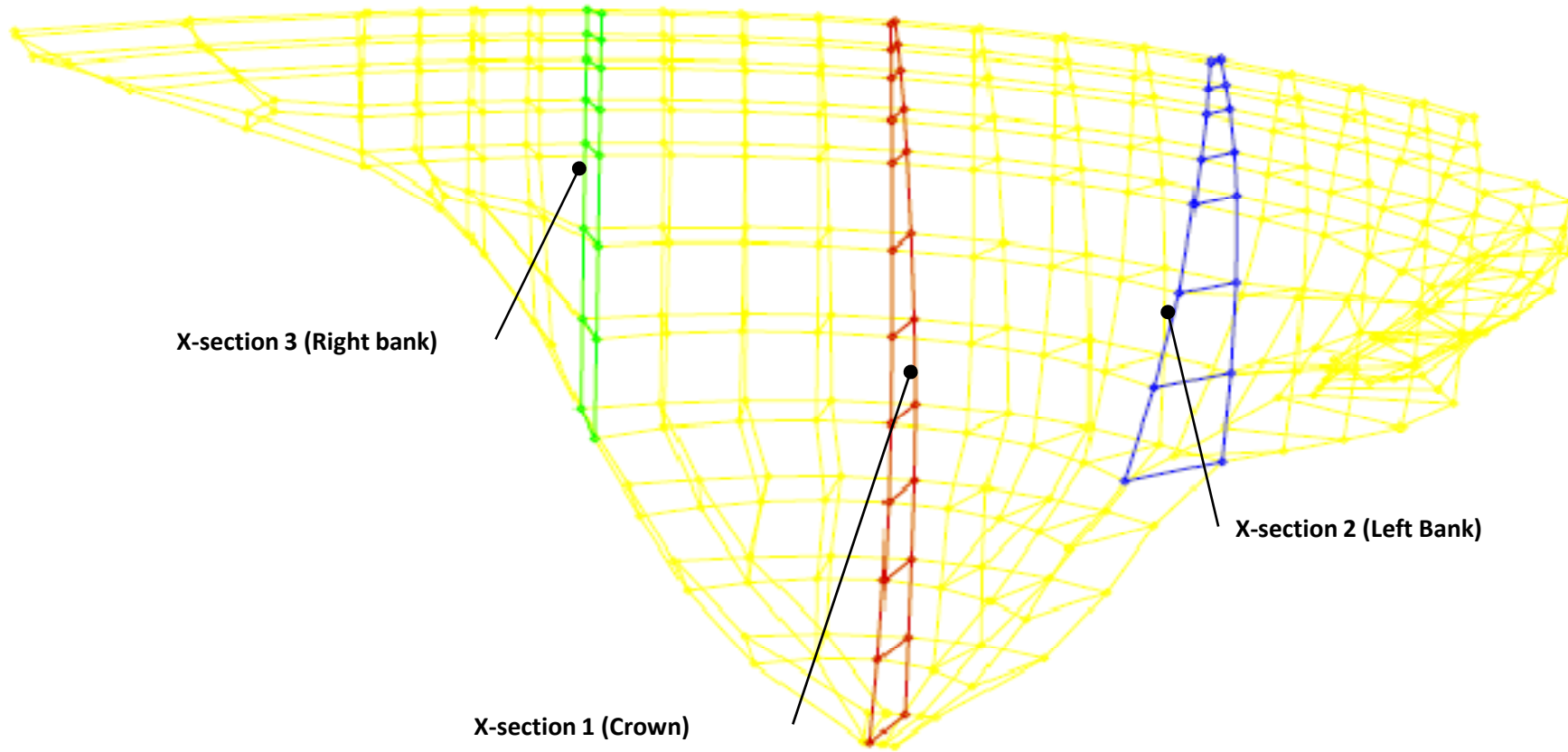
Description of Geometry and Finite Element Model Data Structure and Formatting

Reference: ThemeCModel.fga

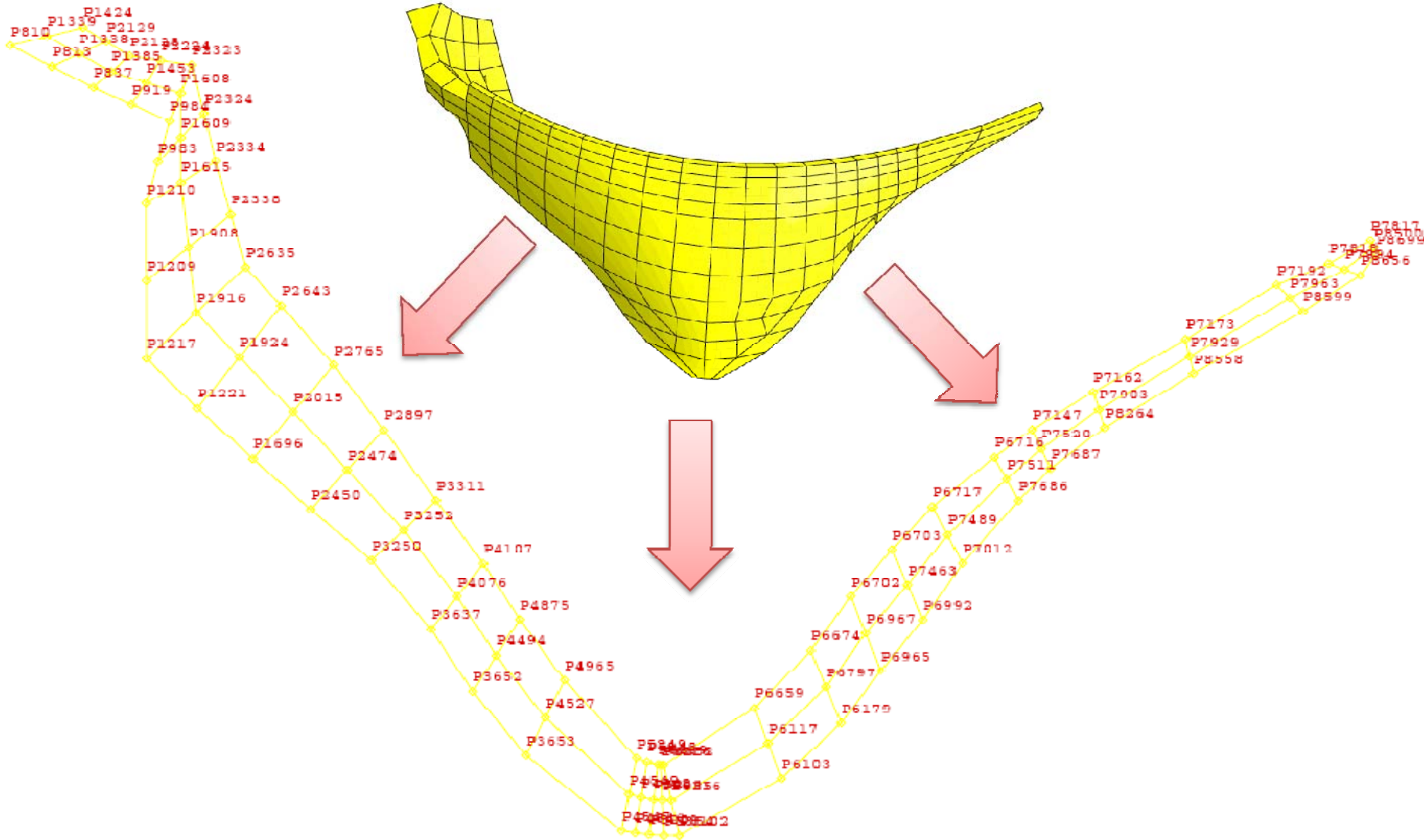
Creation software: DIANA Version 9.2, 2008

<i>File Number Lines</i>	<i>Command</i>	<i>Entity</i>	<i>Description</i>
	PROP ATTACH EQ1 EQT1 PROP LOAD FIXPOT LC6 6 SURF2 = 10 PROP ATTACH LC6 EQT4		Attach property EQ1 to time curve EQT1 Define initial temperature of 10° on surface 2 and attach it to a time curve
43996 - 44000	UTILITY SETUP UNITS LENGTH METER UTILITY SETUP UNITS MASS KILOGRAM UTILITY SETUP UNITS FORCE NEWTON UTILITY SETUP UNITS TIME SECOND UTILITY SETUP UNITS TEMPERATURE CELSIUS		Define analysis units

Luzzone Dam Model - X-section locations and definitions



Luzzone Dam Model - Interface Point numbering and global coordinates (General Overview)

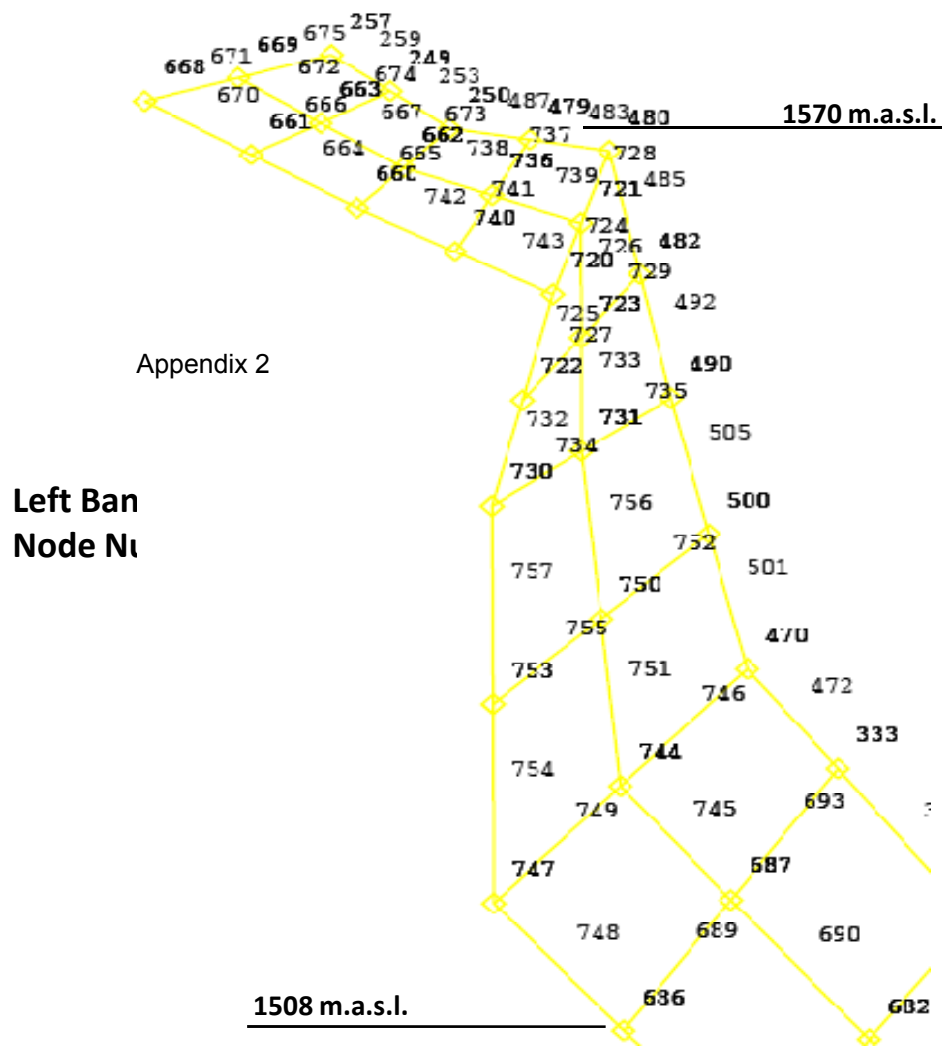


Luzzone Dam Model - Interface Point numbering and global coordinates (Tabulated interface coordinates - Left Bank)

<i>Entity Name</i>	<i>X</i>	<i>Y</i>	<i>Z</i>	<i>Entity Name</i>	<i>X</i>	<i>Y</i>	<i>Z</i>
P810	-235.7	1592	-187.08	P1696	-142.02	1499.2	-74.585
P1339	-224.01	1592	-193.09	P2643	-137.96	1525	-128.54
P813	-221.7	1578.2	-191.1	P2015	-130.37	1504.8	-94.518
P1338	-213.08	1580.5	-196.23	P2450	-121.18	1490.3	-59.359
P1424	-212.33	1592	-199.11	P2765	-118.73	1510.5	-114.45
P837	-207.69	1564.4	-195.12	P2474	-110.61	1493.2	-78.216
P2129	-204.46	1582.8	-201.35	P2897	-100.04	1496	-97.073
P1385	-202.14	1569	-199.36	P3250	-99.273	1481.5	-44.278
P2128	-196.59	1573.6	-203.6	P3252	-89.835	1481.5	-60.628
P919	-194.65	1556.7	-195.2	P3311	-80.397	1481.5	-76.978
P1453	-190.52	1561.7	-202.06	P3637	-77.641	1457.4	-34.043
P2224	-186.38	1566.8	-208.91	P4076	-70.397	1457.4	-51.745
P1210	-186.27	1543	-158.46	P4107	-63.153	1457.4	-69.447
P983	-183.94	1546	-176.87	P3652	-62.351	1433.2	-26.945
P1209	-183.41	1531.5	-130.05	P4494	-56.055	1433.2	-46.041
P984	-181.61	1549	-195.29	P4875	-49.758	1433.2	-65.137
P1217	-180.54	1520	-101.64	P3653	-43.03	1409.1	-19.275
P1608	-178.89	1554.5	-204.76	P4527	-38.224	1409.1	-38.978
P1609	-177.21	1549.2	-187.11	P4965	-33.419	1409.1	-58.681
P2323	-176.17	1560	-214.23	P4547	-9.3001	1385	-7.3266
P1615	-175.54	1544	-169.46	P4549	-8.3215	1385	-26.02
P1908	-170.69	1534.5	-145.66	P5249	-7.3428	1385	-44.713
P2324	-170.49	1552.5	-197.34	P4546	-4.6574	1385	-6.7237
P1916	-165.84	1525	-121.86	P4548	-4.1741	1385	-24.885
P2334	-164.8	1545	-180.46	P5240	-3.6908	1385	-43.045
P1221	-162.19	1508	-89.657	P5211	0	1385	-24.294
P2338	-157.97	1537.5	-161.27	P5209	0	1385	-6.4402
P2635	-151.14	1530	-142.09	P5239	0	1385	-42.148
P1924	-150.07	1516.5	-109.1				

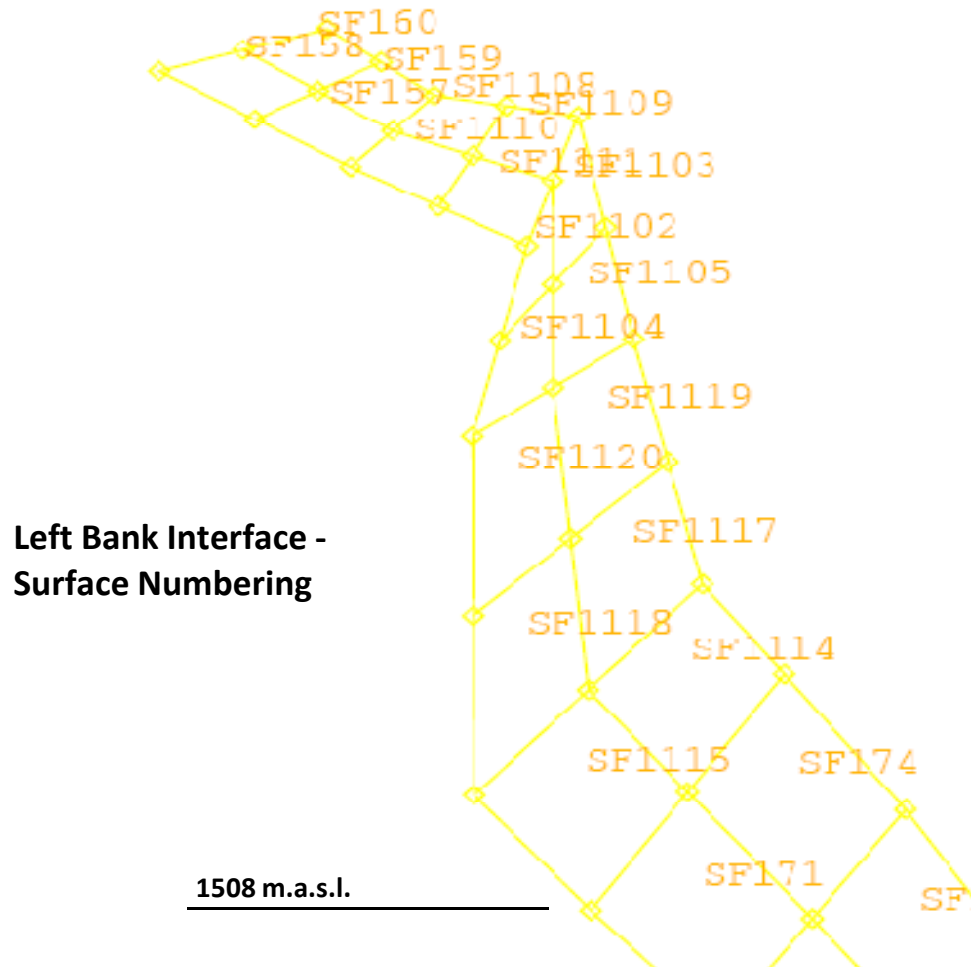
Luzzone Dam Model - Interface Node numbering and global coordinates (Tabulated interface coordinates - Left Bank above elevation 1500)

Entity Name	X	Y	Z
668	-235.7	1592	-187.08
671	-229.86	1592	-190.09
669	-224.01	1592	-193.09
675	-218.17	1592	-196.1
257	-212.33	1592	-199.11
259	-208.39	1587.4	-200.23
672	-218.55	1586.2	-194.66
670	-228.7	1585.1	-189.09
249	-204.46	1582.8	-201.35
674	-208.77	1581.6	-198.79
663	-213.08	1580.5	-196.23
666	-217.39	1579.3	-193.66
661	-221.7	1578.2	-191.1
253	-200.52	1578.2	-202.47
667	-207.61	1574.7	-197.79
250	-196.59	1573.6	-203.6
664	-214.7	1571.3	-193.11
673	-199.37	1571.3	-201.48
487	-191.48	1570.2	-206.25
662	-202.14	1569	-199.36
479	-186.38	1566.8	-208.91
665	-204.92	1566.7	-197.24
738	-196.33	1565.4	-200.71
660	-207.69	1564.4	-195.12
737	-188.45	1564.3	-205.48
483	-181.28	1563.4	-211.57
736	-190.52	1561.7	-202.06
742	-201.17	1560.5	-195.16
480	-176.17	1560	-214.23



Luzzone Dam Model - Interface Node numbering and global coordinates (Tabulated interface coordinates - Left Bank above elevation 1500)

Entity Name	X	Y	Z
741	-192.58	1559.2	-198.63
739	-184.7	1558.1	-203.41
728	-177.53	1557.2	-209.49
740	-194.65	1556.7	-195.2
485	-173.33	1556.2	-205.79
721	-178.89	1554.5	-204.76
743	-188.13	1552.8	-195.24
482	-170.49	1552.5	-197.34
726	-178.05	1551.9	-195.93
724	-180.25	1551.8	-200.02
729	-173.85	1550.9	-192.23
723	-177.21	1549.2	-187.11
720	-181.61	1549	-195.29
492	-167.65	1548.8	-188.9
727	-180.58	1547.6	-181.99
725	-182.77	1547.5	-186.08
733	-176.38	1546.6	-178.28
722	-183.94	1546	-176.87
490	-164.8	1545	-180.46
732	-185.11	1544.5	-167.67
735	-170.17	1544.5	-174.96
731	-175.54	1544	-169.46
734	-180.91	1543.5	-163.96
730	-186.27	1543	-158.46
505	-161.39	1541.2	-170.87
756	-173.11	1539.2	-157.56
500	-157.97	1537.5	-161.27
757	-184.84	1537.2	-144.25
752	-164.33	1536	-153.47

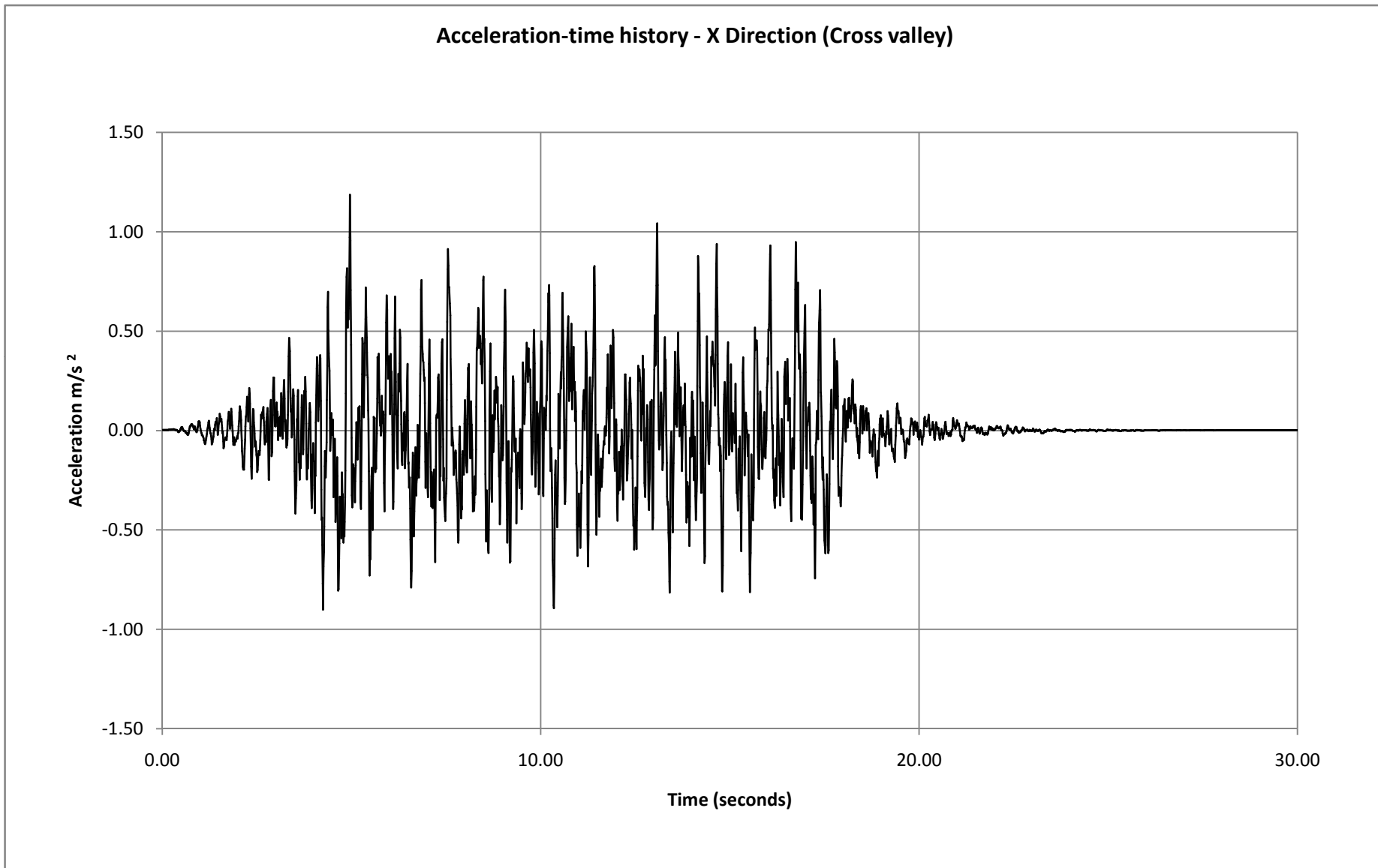


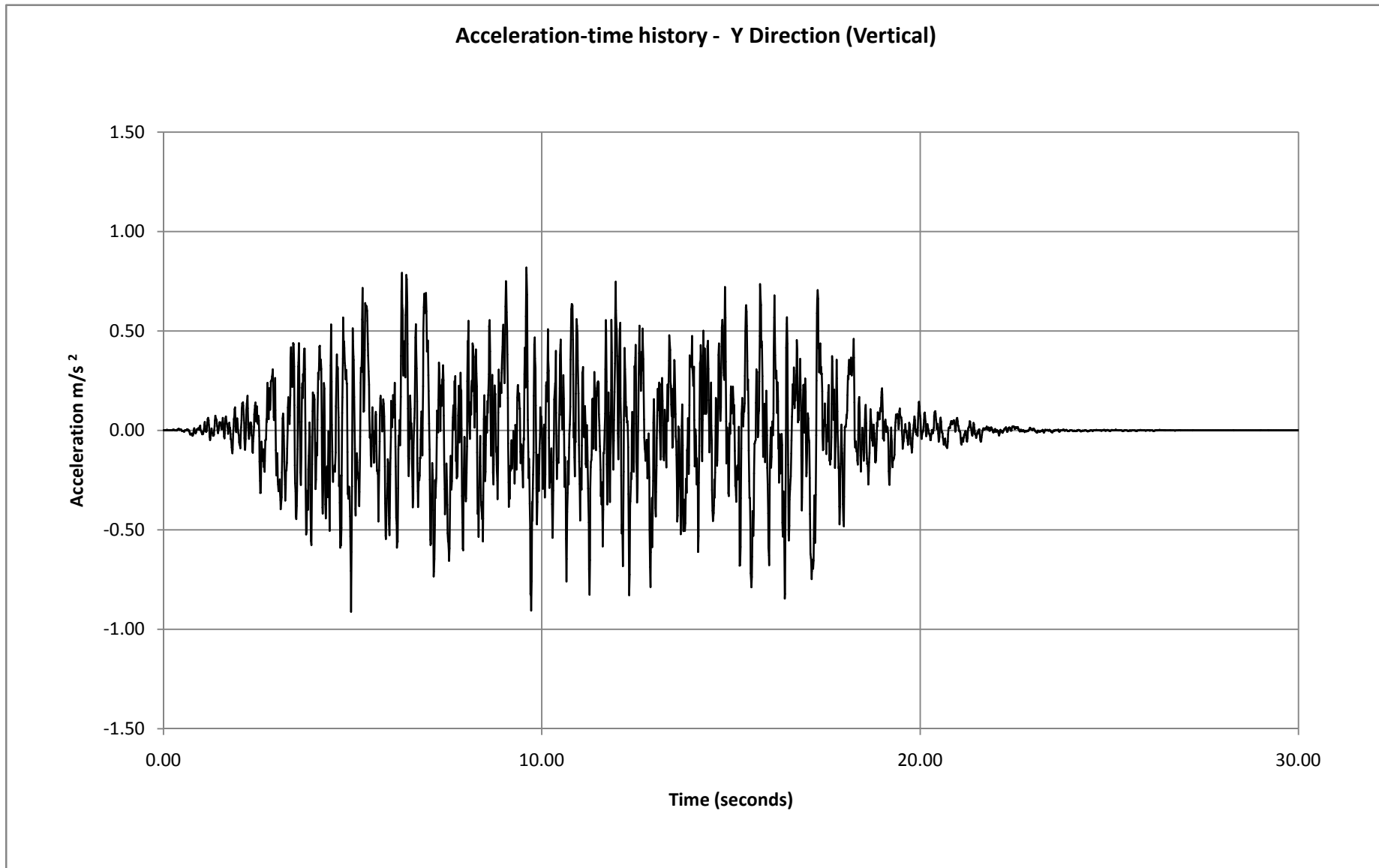
Luzzone Dam Model - Interface Node numbering and global coordinates (Tabulated interface coordinates - Left Bank above elevation 1500)

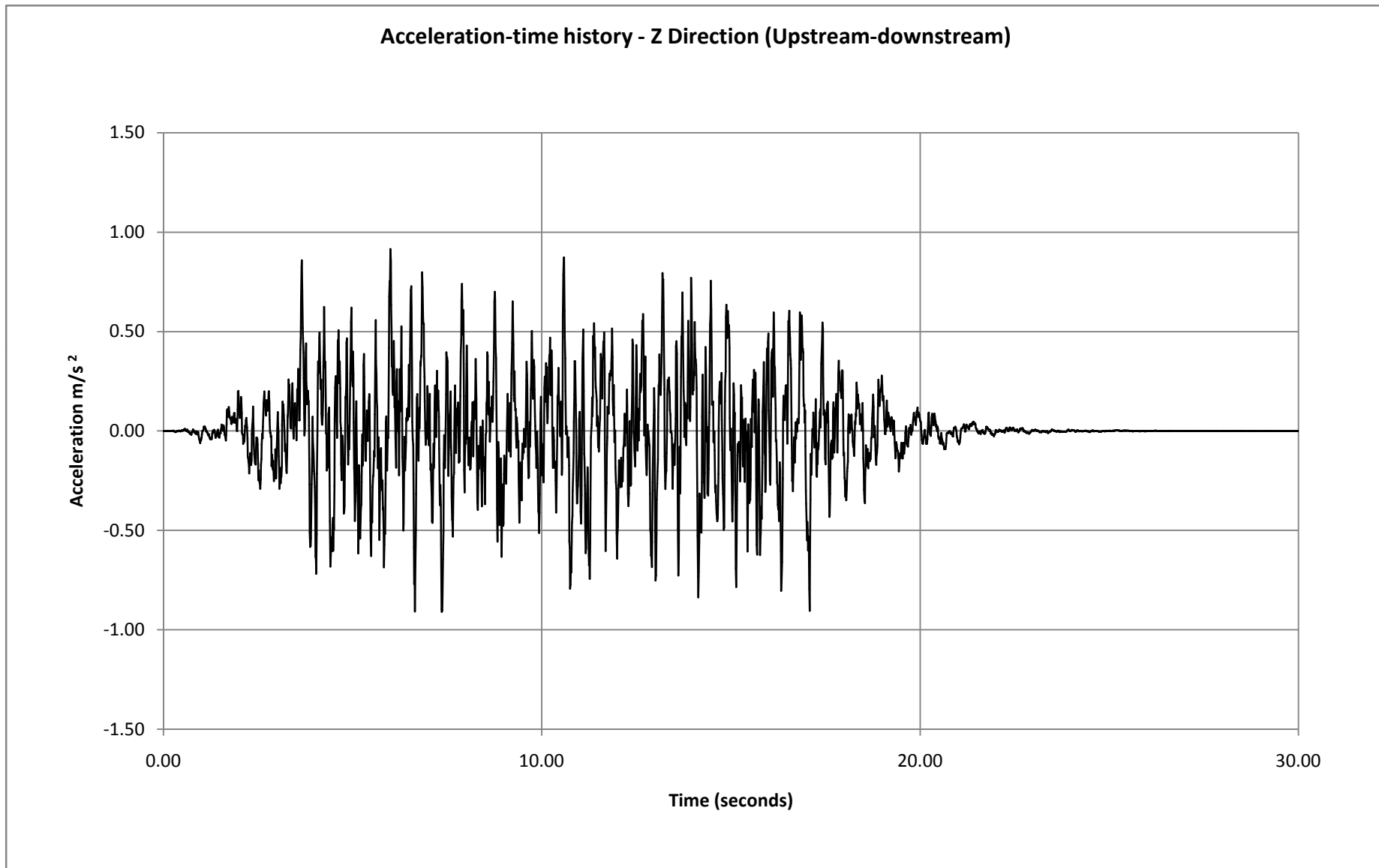
<i>Entity Name</i>	<i>X</i>	<i>Y</i>	<i>Z</i>
750	-170.69	1534.5	-145.66
501	-154.55	1533.8	-151.68
755	-177.05	1533	-137.86
753	-183.41	1531.5	-130.05
470	-151.14	1530	-142.09
751	-168.26	1529.8	-133.76
746	-158.49	1527.5	-131.97
472	-144.55	1527.5	-135.31
754	-181.97	1525.8	-115.84
744	-165.84	1525	-121.86
333	-137.96	1525	-128.54
749	-173.19	1522.5	-111.75
745	-157.96	1520.8	-115.48
693	-144.02	1520.7	-118.82
747	-180.54	1520	-101.64
334	-128.34	1517.7	-121.5
687	-150.07	1516.5	-109.1
748	-171.36	1514	-95.647
689	-156.13	1512.2	-99.378
690	-140.22	1510.7	-101.81
322	-118.73	1510.5	-114.45
686	-162.19	1508	-89.657
692	-124.55	1507.7	-104.49
682	-130.37	1504.8	-94.518
688	-152.1	1503.6	-82.121
323	-109.38	1503.2	-105.76
684	-136.19	1502	-84.552

App. 8 Time-histories X, Y, Z

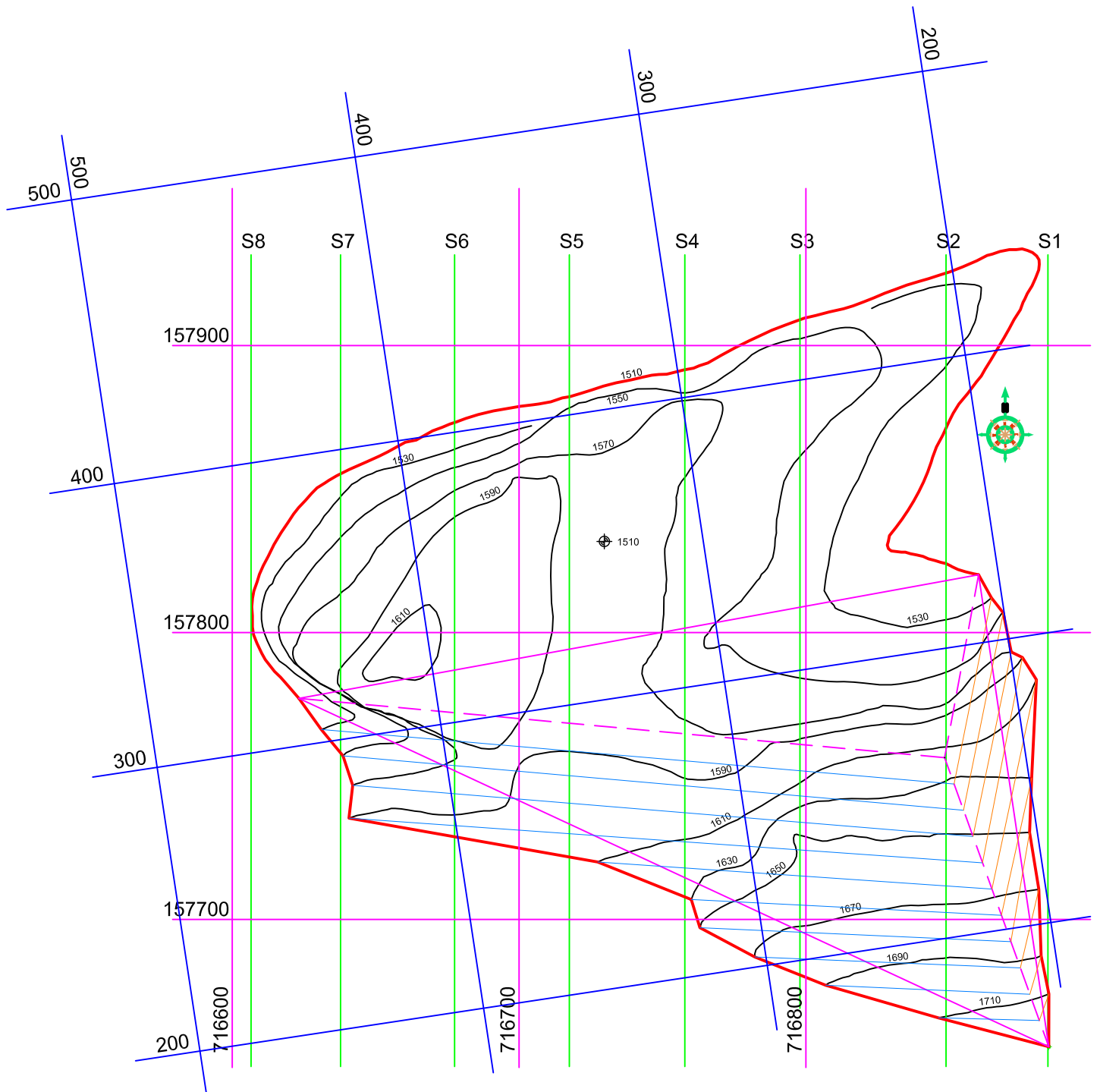
Data	Time	Acceleration	Time	Acceleration	Time	Acceleration
	(secs)	(m/s ²)	(secs)	(m/s ²)	(secs)	(m/s ²)
	X - direction L-R Banks +		Y - direction Vertical +		Z - direction D/S - U/S +	
MAX	3.07E+01	1.19E+00	3.07E+01	8.19E-01	3.07E+01	9.14E-01
MIN	0.00E+00	-9.01E-01	0.00E+00	-9.12E-01	0.00E+00	-9.08E-01
AVE	1.54E+01	1.84E-04	1.54E+01	3.16E-05	1.54E+01	4.21E-06
	0.00E+00	3.38E-03	0.00E+00	1.82E-03	0.00E+00	-3.37E-04
	1.00E-02	3.37E-03	1.00E-02	1.82E-03	1.00E-02	-3.31E-04
	2.00E-02	3.38E-03	2.00E-02	1.81E-03	2.00E-02	-3.17E-04
	3.00E-02	3.38E-03	3.00E-02	1.81E-03	3.00E-02	-3.02E-04
	4.00E-02	3.43E-03	4.00E-02	1.80E-03	4.00E-02	-2.86E-04
	5.00E-02	3.46E-03	5.00E-02	1.82E-03	5.00E-02	-2.48E-04
	6.00E-02	3.46E-03	6.00E-02	1.82E-03	6.00E-02	-1.90E-04
	7.00E-02	3.45E-03	7.00E-02	1.83E-03	7.00E-02	-2.07E-04
	8.00E-02	3.37E-03	8.00E-02	1.86E-03	8.00E-02	-1.94E-04
	9.00E-02	3.20E-03	9.00E-02	1.87E-03	9.00E-02	-1.29E-04
	0.1	3.04E-03	0.1	1.83E-03	0.1	5.30E-05
	0.11	2.86E-03	0.11	1.89E-03	0.11	2.55E-04
	0.12	2.73E-03	0.12	1.79E-03	0.12	1.71E-04
	0.13	2.60E-03	0.13	1.58E-03	0.13	2.19E-04
	0.14	2.67E-03	0.14	1.37E-03	0.14	2.66E-04
	0.15	2.97E-03	0.15	1.14E-03	0.15	4.21E-04
	0.16	3.35E-03	0.16	1.30E-03	0.16	6.02E-04
	0.17	3.72E-03	0.17	1.52E-03	0.17	8.42E-04
	0.18	3.89E-03	0.18	1.40E-03	0.18	1.19E-03
	0.19	4.14E-03	0.19	1.39E-03	0.19	1.12E-03
	0.2	4.18E-03	0.2	1.37E-03	0.2	1.10E-03
	0.21	3.84E-03	0.21	1.33E-03	0.21	1.30E-03
	0.22	3.83E-03	0.22	1.75E-03	0.22	7.75E-04
	0.23	4.04E-03	0.23	1.55E-03	0.23	1.53E-04
	0.24	5.14E-03	0.24	1.87E-03	0.24	5.73E-04
	0.25	5.38E-03	0.25	2.86E-03	0.25	1.51E-03
	0.26	5.78E-03	0.26	3.32E-03	0.26	1.99E-03
	0.27	5.74E-03	0.27	3.08E-03	0.27	8.98E-04
	0.28	5.95E-03	0.28	2.41E-03	0.28	-6.01E-04
	0.29	6.45E-03	0.29	1.50E-03	0.29	-2.06E-03
	0.3	6.63E-03	0.3	6.80E-04	0.3	-3.35E-03
	0.31	6.75E-03	0.31	6.25E-04	0.31	-4.48E-03
	0.32	5.73E-03	0.32	1.46E-03	0.32	-5.09E-03
	0.33	5.27E-03	0.33	7.79E-04	0.33	-4.22E-03
	0.34	3.08E-03	0.34	6.04E-04	0.34	-1.54E-03
	0.35	1.37E-03	0.35	-7.20E-05	0.35	-4.97E-04
	0.36	1.29E-03	0.36	1.01E-03	0.36	-3.66E-04
	0.37	1.46E-03	0.37	3.84E-03	0.37	3.67E-04
	0.38	3.04E-03	0.38	6.14E-03	0.38	-1.38E-03
	0.39	2.80E-03	0.39	7.24E-03	0.39	-1.69E-03
	0.4	1.40E-05	0.4	7.72E-03	0.4	6.51E-04
	0.41	-3.50E-03	0.41	7.24E-03	0.41	1.46E-03
	0.42	-6.42E-03	0.42	4.74E-03	0.42	1.40E-03
	0.43	-7.68E-03	0.43	2.96E-03	0.43	6.27E-04
	0.44	-6.94E-03	0.44	4.45E-03	0.44	-5.18E-04
	0.45	-4.25E-03	0.45	4.56E-03	0.45	-1.95E-03
	0.46	-2.42E-03	0.46	4.43E-03	0.46	-2.64E-04
	0.47	1.53E-03	0.47	3.30E-03	0.47	-1.15E-04
	0.48	6.13E-03	0.48	-4.54E-04	0.48	1.75E-03
	0.49	8.81E-03	0.49	-3.30E-03	0.49	4.37E-03
	0.5	1.34E-02	0.5	-3.21E-03	0.5	3.09E-03







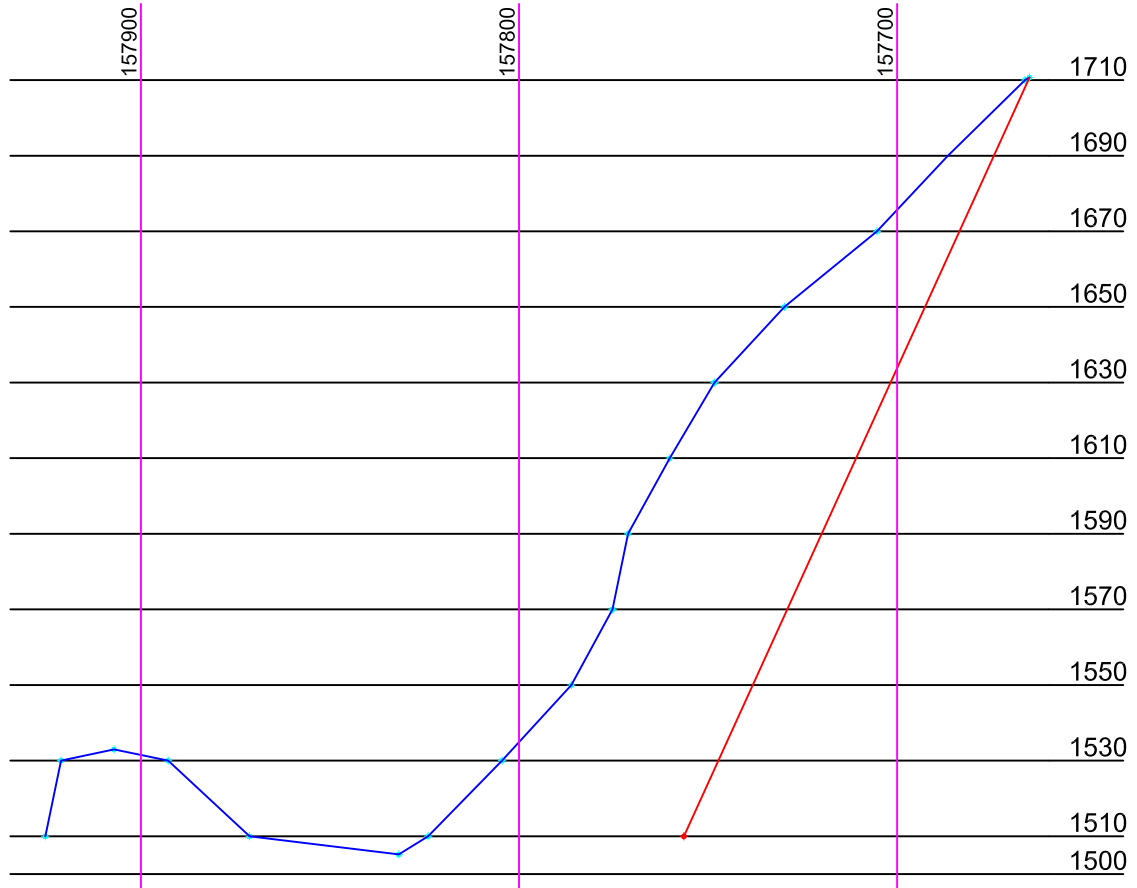
1



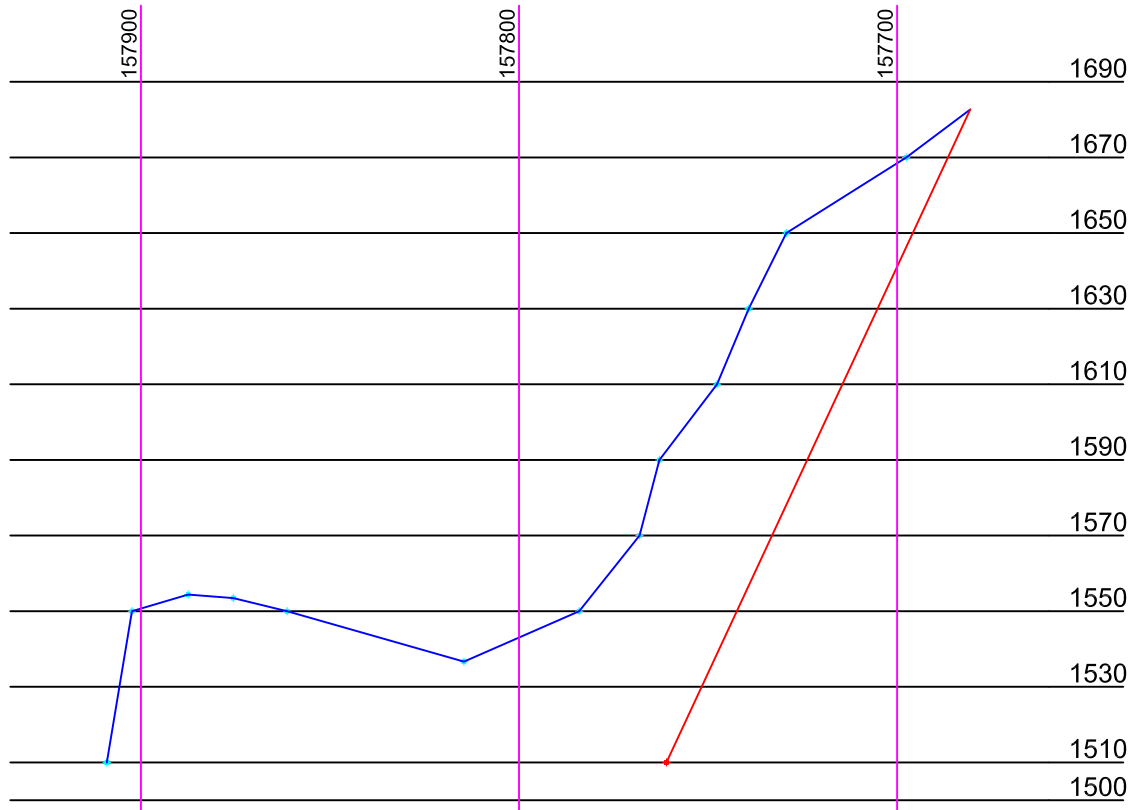
WEDGE ARRANGEMENT

01.04.2009	m	1 : 2000
Date:	Units:	Scale:

SECTION 2 1/2000



SECTION 3 1/2000



WEDGE ARRANGEMENT - SECTIONS 2 & 3

01.04.2009

m

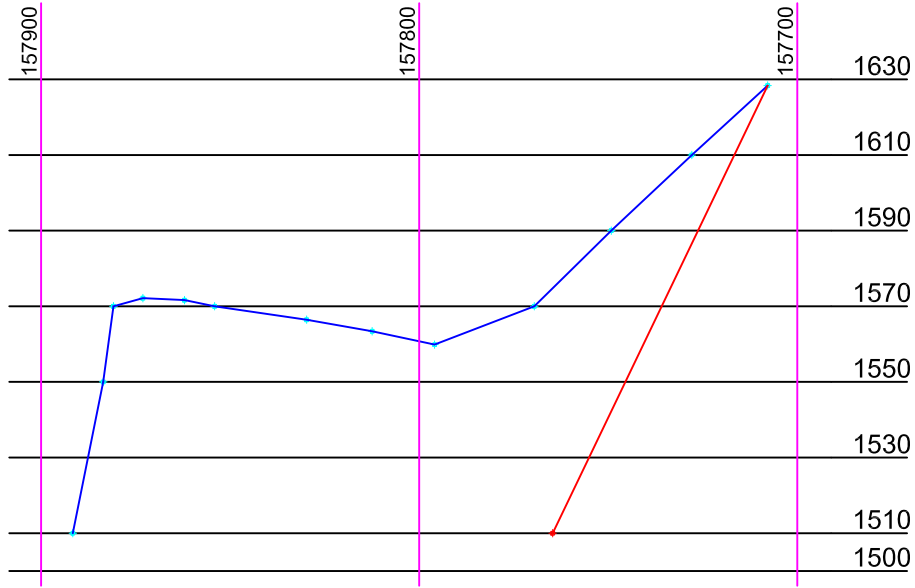
1 : 2000

Date:

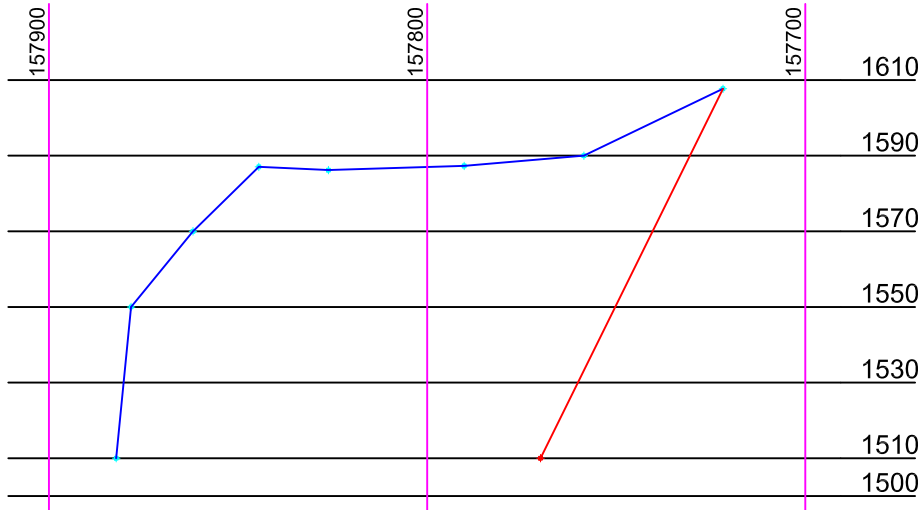
Units:

Scale:

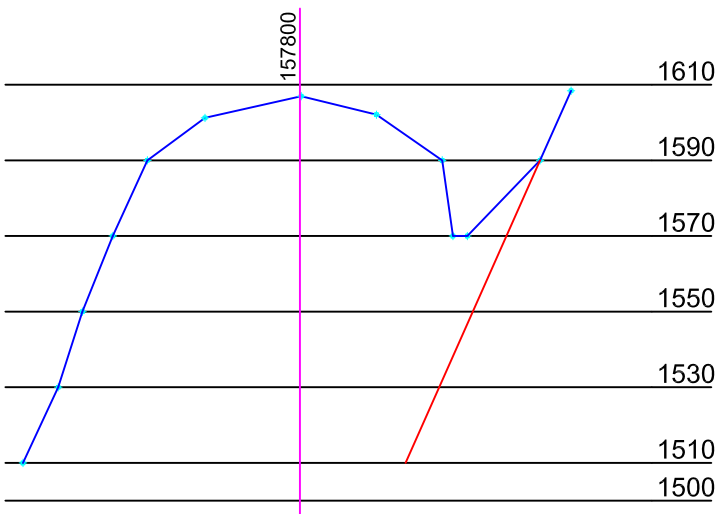
SECTION 4 1/2000



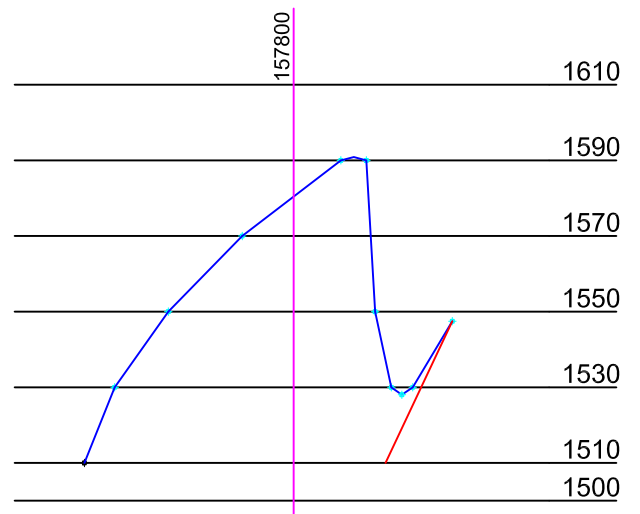
SECTION 5 1/2000



SECTION 6 1/2000



SECTION 7 1/2000



WEDGE ARRANGEMENT - SECTIONS 4 TO 7

Date: 01.04.2009

Units: m

Scale: 1 : 2000

Results Case	Interface Forces (Dam thrust)			Resultant Forces (Dam thrust)			Contact Plane Forces			Stability Forces		Loss of Contact Plane Results		
	F_x MN	F_y MN	F_z MN	F_R MN	F_α °	F_β °	J_h MN	J_1 MN	J_2 MN	D MN	S MN	J_h	J_1	J_2
Static Load $F_{sw(0)}$												Yes	No	Yes
Static Load $F_{hyd(0)}$														
Static Load $F_{tot(0)}$														
Initial Static Load $F_{s(0)}$														
First dynamic step $F_{d(0)}$														
Dynamic steps $F_{d(n+1)}$														
.....														
.....														
Last dynamic step $F_{d(n)}$														

Notes:

Subscripts -

s = static

d = dynamic

α = dip angle (°)

β = dip direction angle (°) with respect to the North

w = wet plane surface area (below reservoir elevation)

δ = displacement (mm)

1 = plane 1

2 = plane 2

h = horizontal plane (elevation indicated)

sw = self-weight

hyd = full hydrostatic loading (Elevation 1610.20 m.a.s.l.)

tot = $sw + hyd$

Loading -

The total load shall consist of self-weight, full hydrostatic pressure and all three component earthquake forces

Stability -

D = Driving force (MN) S = Stabilising force (MN)

Results Case	Wedge displacements						Factor of Safety
	δ_x mm	δ_y mm	δ_z mm	δ_R mm	δ_α °	δ_β °	
Static Load $F_{sw(0)}$							
Static Load $F_{hyd(0)}$							
Static Load $F_{tot(0)}$							
Initial Static Load $F_{s(0)}$							
First dynamic step $F_{d(0)}$							
Dynamic steps $F_{d(n+1)}$							
.....							
.....							
Last dynamic step $F_{d(n)}$							

Notes:

Subscripts -

s = static
 d = dynamic
 α = dip angle (°)
 β = dip direction angle (°) with respect to the North
 w = wet plane surface area (below reservoir elevation)
 δ = displacement (mm)

1 = plane 1
 2 = plane 2
 h = horizontal plane (elevation indicated)
 sw = self-weight
 hyd = full hydrostatic loading (Elevation 1610.20 m.a.s.l.)
 tot = $sw + hyd$

Loading -

The total load shall consist of self-weight, full hydrostatic pressure and all three component earthquake forces

Stability -

D = Driving force (MN) S = Stabilising force (MN)

Manuscript to Civil Engineers
 Re: for the London Institution
 Trans. Inst. Civ. Eng. 1975

EFFECTS OF EARTHQUAKES ON DAMS AND EMBANKMENTS

N. M. NEWMARK, D.Sc., Ph.D., M.S., M.I.C.E.

I wish to thank the British Geotechnical Society for the opportunity of visiting London again and for the honour of appearing before you in the home of the Institution of Civil Engineers, of which I am so proud to be a member.

Several years ago I transmitted some preliminary notes on the topic of earthquake effects on dams to the late Karl Terzaghi, whose invaluable advice and suggestions regarding those notes were freely used in the preparation of this Paper. I wish also to acknowledge the comments and suggestions I have had from time to time concerning the subject from my colleague at the University of Illinois, Dr Ralph B. Peck; from my associate in several consulting assignments, Dr Laurits Bjerrum; and from my colleague for several months, while he was visiting the University of Illinois, Dr N. N. Ambraseys.

Finally, I should like to acknowledge the assistance on some of the calculations for this lecture that were made by two of my associates at the University of Illinois, Dr John W. Melin, and Mr Mohammad Amin.

INTRODUCTION

General description of earthquake motions

In an earthquake, the earth moves in a nearly random fashion in all directions, both horizontally and vertically. Measurements have been made of earthquake motions in a number of instances. In general, those measurements which are of greatest interest are the records of 'strong motion' earthquake accelerations, measured by the U.S. Coast and Geodetic Survey for a number of earthquakes in California in the past three decades. These accelerations, as a function of time, are available for motion in two horizontal directions as well as in the vertical direction, at a number of locations for several earthquakes. From the time-record of the acceleration, the velocities and displacements can be computed by integration.

One of the most intense strong motion records available is that for the El Centro, California earthquake of 18 May, 1940. The record for the north-south component of acceleration of this earthquake is shown in Fig. 1, which also shows the values computed for velocity and displacement in the same direction. From the figure it can be observed that the maximum ground acceleration in the direction of this measurement is about 0.32 *g*, the maximum ground velocity 13.7 in/sec, and the maximum ground displacement 8.3 in.

The general nature of earthquake motions is indicated by this figure. It can be noted that the highest intensity peaks of acceleration have a relatively short period or a relatively high frequency; the most important peaks in the velocity, however, have a longer period which corresponds to a lower frequency; and the important peaks in the ground displacement have a much longer period still. For the ground conditions at El Centro the length of single loops of the highest intensities, in the various records, have durations of the order of the following: for acceleration, about 0.1 to 0.5 sec; for velocity, about 0.3 to 2 sec; and for displacement

about 1 to 4 sec. In other types of soil, the relative durations may differ, with softer soils in general showing lower magnitudes of acceleration, but longer durations and much larger displacements, than in Fig. 1.

It must be remembered that the El Centro earthquake is not the largest earthquake which has been experienced, even in California. It happened only to yield the most intense record at a point where a strong motion accelerograph was located.

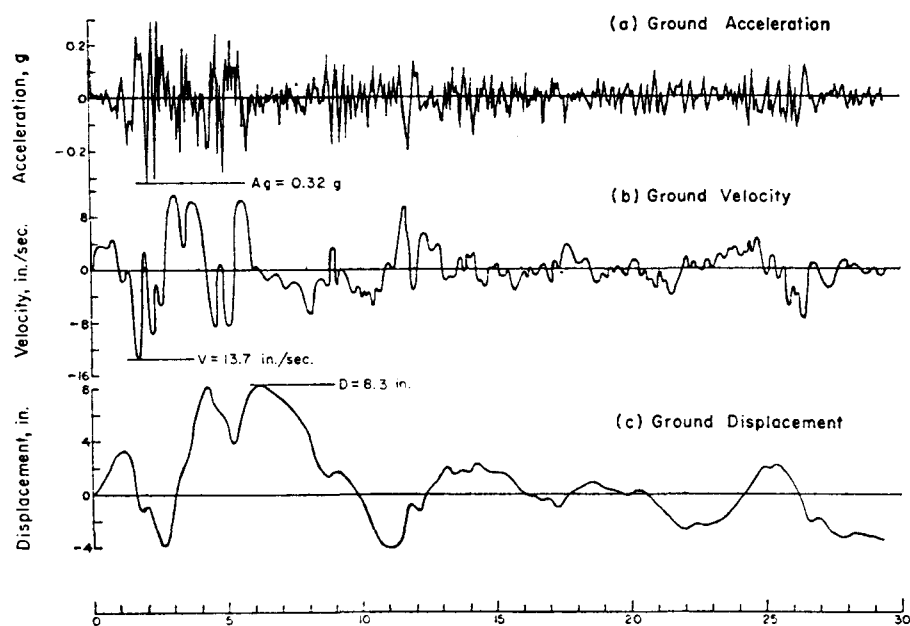


Fig. 1. El Centro, California, earthquake of 18 May, 1940, N-S component

Significant factors of earthquake motion

In considering the effect of an earthquake on a structure such as an earth or rock-fill dam, it is necessary to consider all of the aspects of the motion. In other words, the peak acceleration may not be significant in determining the response of the dam. The effects of the velocities and of the ground displacement, and of the differential displacement of the ground leading to fissures in the ground surface, may be of equal or of even greater importance. It will be shown later that the most important measure of the intensity of an earthquake is the maximum ground velocity reached at any time during the earthquake.

Records of the same general nature as those in Fig. 1 have been obtained for other earthquakes. Some major differences exist in the records, which show distinctive situations: in some cases an earthquake may correspond only to one short series of major pulses, with essentially only one major loop of displacement; and in other cases it may show an almost periodic displacement response for a large portion of time. The El Centro record is typical of a nearly periodic response of moderately low intensity combined with one very large displacement peak.

The durations of large motion in earthquakes vary from less than 10 seconds to as long as several minutes. The total duration and the total number of 'spikes' or peaks of velocity, and the reversals of velocity, are of importance in determining the response of a structure such as an earth or rock-fill dam, or embankment.

In the studies made for this Paper, earthquakes have been considered patterned after those for which records are available in California, but which differ in some respects in terms of the significant frequencies of the various kinds of motion, and in the total duration of motion or number of spikes.

One of the most important special conditions existing at some sites is a relatively soft sedimental deposit of fairly great depth and wide extent. When such a soil deposit is set in to motion at its contact with the bed rock, there is a tendency for the resultant motions of the soil to reflect the natural frequency of the bowl of soil. This has the effect of increasing the magnitude of surface displacements and velocities, but it also causes the resultant motion to be more periodic in character, with many loops of successive displacement or velocity nearly in resonance, that is, having nearly the same period and with successive positive and negative peaks. A structure built on such material and hence subjected to such a motion will generally have a larger response than it would have if it were subjected to the motions of the bed rock.

Intensities of maximum motion for major earthquakes

Although earthquakes in many parts of the world may be less intense than the maximum recorded earthquake in California, in regions in which major seismic activity must be expected one should consider the probability of even larger motions. In any location, it is desirable to design for the maximum probable earthquake, that is, an earthquake that has a reasonable probability of occurring within the lifetime of the structure, with a sufficiently large factor of safety to preclude the necessity for major repairs. One should also consider an extreme earthquake, of about the maximum intensity that might be expected at the site, and for which some damage might be permissible, but collapse or failure should be prevented. Estimates of the maximum probable earthquake that might occur once in a hundred years in California, and an extreme earthquake with only a relatively small chance of occurrence, are given in Table 1, for comparison with the maximum recorded earthquake in California. It is not considered likely that the extreme earthquake indicated in Table 1 would be exceeded anywhere in the world. The parameters indicated in Table 1 describing the intensity of possible earthquakes, are intended to apply to the general motions of the soil or rock away from the regions where the major fault motions occur. Although even at such fault motions, the accelerations and velocities are not likely to exceed the values tabulated, the displacements might be considerably greater, and the relative displacement at a fault may be of such a magnitude that it would cause damage or serious difficulty in a structure or a dam at the fault.

Table 1
Probable intensities of maximum motion for major earthquakes

Condition	Maximum acceleration <i>g</i>	Maximum velocity: in/sec	Maximum displacement: in.	Duration of major motion: sec.
1. Maximum recorded EQ. in California — —	0.32	14	12	30
2. Maximum probable EQ. in California — —	0.50	24 to 30	24	90 to 120
3. Extreme values considered	0.50 to 0.60	30 to 36	36 to 48	120 to 240

Note: Lower values of motions apply to rock, in general.

OBSERVED EFFECTS OF EARTHQUAKES

Ambraseys (1962) points out that no major earth dam has been damaged by an earthquake during the last 25 years. However, he also points out that this argument can not be used as a proof for the adequacy of modern design methods, since no major dam built after the late thirties has been subjected to a severe earthquake. There have been a number of dams that have been damaged, or even destroyed, in earthquakes (Ambraseys, 1960, 1962). Moreover, it is generally true that in all compacted dam-construction materials, and in many natural soil strata, the dynamic shearing resistance is about the same as the static shearing resistance, or slightly greater, and the usual factor of safety is sufficiently large to prevent catastrophic motions. However, at some localities, natural soil strata are encountered which can lose part or almost all of their shearing resistance under shock conditions, either because of increased hydrostatic pressure or owing to loss in shearing strength from even slight remoulding. Under such conditions, major failures can occur, and have occurred, in embankments or under the foundations of dams which otherwise would not have suffered difficulties.

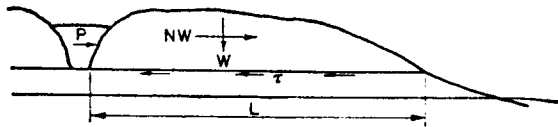


Fig. 2. Sliding of block in Anchorage (after Wilson)

In the recent Anchorage earthquake, large motions and catastrophic failures occurred in natural embankments which slid major distances on sensitive clay strata or on loose, low relative density sand layers. A typical example of the type of failure which occurred is shown in Fig. 2, taken from Shannon and Wilson (1964). The entire block of material of the order of 1000 ft in length and 60 to

100 ft in height, moved bodily tens of feet in an earthquake the maximum acceleration of which has been variously estimated as about 0.15 to 0.18 *g*.

Motions along a sliding surface may occur in a dam, under certain conditions, and a succession of slides of limited displacement on the upstream and downstream faces of a dam are indicated schematically in Fig. 3, taken from Ambraseys (1958). The successive motions coming from the several shocks in different directions produce slides along different surfaces, with the net results shown at the bottom of the figure. The major settlement at the crest and the pattern of the deformations are similar to those which have been observed in several older dams which may not have been designed to have adequate earthquake resistance.

Tests of models of earth or rock-fill dams have been made by Davis and his associates at Berkeley (Davis *et al.*, 1960; Clough and Pirtz, 1958), by Seed and his associates, also at Berkeley (Seed and Clough, 1963; Seed and Goodman, 1964), and by Bustamante (1964) at the University of Mexico. In granular material the patterns of slip are similar to those shown in Fig. 4. The outline marked 1 shows the original slope, that marked 2 shows the deformation after a relatively small shock, and the outline marked 3 shows the deformation after major motions have occurred. Similar motions have been observed when the base of the model was tipped, to simulate a constant acceleration field.

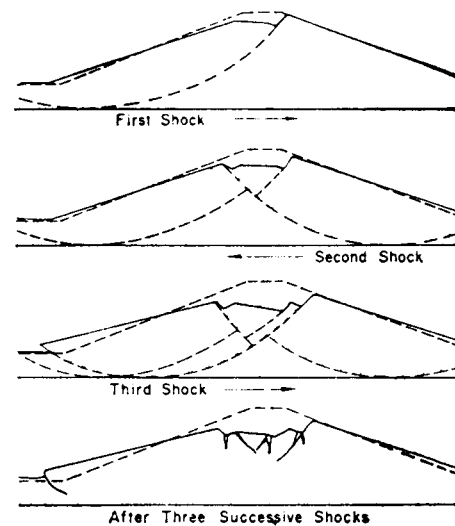
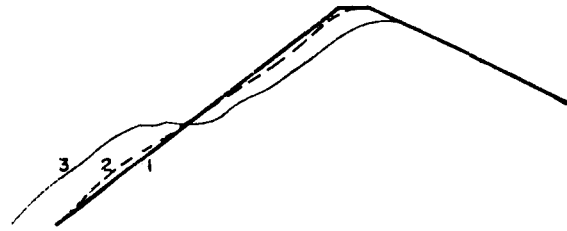


Fig. 3. Major deformation pattern (after Ambraseys)

Fig. 4. Patterns of slip in granular embankment



General concepts of behaviour

The types of motion of earth or rock-fill dams, or of an embankment, subjected to an earthquake can be considered to be of the following forms:

- (a) motion of a block or wedge or slice of the upstream or the downstream slope, generally out and downhill, as indicated in Fig. 5, arcs 'a' or 'b';
- (b) motion of the dam as a whole block, as in Fig. 5, line 'c';
- (c) relative motions in either the dam or the foundation, of such a nature as to cause fissures to open, generally vertical, caused either by relative shearing motions or tensile strains in the earth crust, corresponding to differential movements arising from the wave characteristics of the surface motion of the earth, or from stresses arising when parts of the mass of the dam and foundation are accelerated in one direction and other parts in other directions. This type of effect is illustrated in Fig. 5, by the fissures marked 'd' and 'e'.

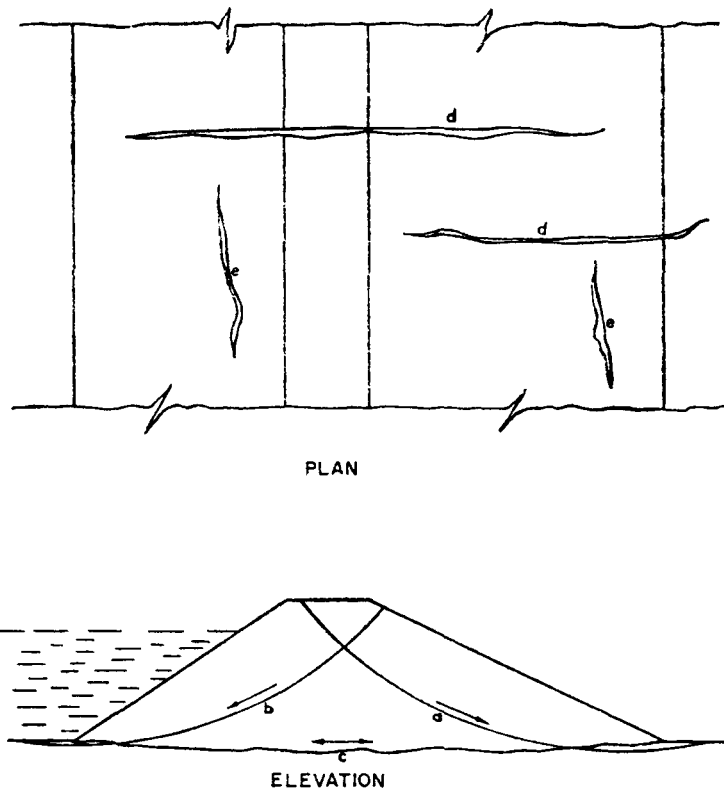
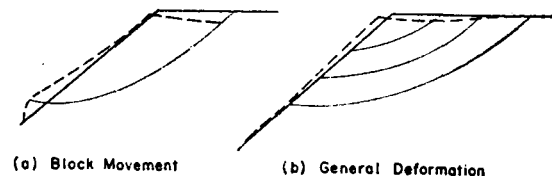


Fig. 5. Possible motions and deformations of an earth dam in an earthquake

Fig. 6. Comparison of two types of gross-motions



(a) Block Movement

(b) General Deformation

The characters of the motions in different types of materials are somewhat different. In general, for non-cohesive materials, and for cohesive materials where a well-defined plane of weakness can develop, the motion occurs along arcs or planes, and is similar to that assumed in the usual static analysis of stability of an embankment, as indicated in Fig. 6(a). However, in highly cohesive materials, the motion is more nearly general and elastic or nearly elastic in character, and a well defined sliding surface may not be formed. This is illustrated in Fig. 6(b). Where movements such as those in Fig. 6(a) occur, a relatively simple analysis can be used to compute the magnitude of dynamic motions produced by earthquake or other shocks. However, where motions such as those in Fig. 6(b) occur, the situation is much more complex, and the analysis cannot be made so readily or so accurately. For this case, the methods described herein can only be used as a crude approximation. In general, we shall devote our further attention in detail to situations of the type illustrated in Fig. 6(a).

Resistance to sliding motion

The resistance to earthquake shock motion of a block of soil or rock that slides on a surface is a function of the shearing resistance of the material under the conditions applicable in the earthquake. Although the magnitude of the resistance depends on the amount of displacement, the displacement necessary to mobilize the average 'yielding' resistance, normally considered in a stability analysis, is not large. For the purpose of simplifying the calculations the resistance which we shall use is measured by (and in fact equal and opposite to) that steady force acting at the centre of gravity of the sliding mass, in the direction in which the force can have its lowest value, which will just overcome the stabilizing forces and will barely keep the mass moving, after it has started to move, or after several pulsations (or reversals) of motion have occurred.

It is convenient to state this resistance in terms of a coefficient N multiplied by the weight of the sliding mass. Then the quantity Ng , where g is the acceleration of gravity, corresponds to that steady acceleration, acting in the proper direction, which would just overcome the resistance to sliding of the element, in the direction indicated, as defined above.

The resistance to sliding downhill, as on lines 'a' or 'b' of Fig. 5, is much lower than the resistance to sliding uphill on the same lines. The uphill resistance, without serious error in the calculations, may be taken as infinitely large. On the other hand, the type of motion characterized in line 'c' of Fig. 5 may have nearly the same resistance in either direction of relative motion of the mass compared with its foundation. This resistance may change as a function of displacement, and with reversal of displacement, but it is not generally greatly affected by the direction of motion other than in these ways.

We are not limited in the argument which follows by the use of a constant or steady-state value of N . We can consider the quantity n to be a coefficient, multiplied by the weight of the sliding material, which is used as a measure of the resistance to sliding, and which can be a function of the amount of deformation, or of time, or of any other parameters which it is desirable to consider. It is convenient to use the single parameter n as a measure of resistance, and to compare it with a single parameter a , as a measure of the acceleration driving the element. In other words, the quantity nW is a measure of the resistance as a generalized force, and the quantity aW , where the transient ground acceleration is ag , is a measure of the disturbing force as a generalized force, which varies with time. For further simplicity, we may use $n=N$, the steady-state resistance; and $a=A$, as a measure of the maximum ground acceleration, in developing approximate relationships.

Dynamic properties of soil and rock

In the determination of the value of sliding resistance, the dynamic properties of the material must be considered. This involves also the dynamic effects on the pore-water pres-

sure, and the effects of the motion or shearing strain itself on the volume change and the pore pressure change. In general, it is the undrained shearing resistance that is of importance. For highly permeable materials, the drained shearing resistance may be appropriate. Because of the fact that our primary concern is with the resistance of the soil or rock and its strength under dynamic conditions, although the dynamic resistance is used in a sort of static analysis, we shall refer to the resistance as the 'pseudostatic' resistance. In other words, the calculation of stability which leads to the determination of the steady-state sliding resistance N is made for properties of the material that are related to the dynamic situation.

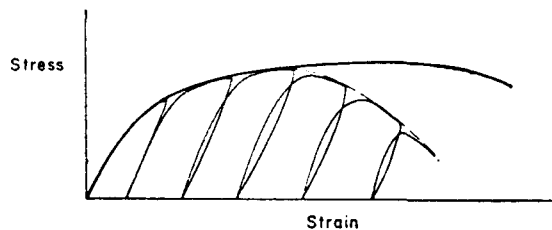


Fig. 7. Stress-strain relations for pulsating loads

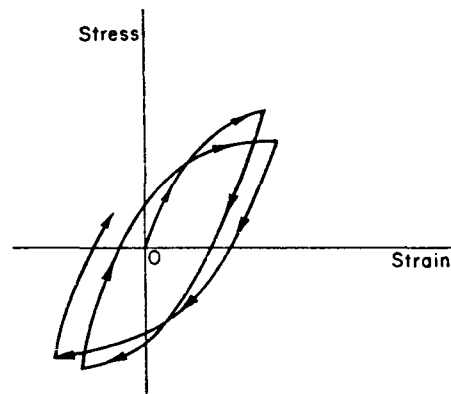


Fig. 8. Stress-strain relations for reversed loading

Effect of pulsation or reversal of stress

Because of the vibratory character of earthquake shock motions, the direction of stresses and of deformations may reverse, or at least pulsate with relatively rapid fluctuations. In Fig. 7 is shown the relation between stress and strain for a load applied and released successively. So long as the strains are relatively small, for many soils the bounding curve to the pulsating stress-strain relation is the same as for a single application of stress. However, for some soils after a certain strain has been reached the stress may drop from the original virgin curve, as indicated by the dashed line on the right-hand side of the figure. The situation shown, with a diminishing resistance beyond the maximum, is not untypical of many sensitive soils. Where the stress is reversed, or where motions can take place in both directions, the reduction may be even greater, and the change in shape of the stress-strain relationship is very marked, possibly even more than is indicated in Fig. 8. Under these conditions a change in the resistance function N , with number of reversals or with time, is necessary if one is to account properly for the behaviour of the embankment.

DYNAMIC RESPONSE THEORY

The dynamic response of a deformable body can be computed by the direct application of Newton's laws of motion. However, in many cases this application is extremely tedious or involved. Some basic concepts and principles are available to permit a relatively simple summary of the responses to earthquake motions to be developed. These are described in some detail by Blume *et al.* (1961).

The maximum responses of a simple system such as that shown in Fig. 9, consisting of a single mass connected by an elastic spring to a movable base, are best described by the so-called 'response spectrum', which is a plot against frequency of one of several measures of the

stress or deformation in the system. One of the most convenient ways of indicating the response for a variety of conditions is the tripartite logarithmic plot indicated in Fig. 10. The frequency f of the mass-spring system is the abscissa. For a particular motion of the base, the maximum strain in the spring or relative displacement of the mass with reference to the base D_f , is plotted along the axis sloping up to the left. A quantity from which the maximum energy absorbed in this system may be readily computed, the pseudo-velocity V_f is plotted as the ordinate, vertically, and the maximum acceleration of the mass A_f is plotted along the axis sloping up to the right. For damping other than zero, the quantity that is plotted is not exactly equal to the acceleration but is the 'pseudo-acceleration'. The relations among the pseudo-velocity, the pseudo-acceleration, and the relative displacement, are indicated in Fig. 10. The spectrum shown in Fig. 10 is plotted against frequency rather than against period, as are those in Blume *et al.* (1961).

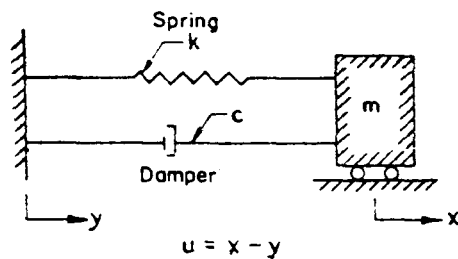


Fig. 9. System considered

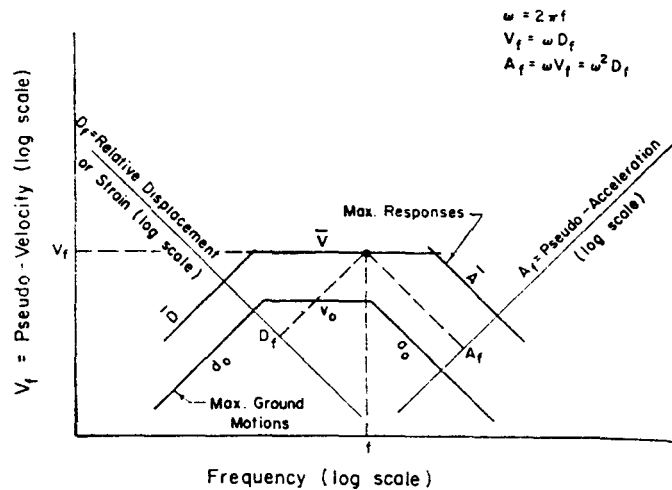


Fig. 10. Tripartite logarithmic response spectrum plot

For a base motion corresponding to the El Centro earthquake described in Fig. 1, the response spectra for several different values of the damping factor β , the proportion of critical damping for the system, are shown in Fig. 11.

The general characteristics of the response spectrum, as summarized from a great many studies of different input motions, are indicated in Fig. 10, where the quantities representing the maximum ground displacement d_0 the maximum ground velocity v_0 , and the maximum ground acceleration a_0 , are indicated schematically in the lower part of the figure by straight lines. Then the response spectrum has the shape shown roughly by the upper series of three straight lines parallel to the lines just described, fairing in at the high and low frequency ends to the ground motion lines. The bounds to the response spectrum for displacement \bar{D} , pseudo-velocity, \bar{V} , and pseudo-acceleration, \bar{A} , are for moderate amounts of damping, of the order of 5 to 10%, given by the relations

$$\bar{D} = d_0, \bar{V} = 1.5 v_0, \bar{A} = 2 a_0 \quad (1)$$

Multi-degree-of-freedom system

The simplicity inherent in the description of the response of a single-degree-of-freedom system is not possible in describing the multi-degree-of-freedom system. A typical multi-

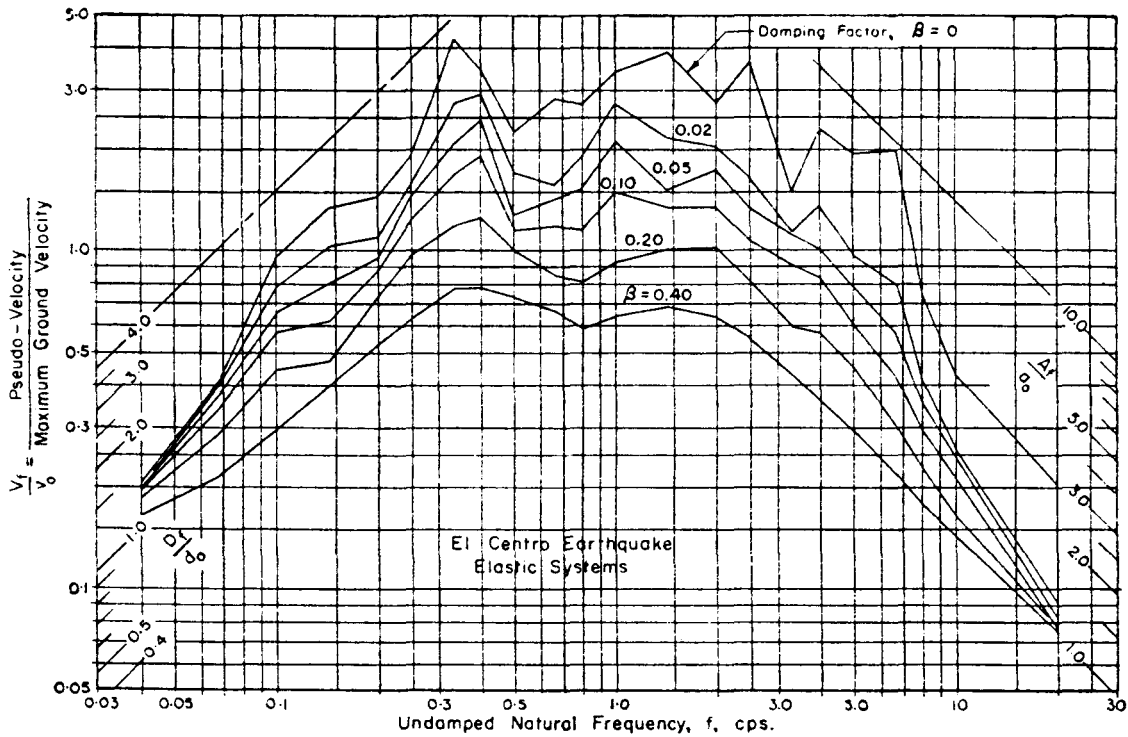


Fig. 11. Deformation spectra for elastic systems subjected to the El Centro quake

degree-of-freedom system having the characteristics of a so-called 'shear beam' is shown in Fig. 12. A shear beam is a system made up of masses which can move horizontally with respect to one another. This is not untypical of the type of motion that occurs in a dam or embankment. Sketches of the modes of vibration of a typical shear beam are also shown in Fig. 12. Each of these modes has a frequency, with the fundamental mode having the lowest frequency, the second mode the next higher frequency, etc.

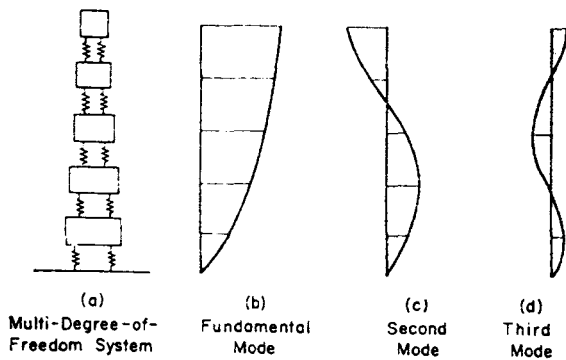


Fig. 12. Modes of vibration of shear beam

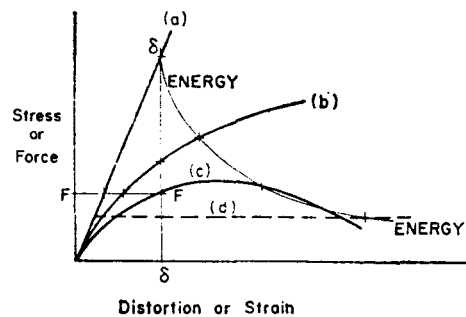


Fig. 13. Comparison of strains for equal displacement, energy, or force

The maximum strains or distortions in the springs, or the maximum stresses at any elevation, in a multi-degree-of-freedom system, can be stated in terms of the corresponding

quantities for a set of single-degree-of-freedom systems corresponding to each of the modes of vibration. For a particular system, a plot similar to that in Fig. 10 can be drawn, as a function of the fundamental frequency.

Inelastic relations between stress and strain

The spectra indicated previously in Figs 10 and 11, for an elastic system, correspond to elastic behaviour, which is represented by the upper inclined straight line (a) in Fig. 13. There are also shown in Fig. 13 several inelastic relations between stress and strain, or between force and deformation. For an inelastic relation between stress and strain, corresponding to one of the curved lines such as (b) or (c) in Fig. 13, the spectrum as described previously cannot be used directly. Curve (b) corresponds to a strain hardening situation, and curve (c) to an unstable one. An elasto-plastic resistance is indicated by the dashed line (d), in Fig. 13.

Spectrum bounds for the distortion or strain can be derived from Fig. 10, as indicated by the schematic plot in Fig. 14. Here three different regimes are considered. At the left, for a frequency f , the inelastic spectrum bound \bar{D}_1 is the same as \bar{D} . At the right, the inelastic spectrum gives the displacement bound \bar{A}_1 corresponding to the same force as the elastic spectrum bound \bar{A} . Where we have an elasto-plastic resistance, the bound \bar{A}_1 may be infinitely far above \bar{A} .

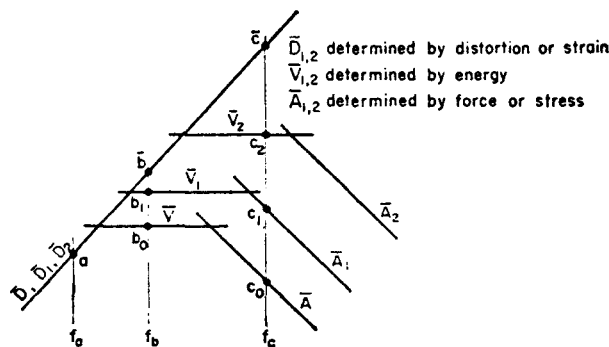


Fig. 14. Response spectrum displacement limits

In the intermediate range of frequencies, the spectrum bound \bar{V}_1 corresponds to the same total energy or area under the stress-strain curve as \bar{V} . These three conditions are illustrated in Fig. 13 by the lines marked FF at a constant force level, which intersects three of the curves but not the elasto-plastic curve; the line marked $\delta\delta$ which intersects all of the curves at the same displacement, and the line marked 'energy' which intersects all of the curves at such a point that the area up to that displacement is the same. In Fig. 14 two different levels of inelastic displacement are considered, corresponding to \bar{V}_1 and \bar{V}_2 , or \bar{A}_1 and \bar{A}_2 .

Results of a number of studies, still under way, indicate that in general the displacement for an inelastic system is bounded by the *least* of the following three quantities:

- (1) a displacement corresponding to the same force as for the elastic spectrum bound \bar{A} ;
- (2) a displacement corresponding to the same energy as for the elastic spectrum bound \bar{V} ;

(3) a displacement corresponding to the elastic spectrum bound \bar{D} . In other words, one can compute the displacement of the inelastic system by taking the smallest of the displacements that correspond to force, energy or maximum ground displacement, as indicated in Fig. 14.

For very large amounts of plastic deformation, the acceleration bound for the inelastic spectrum lies so high that the energy bound is the only one of importance other than the displacement bound. Consequently, for large amounts of plastic deformation, it is appropriate to consider the preservation of energy, and to neglect the preservation of force, provided the stipulation is made that the displacement does not exceed the maximum ground displacement. Actually the displacement bound that should be considered is the maximum elastic spectrum displacement which may be slightly greater than the maximum ground displacement.

The methods described heuristically in the foregoing can be used for the analysis of systems in which the resistance varies with displacement. However, when the resistance is essentially rigid-plastic, corresponding to no displacement until the yield point is reached, after which the displacement may have any value, the analysis is particularly simple. In the remainder of the analytical discussion herein, this is the type of resistance that is considered. We shall simplify the cases of motion to that of a rigid block of weight W , supported on a base which moves as a function of time. We are concerned with the motion u of the block relative to the base. This model will be used for all of the cases of sliding that we have defined for a dam or embankment.

The three important cases of sliding for a dam, on a circular sliding surface, on a plane sliding surface, or block sliding horizontally, are shown in Fig. 15. Of course, one might consider even more complex sliding surfaces if one can make the appropriate analysis for the resistance. For a general non-circular sliding surface the distortions within the sliding mass must be taken into account in arriving at the value of N for the entire mass.

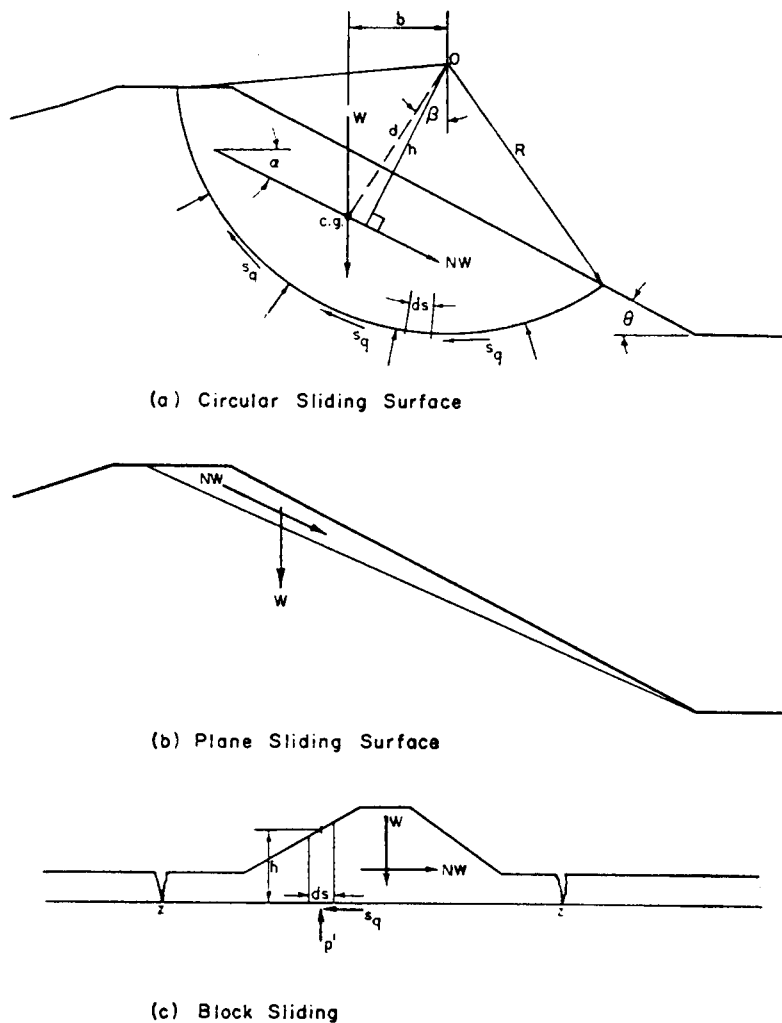


Fig. 15. Forces acting on a sliding element

Measures of dynamic resistance to sliding

In order that a dam or embankment have any dynamic resistance to sliding in an earthquake, it must have a margin of safety against static failure. Values of the static factor of

safety against sliding are determined by conventional analysis with no consideration of horizontal or inclined accelerations. Values of the dynamic factor of safety against sliding may be determined in a similar manner, but one must use in such an analysis the appropriate properties of the materials, which may involve considerably reduced shearing strengths owing to the dynamic effects on the pore pressures.

The method of analysis described here is a simplified approach permitting a rapid estimate to be made of the order of magnitude of the displacement or deformation in an earthquake.

Circular cylindrical sliding surface

Consider the sliding element of the dam shown in Fig. 15(a), where a circular arc of radius R defines the sliding surface. The weight of the element W has a lever arm b about the centre of rotation O . Consider a force NW which corresponds to a constant acceleration N times that of gravity, acting along the line shown making an angle α with the horizontal, which may be different from the angle θ of the surface slope of the element. For constant values of acceleration less than Ng , no sliding occurs, but for greater values, sliding of the element will take place. For any arbitrary acceleration $N'g$, we may define a dynamic factor of safety \overline{FS}' , which becomes unity if $N' = N$.

Now, when N' is taken as zero, the dynamic factor of safety, \overline{FS}' for this definition becomes equal to \overline{FS} , defined as the ratio of moment of the resisting forces on the sliding surface to the disturbing moment Wb . This dynamic factor of safety is defined differently from the usual static factor of safety. Drawdown seepage forces, etc. should be taken into account, also, in defining the factor of safety.

The shearing stresses τ for static conditions are to some extent indeterminate, but their total or their average value can be determined from the relation between the disturbing moment Wb and the restoring moment $R \sum \tau ds$, when $N' = 0$:

$$Wb = R \sum \tau ds. \quad \dots \dots \dots (2)$$

The moment of the resisting forces on the arc is $R \sum s_q ds$. Hence the dynamic factor of safety is:

$$\overline{FS} = R \sum s_q ds / R \sum \tau ds = \sum s_q ds / \sum \tau ds.$$

An approximate value of N which will just cause sliding is obtained by equating disturbing and resisting moments as follows:

$$Wb + NWh = R \sum s_q ds. \quad \dots \dots \dots (3)$$

Therefore, by subtracting equation (2) from equation (3), one obtains:

$$NWh = R \sum s_q ds - R \sum \tau ds.$$

On dividing this equation by equation (2), and multiplying through by b/h , one obtains the result:

$$N = \frac{b}{h} \left(\frac{\sum s_q ds}{\sum \tau ds} - 1 \right)$$

which can be written:

$$N = \frac{b}{h} \left(\frac{\bar{s}_q}{\bar{\tau}} - 1 \right) \quad \dots \dots \dots (4)$$

if \bar{s}_q and $\bar{\tau}$ are considered as average values. This expression is valid for any case such as steady seepage or after rapid drawdown, but the value of $\bar{\tau}$ and \bar{s}_q have to be determined separately for each case. Equation (4) can also be written as:

$$N = (\overline{FS} - 1) \frac{b}{h} \quad \dots \dots \dots (5)$$

Since the maximum value of h for a given sliding surface occurs when h equals d , the distance from O to the c.g. of the element, the minimum value of N occurs for a slope perpendicular to d , and one finds for this:

$$N = (\overline{FS} - 1) b/d = (\overline{FS} - 1) \sin \beta \quad (6)$$

where β is the angle between d and the vertical, and $\overline{FS} = \bar{s}_q/\bar{\tau}$.

For N horizontal, the result would be:

$$N = (\overline{FS} - 1) \tan \beta. \quad (7)$$

In the calculations, N is taken as inclined rather than horizontal, in order to be conservative, and also because the earth moves vertically as well as horizontally in an earthquake.

For soils which have nearly the same static and dynamic shear resistance, equation (5) may be approximated as:

$$N = (FS - 1) \sin \beta \quad (8)$$

in which FS is the conventional static safety factor. This equation will hold good for free-draining materials and can also be used for dilatant soils in which only small or negative pore pressures will be developed.

When N' is different from zero, the same type of derivation leads to the relation:

$$R \sum s_q ds = \overline{FS}' (Wb + N'Wh) \quad (9)$$

By equating equation (9) with (3), one obtains

$$N = N'(\overline{FS}') + (\overline{FS}' - 1)b/h \quad (10)$$

which reduces to equation (5) when $N' = 0$ and $\overline{FS}' = \overline{FS}$. Note, however, that equation (10) is valid even if \overline{FS}' is less than unity.

Because we are concerned with the minimum value of N for all of the possible sliding surfaces, and because the minimum value does not necessarily occur for the sliding surface for which \overline{FS} has a minimum value, use of equation (10), involving a trial value of N' , will lead to more accurate results than use of equations (4) and (5) in which no assumed value of accelerating force is included in the basic computation. The most accurate results are obtained when \overline{FS}' is nearly equal to unity. The poorest results are obtained from the static factor of safety computed for the case of zero lateral force.

For completeness, the relations corresponding to (6) and (7) are given, for the case in which N' is different from zero:

for N perpendicular to d ,

$$N = N'(\overline{FS}') + (\overline{FS}' - 1) \sin \beta \quad (11)$$

for N horizontal,

$$N = N'(\overline{FS}') + (\overline{FS}' - 1) \tan \beta. \quad (12)$$

Block sliding

For block sliding of the entire dam along a surface such as $z-z$ in Fig. 15(c), between fissures or embankment surfaces, the relationships to be used involve summation of forces rather than summation of moments. For the static condition of equilibrium it can be assumed without significant error that the average static shear stress along the horizontal surface is zero and the only disturbing force is thus the effect of the horizontal constant acceleration. The maximum shear strength which can be mobilized for earthquake conditions is the undrained shear strength s_q .

Since the sum of the disturbing forces NW per unit of width of dam must equal the sum of the shearing resistances per unit of width,

$$NW = \sum s_q ds \quad (13)$$

where ds is the length of the element on which the resistances act. Hence N is the ratio of the total horizontal resistance to the weight of the dam.

The effective overburden pressure p' is equal to the weight of the material above minus the pore pressure; hence

$$p' = \gamma h - u_p \quad (14)$$

where γ is the bulk density of the soil, h the height of the element, and u_p the pore pressure. However,

$$W = \sum \gamma h ds. \quad (15)$$

In general the undrained shear strength is a function of the effective overburden pressure. For the special case of a normally consolidated soil the ratio of s_q to p' is a constant.

From equations (13) and (14), for a normally consolidated soil, one can determine N as follows:

$$\begin{aligned} N &= \frac{1}{W} \sum s_q ds = \frac{1}{W} \sum \frac{s_q}{p'} p' ds \\ &= \frac{1}{W} \left(\frac{s_q}{p'} \right) \sum p' ds \\ &= \frac{s_q}{p'} \frac{\sum \gamma h ds - \sum u_p ds}{\sum \gamma h ds} \\ &= \frac{s_q}{p'} \left(1 - \frac{\sum u_p ds}{\sum \gamma h ds} \right) \quad (16) \end{aligned}$$

This equation can be written as

$$N = \frac{s_q}{p'} (1 - r_u) \quad (17)$$

where

$$r_u = \frac{\sum u_p ds}{\sum \gamma h ds} \quad (18)$$

The quantity r_u is in general not a constant and has to be determined in each case as an average value. It should be taken at a conservative value to provide for pore pressure increase in an earthquake.

Plane sliding surface

For cohesionless and free-draining materials, with a plane sliding surface, as in Fig. 15(b), it is found that the most dangerous sliding plane is the upper slope, making an angle θ with the horizontal. Under these conditions, for a material with an angle of internal friction ϕ when sliding is taking place, the value of factor of safety against sliding is

$$\overline{FS} = \frac{\tan \phi}{\tan \theta} \quad (19)$$

It can be determined under these conditions that the minimum value of N is

$$N = (\overline{FS} - 1) \sin \theta. \quad (20)$$

Sliding of a rigid-plastic mass

A simple derivation for a rigid-plastic resistance is developed to give a quick estimate of the magnitude of the motions to be expected in a sliding wedge of rock or earth in a dam,

when it is subjected to the influence of dynamic forces from an earthquake. The calculation is based on the assumptions that the whole moving mass moves as a single rigid body with resistance mobilized along the sliding surface.

Consider the rigid body having a weight W , and a mass M , shown in Fig. 16, having a motion x . The motion of the ground on which the mass rests is designated by $y(t)$, where y is a function of time t . The relative motion of the mass, compared with the ground, is designated by u , where

$$u = x - y. \quad \dots \dots \dots (21)$$

The resistance to motion is accounted for by a shearing resistance, which can be expressed as being proportional to the weight W , of magnitude NW . This corresponds to an acceleration of the ground of magnitude Ng that would cause the mass to move relative to the ground.

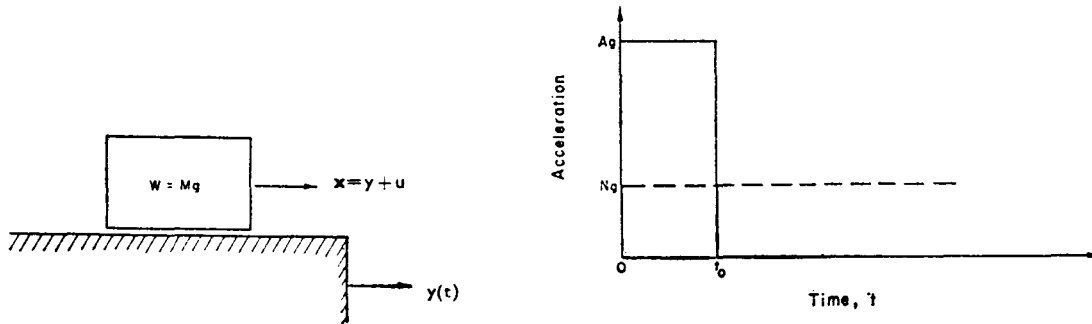


Fig. 16. Rigid block on a moving support Fig. 17. Rectangular block acceleration pulse

In Fig. 17, the accelerating forces acting on the mass M are shown. The acceleration considered is a single pulse of magnitude Ag , lasting for a time interval t_0 . It would be possible to consider a sinusoidal pulse, but this complicates the expressions unnecessarily. The resisting acceleration, Ng , is shown by the dashed line in Fig. 17. The accelerating force lasts only for the short time interval indicated, but the decelerating force lasts until the direction of motion changes.

In Fig. 18, the velocities are shown as a function of time for both the accelerating force and the resisting force. The maximum velocity for the accelerating force has a magnitude V given by the expression

$$V = Agt_0.$$

After the time t_0 is reached, the velocity due to the accelerating force remains constant. The velocity due to the resisting acceleration has the magnitude $Ng t$. At a time t_m , the two

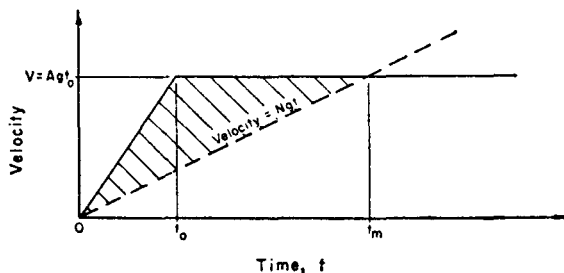


Fig. 18. Velocity response to rectangular block acceleration

*

velocities are equal and the net velocity becomes zero, or the body comes to rest relative to the ground. The formulation for t_m is obtained by equating the velocity V to the quantity Ngt , giving as a result the expression

$$t_m = \frac{V}{Ng} \quad \dots \dots \dots (22)$$

The maximum displacement of the mass relative to the ground u_m is obtained by computing the shaded triangular area in Fig. 18. The calculation is made as follows:

$$u_m = \frac{1}{2} Vt_m - \frac{1}{2} Vt_0$$

or

$$u_m = \frac{1}{2} \frac{V^2}{Ng} - \frac{1}{2} \frac{V^2}{Ag}$$

whence

$$u_m = \frac{V^2}{2gN} \left(1 - \frac{N}{A} \right) \quad \dots \dots \dots (23)$$

The acceleration pulse shown in Fig. 17 corresponds to an infinite ground displacement. The actual situation corresponds to a number of pulses in random order, some positive and some negative. If we consider a second pulse, of a negative magnitude, to bring the velocity to zero even without the resisting force, it can be shown that the net displacement with the resistance generally cannot exceed that which would occur without resistance.

The result given in equation (23) generally overestimates the relative displacement for an earthquake because it does not take into account the pulses in opposite directions. However, it should give a reasonable order of magnitude for the relative displacement. It does indicate that the displacement is proportional to the square of the maximum ground velocity.

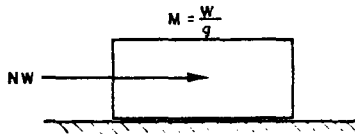


Fig. 19. Mass sliding under constant force

The result derived above is applicable also for a group of pulses when the resistance in either direction of possible motion is the same. For a situation in which the body has a resistance to motion greater in one direction than in another, one must take into account the cumulative effect of the displacements. A simple example where this must be considered would be found if Fig. 16 were rotated clockwise, as in Fig. 19, so that the body has a tendency to slide downhill. In this situation, ground motions in the direction of the downward slope tend to move the mass downhill, but ground motions in the upward direction along the slope leave the mass without relative additional motion except where these are extremely large in magnitude. One may consider that this case is applicable to the dam.

Energy concepts

Another interpretation of equation (23) may be useful. Consider the situation where the sliding mass of material acquires somehow a velocity V relative to the ground or foundation. This velocity may be imparted by motion of the foundation and that part of the dam which presses against the sliding wedge, but in any event, it is the velocity of the mass, relative to the ground or foundation on which it slides, that is needed. This is not necessarily the same as the maximum ground velocity.

The kinetic energy of the moving mass, with this velocity, then is given by the relation $WV^2/2g$. The resistance to sliding is given by the quantity NW and the energy absorbed in the sliding resistance is NW times the displacement. It follows, therefore, that the displacement required to absorb the kinetic energy is given by the first term on the right of equation

(23), namely, $V^2/2gN$. The solidus term takes into account to some extent the manner by which the mass acquires its velocity.

We may extend the energy concept to other types of force displacement relationships such as shown in Fig. 13 or even more complex relations. It is of particular interest to compute the relative displacement for an elasto-plastic resistance as compared with a purely elastic resistance. To do so one can compare the two types of resistance shown in Fig. 20 and note that areas 1 plus 2 plus 3, for the elastic resistance energy, must be equal to areas 1 plus 2 plus 4 for the elasto-plastic resistance energy.

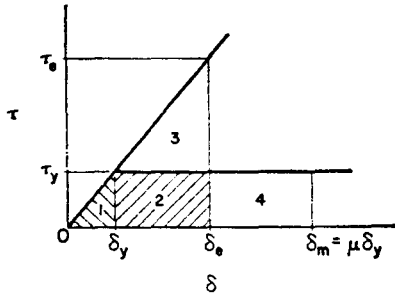


Fig. 20. Conventionalized elastic and elasto-plastic stress-strain diagrams

From this relation, taking note of the fact that

$$\tau_e/\tau_y = \delta_e/\delta_y \quad \dots \dots \dots (24)$$

one derives the result

$$\frac{\delta_y}{\delta_e} = \frac{1}{\sqrt{(2\mu - 1)}} \quad \dots \dots \dots (25)$$

$$\frac{\delta_m}{\delta_e} = \frac{\mu}{\sqrt{(2\mu - 1)}} \quad \dots \dots \dots (26)$$

In these equations, as indicated in Fig. 20, μ is the ratio of the maximum total displacement to the elastic component of displacement. For purely elastic conditions, $\mu = 1$.

For a rigid-plastic resistance, the energy absorbed at a maximum displacement δ_{mp} is $\delta_{mp}\tau_y$, whereas for the elasto-plastic resistance, the energy absorbed at a maximum displacement δ_m is

$$\delta_m\tau_y(1 - 1/2\mu) \quad \dots \dots \dots (27)$$

Then, for the same energy the relative value of maximum displacement is:

$$\delta_m/\delta_{mp} = 1/(1 - 1/2\mu) \quad \dots \dots \dots (28)$$

The maximum value of this ratio is 2.0. For even moderate values of μ , however, the ratio is close to unity.

Number of effective shocks in an earthquake

Since the sliding of either the upstream or downstream slopes in an earthquake can only occur downhill, if sliding occurs at all there will be a lowering of the crest of the dam caused by a cumulative slip on both slopes, always downhill. The net motions of either slope can be determined only after assumptions are made of: (a) the input motions of the ground; (b) the effective number of spikes of accelerations similar to one of the single spikes considered in Fig. 17 and in the derivation of equation (23); and (c) the resistance of the sliding elements.

The effective number of pulses in an actual earthquake can be determined by an analysis of the response of simple systems to the earthquake motion. This has been done for four of the West Coast United States earthquakes for which strong motion records are available. These four are described in Table 2.

For convenience in interpreting the results the four earthquakes were normalized to a

maximum acceleration of 0.5 g and a maximum ground velocity of 30 in/sec, by modifying the acceleration and time scales appropriately. Normalized displacements are given in Table 2 for each of the earthquakes.

The analysis was made on the high-speed digital computer at the University of Illinois Digital Computer Laboratory for the normalized accelerograms for the earthquakes. The results are plotted in Fig. 21 for a symmetrical resistance function, in which the resistance is rigid-plastic but having the same value in each direction of motion. It appears from Fig. 21 that the results are bounded by the expression for energy $V^2/2gN$, and also by the maximum displacement y_0 of the ground. Where the value of N approaches the maximum earthquake acceleration, there is a reduction in response from that given by the energy expression, as shown by the equation in the lower right-hand part of the figure, in which the correction factor derived in equation (23) appears to be applicable. Apparently this is important only beyond a value of N/A greater than 0.5.

Table 2
Earthquakes considered in analysis

Earthquake	Maximum ground motions				Normalized * displacement : in.
	Acceleration g	Velocity in/sec	Displacement : in.	Duration : sec.	
1. Ferndale, 21 Dec., 1954, N45E —	0.205	10.5	8.26	20	27.7
2. Eureka, 21 Dec., 1954, S11W —	0.178	12.5	10.0	26	51.2
3. Olympia, 13 April, 1949, S40W —	0.210	8.28	9.29	26	20.5
4. El Centro, 18 May, 1940, N-S —	0.32	13.7	8.28	30	25.5

* Normalized to give acceleration = 0.50 g and velocity = 30 in/sec.

Unsymmetrical resistance

When the motion takes place with a different resistance in the two directions, corresponding to a mass sliding downhill, as in Fig. 19, the displacement is increased greatly. Although there is a smooth transition between the value given in Fig. 21 and the greatly increased value corresponding to completely unsymmetrical resistance, the results approach very rapidly those corresponding to an infinite resistance in one direction. The results of calculations for this case are summarized on Fig. 22. A conservative upper bound to the computed values of displacement is given by the relation

$$\frac{V^2}{2gN} \cdot \frac{A}{N} \dots \dots \dots (29)$$

This appears to indicate that the effective number of pulses in the earthquakes considered is equal to the quantity A/N . If one multiplies equation (23) by A/N , one obtains a bound which is somewhat closer in the region where N/A is larger than about 0.5, but is not conservative for somewhat smaller values. For very low values of N/A , the number of effective pulses in the earthquake apparently is no greater than 6 for the earthquakes considered. This, however, may be considered a peculiarity of the particular earthquakes examined. It would be undoubtedly true that for earthquakes lasting for a longer time the number of effective pulses would be greater. Preliminary studies indicate a relative value for longer durations roughly proportional to the square root of the duration.

Comparisons with model tests

The theoretical procedures described herein have been applied to tests of a model of a rock-fill dam, described by Davis *et al.* (1960). The scale of the model was 1/300 of the prototype. The dynamic tests of the model were made by striking a shaking table with a heavy pendulum. A rebound of the pendulum caused a second input at a lower acceleration. Hence, data could be obtained both for the initial strike and for the first rebound.

On the whole, the model tests indicated a fair agreement with the calculations, for comparable conditions. Within the accuracy of the records obtained in the tests, the measured motions were in fairly good agreement with the results computed by means of equation (23) and Fig. 21.

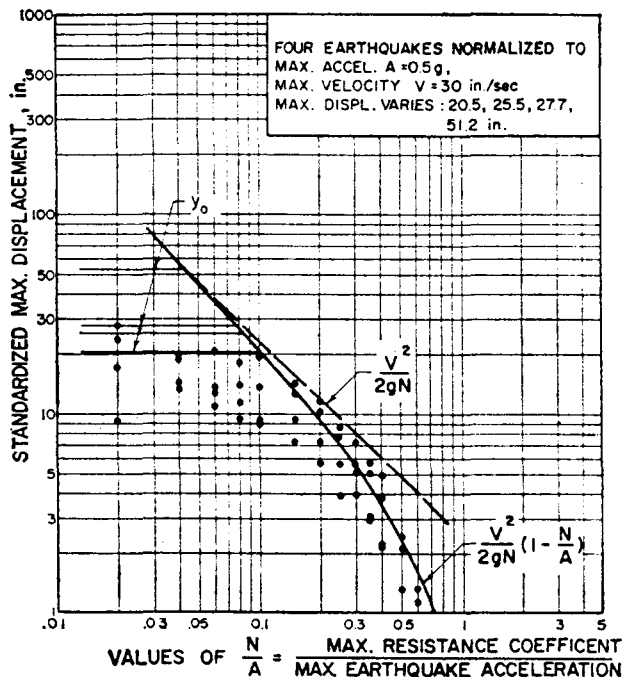


Fig. 21. Standardized displacement for normalized earthquakes (symmetrical resistance)

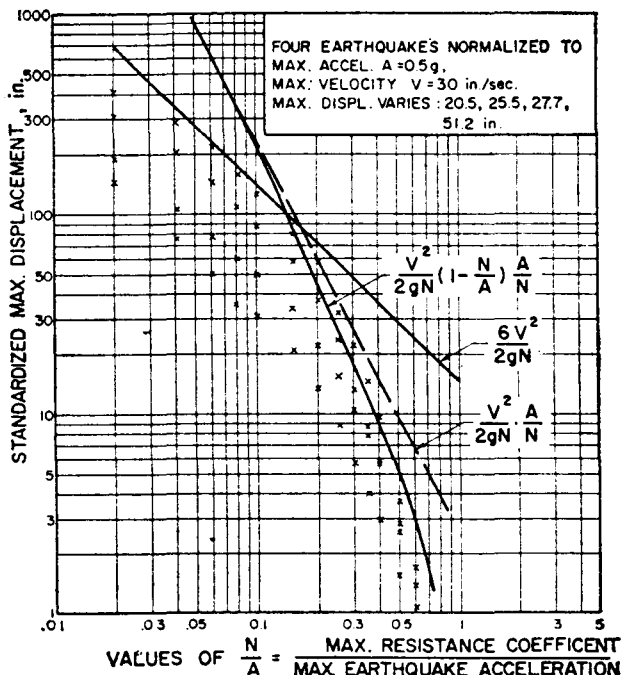


Fig. 22. Standardized displacement for normalized earthquakes (unsymmetrical resistance)

Comments and conclusions

For the maximum probable earthquake in California, which is a reasonable maximum earthquake for many other areas of the world, Fig. 22 may be used directly to obtain a measure of the maximum displacement for unsymmetrical sliding. If the maximum resistance coefficient is about 0.16, or about one-third the maximum earthquake acceleration, the net displacement will be about 1 ft. If the maximum resistance coefficient N is about 0.20 times the maximum earthquake acceleration, or N equals 0.1, the maximum displacement is about 5 ft. The maximum displacement increases rapidly as N decreases. Values of N in the range of 0.1 to 0.15 are not uncommon for earth dams designed for earthquake resistance. Of course, a design with a somewhat smaller value of N would have a smaller displacement if the earthquake were less intense. For an earthquake with a maximum acceleration of 0.25 g , and a maximum velocity of 15 in/sec, the displacements computed would be one-fourth those quoted, if the value of the ratio of N to A were the same. In other words, for the same relative value of resistance coefficient, the displacement varies as the square of the ground velocity. This displacement lowers the crest of the dam.

Another factor that must be considered in the design of a dam is overtopping caused by wave action. Such wave action can be initiated by slumping of the dam but it is more likely to be caused by slides from unstable natural areas in the reservoir. Slides of this sort caused failure of the Vaiont Reservoir in Italy; the dam itself did not fail structurally.

Faulting or sudden settlement may also cause wave action. Such a settlement that took place very rapidly at the dam itself caused the large waves at Hegben Lake (Anon, 1964).

Damage and serious danger may occur if an earth dam is in the neighbourhood of the fault where the fault may intersect the dam and cause a break or fissure through it. When an earth dam is founded on rock or a firm soil stratum, and is made of well compacted material, the danger in an earthquake may be minimal. However, if the dam is located above a stratum which can liquefy or lose its shearing strength an earthquake may cause a failure by spreading of the dam even though the dam itself may have an ample factor of safety with respect to failure in the material of the dam itself. In general, sites underlain by strata which may suffer a major reduction in shearing resistance should be considered unsuitable unless the sensitive strata can be removed.

Open cracks across the impervious section of an earth dam can form as a result of differential settlement of the base of the dam, or as a result of differential movements within the body of the dam, as well as a result of earthquakes. Transverse cracks may develop even in earthquake-free regions. Because an earthquake with even moderately large motions may introduce fissures and cracking which may lead to piping, provisions should be made to induce self-healing of open cracks. Dr Terzaghi has suggested that such provisions might consist of establishing the impervious section of the dam, or core, between two layers of properly graded cohesionless material. These layers should be only moderately compacted, and in each layer the grain size should increase with increasing distance from the contact surface with the impervious core. A method of this sort was adopted by Terzaghi for Mission Dam.

In arriving at the design of a dam which is required to resist earthquake motions one may either adopt a procedure in which the static resistance of the dam is greater than the maximum earthquake acceleration likely to be encountered, or one can make the dam capable of resisting displacements corresponding to those computed by the methods described herein. The former approach gives a misleading sense of security because of the fact that there are small displacements that take place even when N equals A or exceeds it, owing to the fact that resisting forces are developed even by elastic displacements less than the yield point. Hence the motions can be of such a nature as to cause a reduction in shearing stress and a consequent amplified displacement.

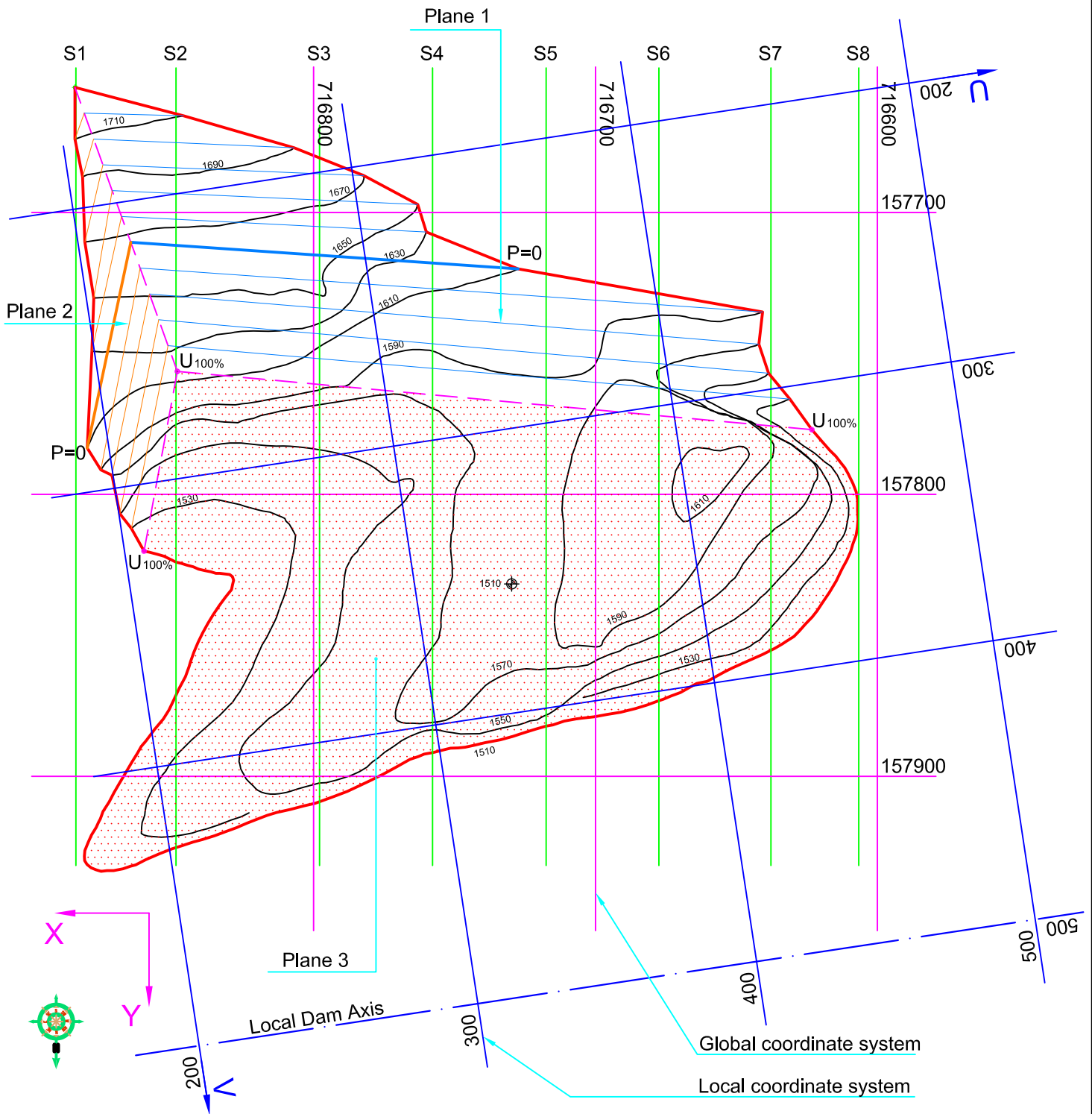
It may be required, to avoid permanent displacements altogether, that the value of N be well in excess of the maximum earthquake acceleration. This appears to be too uneconomical a procedure for general use.

For years engineers were convinced that foundations did not settle if they were adequately designed. The methods introduced by Terzaghi concentrated attention on methods by which the settlements could be determined and subsequent measurements indicated that almost all foundations settle. One might expect that the same situation applies to earth and rock-fill dams and embankments. When one concentrates attention only on the strengths and neglects the displacements or motions, one is not likely to realize that these motions will take place. It is desirable to try to keep them at a level such that they can cause no danger.

REFERENCES

- AMBRASEYS, N. N., 1958. 'The seismic stability of earth dams.' *Ph.D. dissertation, University of London.*
AMBRASEYS, N. N., 1960. 'On the seismic behaviour of earth dams.' *Proc. 2nd World Conf. on Earthquake Engng, Tokyo*, vol. 1, p. 331.
AMBRASEYS, N. N., 1962. 'The seismic stability analysis of earth dams.' *Second Symposium on Earthquake Engineering, University of Roorkee, Roorkee, India.*

- ANON, 1964. 'The Hegben Lake, Montana, earthquake of August 17, 1959.' Geological Survey Professional Paper 435. U.S. Government Printing Office, Washington, D.C.
- BLUME, J. A., N. M. NEWMARK, and L. H. CORNING, 1961. 'Design of multi-storey reinforced concrete buildings for earthquake motions.' *Portland Cement Association, Chicago.*
- BUSTAMANTE, J. I., 1964. 'Dynamic behaviour of non-cohesive embankment models.' *Ph.D. dissertation, University of Illinois.*
- CLOUGH, R. W. and D. PIRTZ, 1958. 'Earthquake resistance of rock-fill dams.' *Trans. Amer. Soc. civ. Engrs.*, 123: 792-810.
- DAVIS, R. E. and associates, 1960. 'Model study of stability of Portage Mountain Dam during earthquakes. Berkeley, California, November 1960. (Report to International Power and Engineering Consultants Ltd, Vancouver, Canada.)
- SEED, H. B. and R. W. CLOUGH, 1963. 'Earthquake resistance of sloping core dams.' *Proc. Amer. Soc. civ. Engrs.*, 89 (SM1): 209-242.
- SEED, H. B. and R. E. GOODMAN, 1964. 'Earthquake stability of slopes of cohesionless soils.' *Proc. Amer. Soc. civ. Engrs.*, 90 (SM6): 43-73.
- SHANNON and WILSON, Inc., 1964. Report on Anchorage area soil studies, Alaska, to U.S. Army Engineer District at Anchorage, Alaska, 28 August, 1964.



COORDINATE TRANSFORMATIONS

From Global To Local

$$V = (X - X_0) \cos \phi + (Y - Y_0) \sin \phi$$

$$U = (Y - Y_0) \cos \phi - (X - X_0) \sin \phi$$

From Local To Global

$$Y = U \cos \phi + V \sin \phi + Y_0$$

$$X = V \cos \phi - U \sin \phi + X_0$$

Local System Definition

$$X_0 = 717'113.033$$

$$Y_0 = 157'531.036$$

$$\phi = 109.54088 \text{ g } (\approx 98.5868^\circ)$$

NOTES:

1. Uplift pressures vary linearly from the intersection of planes and the out-cropping topography.
2. Uplift pressure is zero at the limit point of the out-cropping topography.
3. Reservoir elevation = 1610.20 m.a.s.l.
4. Intersection of Plane 1-3 uplift pressure ($U_{100\%}$) is 100% of hydrostatic head
5. Intersection of Plane 2-3 uplift pressure ($U_{100\%}$) is 100% of hydrostatic head

WEDGE ARRANGEMENT

01.04.2009	m	1 : 2000
Date:	Units:	Scale:

Theme C “Stability of a dam abutment including seismic loading” Contribution by Coyne et Bellier

Presented by C. Vibert, O.J. Gastebled & J.S. Garbuio

Coyne & Bellier Consulting Engineers, Tractebel Engineering, Gennevilliers, France

ABSTRACT:

The problem statement of theme C consists of the static and seismic stability assessment of a multi-faced rock "wedge" of an arch dam abutment. The exercise is based on the actual configuration of an existing double curvature arch dam located in Switzerland (Luzzone dam). In the problem statement, the dam and foundation rock geometry is expressed in finite element format. This model has been imported and validated in the finite element software midasGTS. Linear static analysis of the dam and the foundation rock (reservoir not modelled) has been carried out under self-weight, hydrostatic pressure, Westergaard hydrodynamic pressure and dam inertia forces when submitted to 1g unit acceleration in each direction. The resulting interface forces transferred from the abutment to the rock wedge have been post-processed for each considered load case. Uplift pressures (joint water pressures) have been independently assessed by surface integration. The assessed static forces acting on the rock wedge have been summed up and the static stability has been assessed using the Londe method. Three stochastically independent ground acceleration time-histories were provided in the problem statement to describe the earthquake to be considered when checking seismic stability of the wedge. Combinations of peak ground acceleration values have been used to determine the worst-case contribution of hydrodynamic pressures and dam inertia forces acting on the wedge during the earthquake. Considering that these dynamic contributions are small compared to the stabilizing effect of the wedge weight (<10%) and compared to the inertia forces of the wedge (<15%), it was chosen to keep these contribution constant and equal to their envelop values over the full earthquake time history. The uplift pressures were also assumed to remain constant and equal to their static values over the time history. Therefore, in the adopted approach, the inertia forces of the rock wedge were the sole forces that were instantaneously varied over time. The dynamic stability was assessed at each time step according to the Londe method. It was checked that the wedge was only submitted to sliding on its horizontal plane (base), while the two other planes remained open. The sliding displacements (sliding path) of the wedge were derived using the Newmark method. If the peak ground accelerations provided in the problem statement are assumed to apply locally to the wedge, no sliding is predicted and a minimum safety factor of 1.48 is found. If the effect of the site topography is assumed to lead to an amplification of the cross-valley acceleration by a factor 3, the adopted approach predicts a minimum safety factor of 0.76 and a total sliding displacement of 2.5mm.

Introduction

3D numerical analysis based on non-linear continuum mechanics is not commonly used in the current engineering practice to investigate the static and seismic stability of the abutment of arch dams. Such analyses are still costly to perform and it can be argued that the accuracy gained in the solution of the physical problem is not necessarily relevant in the view of the uncertainty with which certain input parameters are known. That is the reason why other approaches based on simplification assumptions are commonly preferred. Such methods have the advantage of allowing variation analysis at low cost to assess the relative weight of various parameters.

The objectives of the current benchmark are multiple:

- compare the performance of the various solution methods now available to the engineer,
- compare the capabilities of the various numerical analysis software available to the engineer,
- show the relevance and the influence of various physical phenomena,
- show the relevance and the influence of various modelling assumptions,
- assess the “human factor” in the spread of the presented solutions,
- establish the current state-of-the-art,
- conclude with a number of recommendations regarding the solution method, the modelling assumptions, the required capabilities of the numerical tool etc...

This contribution aims at providing a solution using only tools which are steadily available in modern engineering firms: 3D solid linear static finite element analysis and standard spreadsheet application. Such a solution can constitute a basis against which the added value brought by the use of more advanced non-linear dynamic continuum mechanics might be assessed. The proposed approach has the advantage of clearly identifying the relative weight of the various parameters of the problem.

Evaluation of Static Forces

The finite element model provided in the problem statement has been imported in the software midasGTS, the 2D and 3D finite element software for geotechnical and tunnel analysis, distributed by TNO DIANA BV, the Netherlands. After fixing the connectivity between the dam and the foundation in the region of the dam toe, deleting the reservoir elements and adopting the concrete and rock properties provided in table 2.1 of the subject, the model has been run in linear static analysis under the following independent load cases:

- self-weight ($g = 9.81 \text{ m/s}^2$)
- hydrostatic water pressure with a reservoir level at 1610.20 m.a.s.l. (triangular pressure distribution over depth).

The finite element model, the orientation of the global axis system and the relative positioning of the rock wedge are shown in Figures 1 to 3. Displacement results for both load cases are shown in Figures 4 and 5.

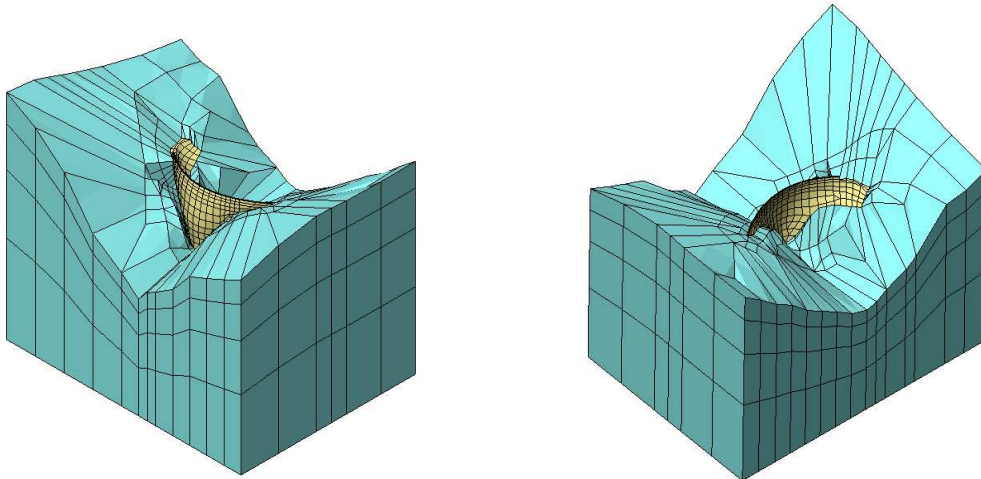


Figure 1 : Birdseye views of the finite element mesh of the dam and rock foundation

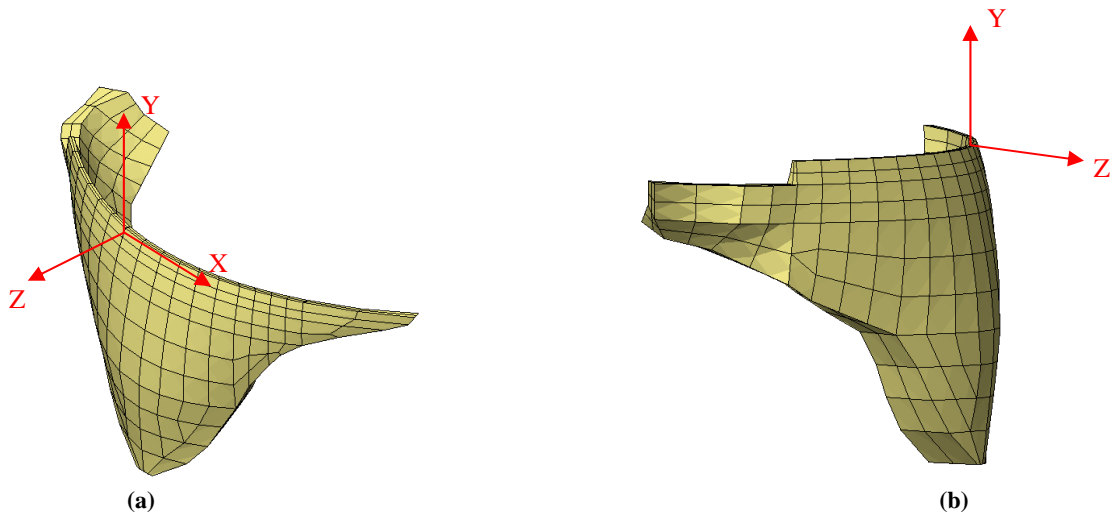


Figure 2 : 3D views of the finite element mesh of the dam, from upstream (a) and from the left bank (b)

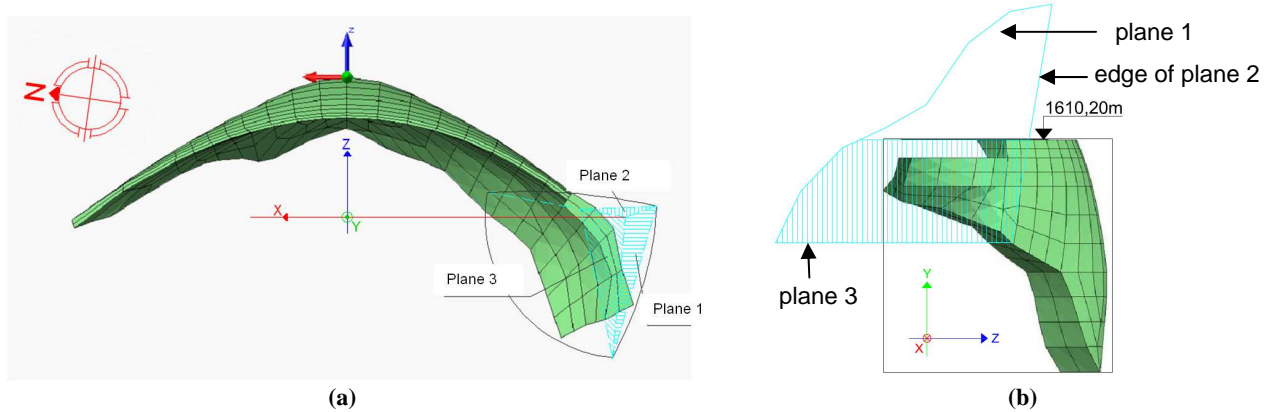


Figure 3 : Positioning of the north and the rock wedge with respect to the dam. Top view (a) and side view (b).

For each load case, the total force transferred from the left abutment to the rock wedge above 1510 m.a.s.l. has been computed by vector summation of all nodal internal forces at the interface between the abutment and the rock. The obtained static forces are presented in Table 1.

Table 1 : Finite element static results

FE results Static forces	F _X	F _Y	F _Z
	[MN]	[MN]	[MN]
Hydrostatic pressure (Q _{hs})	-3236	-698	-3237
Dam self-weight (W _d)	858.0	-3305.8	739.7

Due to load redistribution in the dam body, the vertical component of the computed dam self-weight force, F_Y, is smaller than the weight of the dam volume above the rock wedge (abutment volume = 150 000 m³, abutment weight = 3800 MN). The finite element model does not take into account the fact that equilibrium under dam self-weight is actually achieved before grouting of the joints. Since the problem statement does not give any details on the dam joint locations and the dam construction sequence, the lower value computed by finite element is adopted, which is conservative with respect to rock wedge stability.

The volume of the rock wedge is given equal to 1.92x10⁶ m³. This leads to a large self-weight force for the wedge, equal to W_{ws} = 49920 MN. This is the main factor contributing to the stability of the rock wedge.

The joint water pressure forces acting on the faces of the rock wedge, i.e. the uplift pressures, are assessed using numerical integration based on Figure 6. The in-plane geometry of the wedge faces is deduced from the natural terrain topography provided in appendix 12.a. Water pressures are assumed to vary linearly with depth. The water height distribution is determined based on the following assumptions:

- water height is equal to reservoir level in areas 1 of plane 1, 2 and 3;
 - water height is equal to the local natural terrain level in the area 2 of plane 1;
 - water height decreases linearly from reservoir level to natural terrain level in the areas 2, 3 and 4 of plane 3.
- The linear distributions follow locally the direction of the blue lines shown in Figure 6.

These assumptions result in the values of “uplift” forces presented in Table 2.

Table 2 : Uplift forces obtained by surface integration

Surface integration	U _{P1}	U _{P2}	U _{P3}
	[MN]	[MN]	[MN]
Uplift forces	10406	3226	14938

Considering the orientation of the wedge faces, the uplift pressures can be expressed in the global coordinate system, see Table 3.

Table 3 : Uplift forces expressed in XYZ system

Uplift pressures	F _X	F _Y	F _Z
	[MN]	[MN]	[MN]
U _{P1}	9167	4397	2215
U _{P2}	997	780	-2966
U _{P3}	0	14938	0
ΣU _{Pi}	10165	20116.2	751

The summation of all forces acting on the wedge (self-weight, hydrostatic force and uplift pressures) results in the values presented in Table 4.

Table 4 : Total static force acting on the wedge

Static forces	F _X	F _Y	F _Z
	[MN]	[MN]	[MN]
Total force	7787	-33807	-3249

Static Stability

Using the Londe method, see ref. [1] and [2], it can be checked that, for the considered wedge and the obtained static forces, the likely mechanism corresponds to sliding on the base face (plane 3), opening of the back face (plane 2) and opening of the side face (plane 1). With respect to this mechanism and assuming that the characteristic friction angle of the base face is 35°, static stability is worked out and presented in Table 5.

Table 5 : Static stability analysis of the wedge

Stability analysis static equilibrium	D	S	SF
	[MN]	[MN]	[-]
Results	8437	23671	2.81

D = destabilizing force,
i.e. projection of the total force on plane 3

S = stabilizing force
i.e. friction capacity of plane 3

SF = S/D safety factor

In static equilibrium, the rock wedge is very stable. Under these forces, the critical friction angle would be equal to 14°.

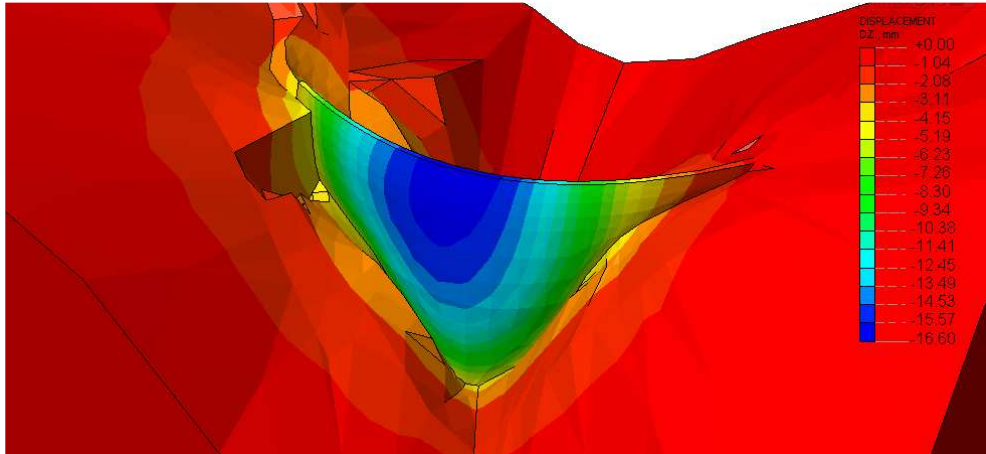


Figure 4 : Vertical displacement under self-weight.

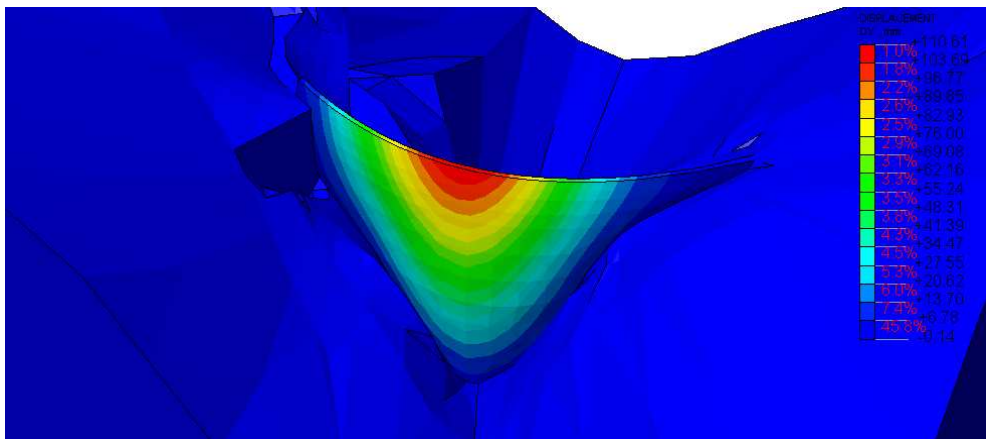


Figure 5 : Horizontal displacement under hydrostatic pressure: 110 mm max.

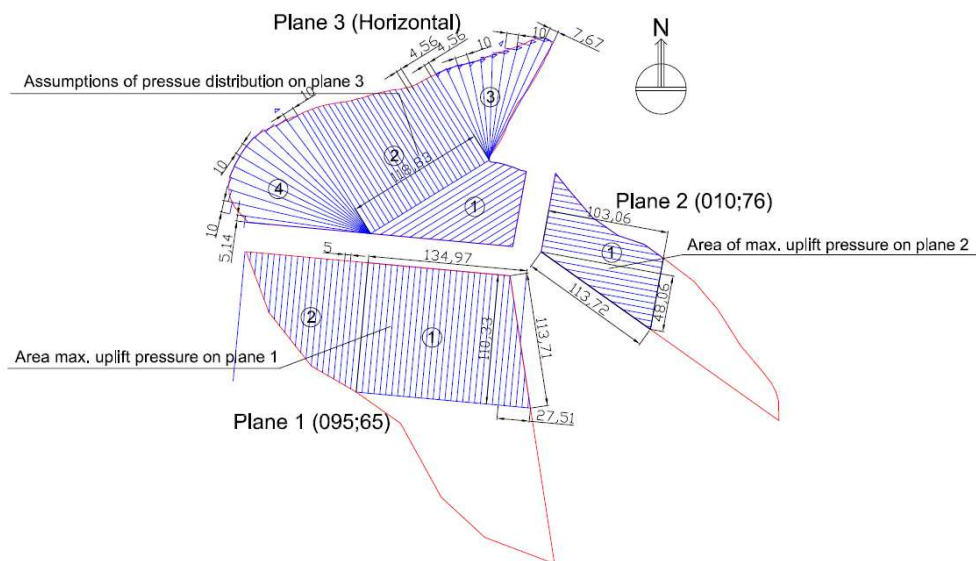


Figure 6 : Assumed distribution of joint water pressures on the faces of the rock wedge

Evaluation of Dynamic Forces

Under seismic loading, the rock wedge will be subjected to the following additional forces:

- inertia forces of the rock wedge;
- inertia forces of the dam acting on the abutment;
- hydrodynamic forces of the reservoir acting on the dam and transmitted to the abutment.

It is assumed that uplift pressures are unaffected by dynamic effects. Consequently the dynamic stability analysis is performed using the same value for the uplift pressures than in static analysis. This assumption is supposed to remain valid even in case of joint opening.

Since the rock wedge is a solid embedded in the surrounding ground, the inertia forces acting on the wedge are obtained by multiplying the wedge total weight by the ground acceleration vector at each time step: $I_w = 4992 [10^6 \text{ kg}] \times a(t) [\text{m/s}^2]$.

The instantaneous inertia forces of the dam depend on the dynamic response of the dam structure to the earthquake and on the boundary condition provided by the reservoir. An eigen mode analysis of the dam alone (reservoir and foundation not modelled) is performed using the finite element model. The two first eigen modes (antisymmetric and symmetric) have an eigen frequency close to 2 Hz. On the other hand, the spectra of the seismic signals show significant magnitude in the range 1 to 5 Hz. It can therefore be concluded that adopting an “instantaneous pseudo-static approach” for the dam mass subjected to ground acceleration would not provide realistic assessment of the instantaneous dam inertia forces. Similarly, using an added water mass in an “instantaneous pseudo-static approach” to assess the hydro-dynamic effect would certainly not yield realistic results.

Considering that the magnitude of dam inertia forces and hydrodynamic forces are small compared to the stabilizing effect of the wedge weight (<10%) and compared to the inertia forces of the wedge (<15%), it is chosen to make an assessment of the peak values of these contributions based on an “envelop pseudo-static approach” and keep these contributions constant over time during the dynamic wedge stability analysis.

The peak hydrodynamic forces are assessed by considering added water mass subjected to the peak upstream-downstream component of the acceleration. It is assumed that vertical and cross-valley components of the accelerations would not have a significant hydro-dynamic effect. The Westergaard formula, see ref [3], is therefore applied with the peak acceleration in the Z direction, a_z , in order to assess the peak hydrodynamic pressure on the dam:

$$P_{(y)} = \frac{7}{8} \cdot a_z \cdot \gamma_w \cdot (H \cdot y)^{\frac{1}{2}}$$

This pressure is applied as a static load in the finite element model and the corresponding force transferred from the abutment to the rock wedge is computed, see Q_{ds} in Table 6.

Regarding the inertia forces of the dam, each acceleration direction contributes differently to the destabilization of

the wedge. Since the oscillation of the dam will produce filtering and out-phasing of the signals coming from the various directions, any combination of positive/negative peak values is possible. The worst-case directional combination with respect to wedge stability cannot be decided “a priori”. The following procedure is therefore adopted:

- the finite element model of the dam and its rock foundation is submitted to 1g acceleration in each direction X, Y and Z and solved in linear static analysis;
- the resulting inertia forces transmitted from the abutment to the rock wedge are computed for each acceleration direction, see Table 6;
- 26 acceleration combinations are generated considering that, for each direction, the acceleration can have the value +peak, zero or -peak;
- for each acceleration combination, the inertia forces are multiplied by the corresponding acceleration value (expressed in g unit) and the total dam inertia force is deduced by superposition (linear system assumption);
- for each combination, the dynamic stability analysis of the wedge is performed keeping the dam inertia forces constant;
- the worst-case combination regarding stability is selected.

Table 6 : Finite element pseudo-static results

FE results Pseudo-static forces	F_X	F_Y	F_Z
	[MN]	[MN]	[MN]
Hydrodynamic force (Q_{ds})	-1119	-299	-1149
Dam inertia force under 1g acceleration in X	4177	82.7	1134
Dam inertia force under 1g acceleration in Y	-858.0	3305.8	-739.7
Dam inertia force under 1g acceleration in Z	3180	995.2	6098

Dynamic Stability

Two cases have been investigated:

- a- provided ground acceleration histories are assume to apply to the rock wedge without modification;
- b- site effect is assumed to lead to an amplification of the cross-valley component of the acceleration by a factor 3.

For both cases, the wedge stability has been studied by applying the Londe method at each time step. When the computed safety factor is smaller than 1, the wedge is supposed to slide in the direction of the destabilizing force. It should be noted that the destabilizing force, having a static and a dynamic contribution, is not necessarily collinear with the acceleration vector. The stabilizing force, i.e. the friction capacity of the base plane, is assumed to instantaneously adopt the same direction as the destabilizing force.

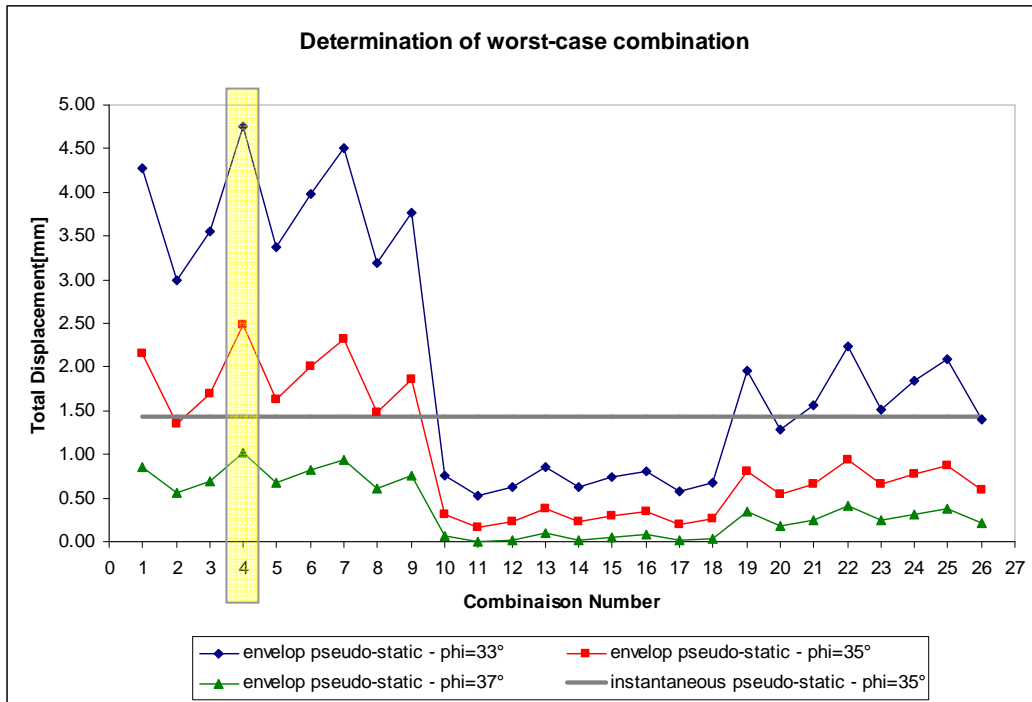


Figure 7 : Determination of worst-case acceleration combination with respect to sliding displacement for case b-

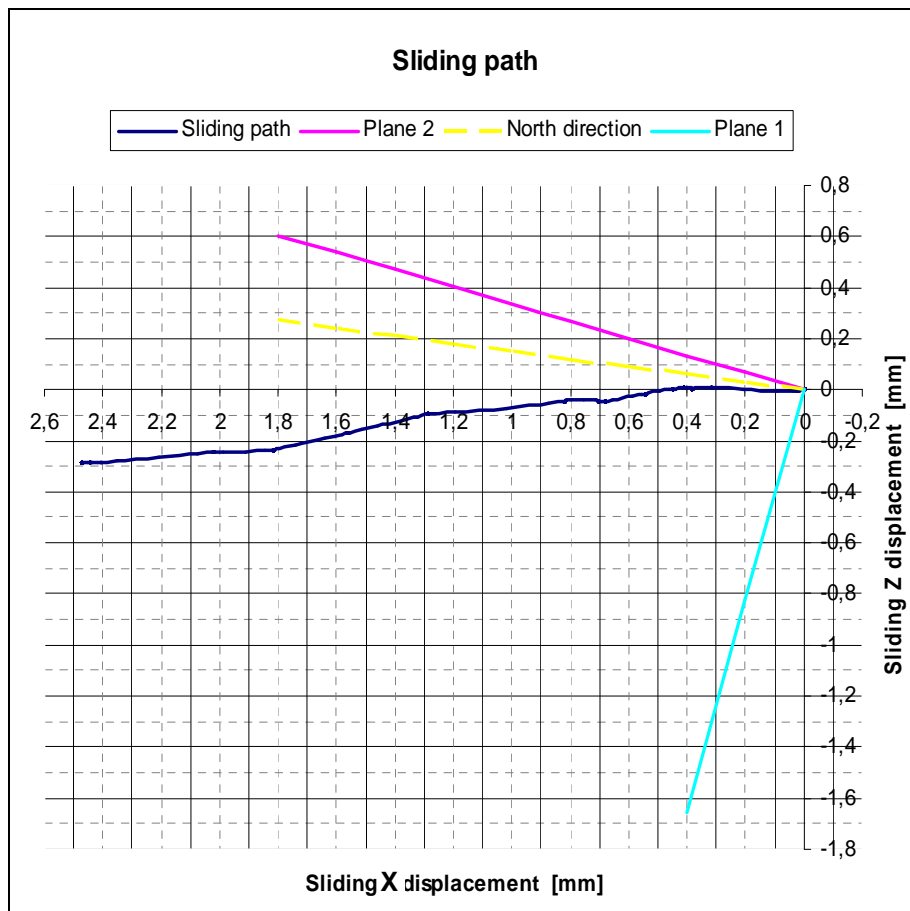


Figure 8 : Sliding path on the horizontal plane 3 for case b-

The obtained out-of-balance force produces a relative acceleration of the wedge, which is integrated over time steps using the Newmark method, see ref [4].

In case a-, this approach leads to predicting no sliding and a minimum safety factor of 1.48. In case b-, it results in a minimum safety factor of 0.76, and to a total sliding displacement of 2.5 mm. Sliding occurs over a short cumulated period of time of 340 ms.

Detailed results are delivered in excel format for cases a- and b-. Figure 7 and 8 present the results of case b- (cross-valley acceleration multiplied by 3) in graphical format. Figure 7 shows the sliding displacement obtained for each of the 26 possible combinations of acceleration components. The worst-case combination with respect to stability is case 4, which corresponds to the values:

$$a_x = +0.48g; \quad a_y = +0.1067g; \quad a_z = -0.16g$$

The sliding path on plane 3 is shown in Figure 8. It can be checked that the wedge slides away from planes 1 and 2.

Discussion

The presented solution is based on a number of assumptions which are discussed below.

The uplift pressures have been assessed based on an “assumed” conservative distribution of water height in the rock wedge. In reality the water height distribution depends on the location and the performance of the drainage curtain. Taking into account a less conservative distribution of water heights, for instance a more efficient drainage, would significantly increase the stability of the rock wedge.

The water pressure in joints during seismic loading is traditionally assumed to remain constant over time and equal to its static value. It is not well known however how these pressures actually evolve during an earthquake, especially when joints are opening due to wedge sliding. It could be argued that, under the high frequency of earthquake loading, undrained effects will take place. To what extent does water have time to flow into the joint to fill the opening gap?

In the presented assessment of the forces acting on the wedge, the arch dam was assumed to behave linear elastically. The sources of non-linearity in the behaviour of the arch dam are however multiple:

- equilibrium under dam self-weight takes place before construction joints are grouted;
- gap opening at dam-rock interface is likely to occur locally, especially at dam toe;
- plain concrete is subject to non-linear behaviour such as cracking and creep.

Similarly, the rock foundation was assumed to be homogenous and to behave linear elastically. However, this natural material is likely to be non-homogeneous, non-anisotropic and to behave non-linearly. For instance, the presence of fault or local alteration of the rock might influence significantly the static and dynamic response of the dam.

As is commonly the case, the eigen frequencies of the dam lie in the frequency range of the earthquake spectrum. This implies that, compared to the ground motion, amplification for certain frequencies and out-of-phase arrivals of dam motion will occur. Regarding the rock wedge stability, and compared to forces assessed using a pseudo-static approach, this effect will induce differences in magnitude, in direction and timing of the dynamic forces acting on the rock wedge. In our case, the relatively large weight of the considered wedge can justify neglecting these effects. If the wedge was however smaller, such effects might become prominent when checking wedge stability.

The site topography (valley) can have a significant effect on the seismic wave when reaching the ground surface. The site effect can include amplification and deamplification, differences in frequency content and out-of-phase arrivals of the ground motion at different locations of the interface of the ground and the structure. At present, such analyses are not commonly performed because realistic modelling of the site with the irregular topography and geology would be either too costly or not well constrained by data on the characteristics of the geologic materials. It is known however that deep valley topography, common for arch dams, can be the cause for significant amplification of the cross-valley ground motion. It was shown in the present case study that an amplification of the cross-valley acceleration by a factor 3 can make the difference between a stable and a sliding abutment wedge. This is therefore identified as a key factor influencing abutment stability which should not be overlooked for design.

References

- [1] LONDE P. (1972) – The mechanics of rock slopes and foundations - Rock Mechanics Research Report N°17, Imperial College, Gresham Press.
- [2] LONDE P. (1965) - Une Méthode d'analyse à trois dimensions de la stabilité d'une rive rocheuse.
- [3] WESTERGAARD, H.M. (1933), "Water pressure on dams during earthquakes", ASCE, Transactions 98 Paper No. 1835 (1933) 418–433.
- [4] NEWMARK N.M. (1965) – Effects of earthquakes on dams and embankments - Fifth Rankine lecture, Geotechnique, vol. 15, no. 2, p. 139-160.

Stability of dam abutment including seismic loading

Morteza Sohrabi Gilani

Civil Engineering
Department
Sharif University
of Technology
Azadi Ave.- Tehran- Iran

mortezasohrabigilani@Yahoo.com

Rupert Feldbacher

Institute of Hydraulic Engineering
and Water Resources Management
Graz University of Technology
Stremayrgasse 10/II
8010 – Graz

rupert.feldbacher@tugraz.at

Gerald Zenz

Institute of Hydraulic Engineering
and Water Resources Management
Graz University of Technology
Stremayrgasse 10/II
8010 – Graz

gerald.zenz@tugraz.at

1. Introduction

One of the most important aspects in the stability analysis of arch dams, which has been encountered for many years, is the stability of the abutment. This study is aimed to evaluate within the Tenth Benchmark Workshop on Numerical Analysis of Dams-Theme C, the abutment stability of Luzzzone arch dam under static and seismic loadings. At first the three dimensional model of the dam has been transferred for being applicable in the finite element program of Abaqus 6.7.

With the FEM the interface forces between concrete dam and wedge are calculated for the required loading cases. The stability analysis of the given wedge is evaluated by Londe method.

2. System Assumption

2.1. Luzzzone dam

The Luzzzone dam is a double curved concrete arch dam which was initially built in the sixties. The dam was heightened within the ninetieths. The total height of the dam is 225 m.

Figure 1 shows the Luzzzone dam.



Fig. 1: Luzzzone dam

2.2. Wedge definition

For the benchmark in the left bank of the dam are two geological joints. With these joints a wedge is defined and has a potential to slide under arch dam and uplift loading. To verify about this situation a stability assessment is necessary. The volume of the wedge has been estimated as $1.92 \times 10^6 m^3$. The wedge position is shown in figure 2.

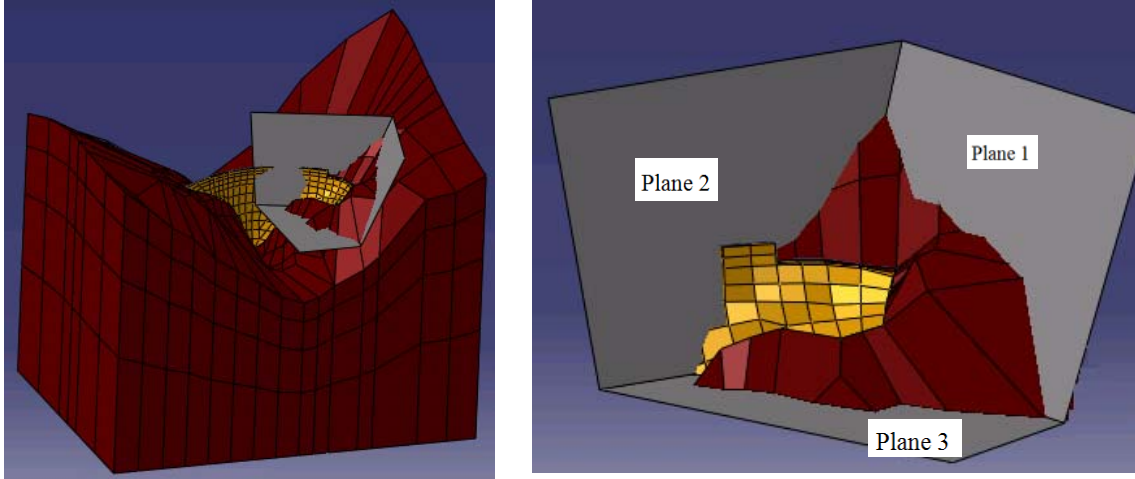


Fig.2: Finite element model of dam and foundation and Geometry of the wedge

2.3. Material properties

The material property of the mass concrete dam and foundation are defined as:

Concrete of dam:

Density (ρ) = 2400 kg/m³

Poisson ratio (ν) = 0.167

Modulus of elasticity (E) = 27 GPa

Rayleigh damping coefficients: α = 0.6 and β = 0.001

Foundation rock:

Density (ρ) = 2600 kg/m³

Poisson ratio (ν) = 0.2

Modulus of elasticity (E) = 25 GPa

Rayleigh damping coefficients: α = 0.6 and β = 0.001

Water:

Density (ρ) = 1000 kg/m³

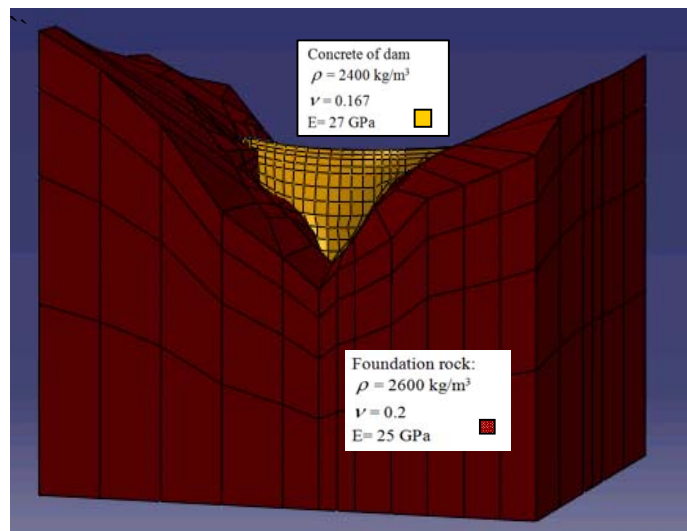


Fig 3: Material properties of dam and foundation

It should be mentioned that in calculating the interface forces between dam and wedge, only the stiffness of foundation is considered and density of it is taken as zero. In other words a massless foundation is considered.

2.4. Loading

The static and seismic load cases are considered to calculate the dam-foundation interface forces. In the self-weight condition the dam is considered monolithic and isotropic material behavior is used.

Under the reservoir full condition the hydrostatic pressure is applied to the dam's upstream surface according to the programs loading definition.

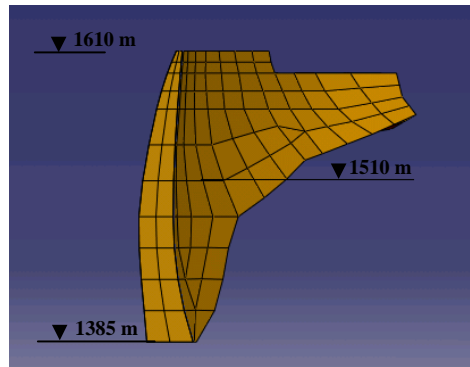


Fig 4: Cross section of the dam

For seismic analysis, three stochastically independent acceleration time histories are used according to the data provided by the formulator. These accelerations are scaled according to the peak ground accelerations of these components are:

Downstream-upstream (X- direction) = 0.16 g

Vertically upwards (Y- direction) = 0.1063 g

Cross valley direction (Z- direction) = 0.16 g

In wedge stability assessment uplift pressure at the wedge interfaces is considered very conservative, and all planes are under full uplift pressure.

3. Calculation Procedure

Figure 2 presents the finite element model of the dam. This model is created within *Abaqus 6.7* and linear elements (C3D8) are used to define dam and foundation body.

The dam-foundation interface is modeled as a joint with a high friction coefficient to reduce relative displacement between dam and foundation to a minimum. The resultant forces transmitted between dam and wedge are computed as the sum of pressure and shear stresses at the wedge dam interface.

For the seismic analysis direct time history approach is used and hydrodynamic pressure is computed by Westergaard's added mass method. According to Westergaard, the hydrodynamic pressures that the water exerts on the dam during an earthquake are the same as if a certain body of water moves back and forth with the dam while the remainder of the reservoir is left inactive. The added mass per unit area of the upstream wall is given in approximate form by the expression $\frac{7}{8} \rho_w \sqrt{h_w (h_w - y)}$, where ρ_w is the density of water.

It should be mentioned that in calculating the interface forces between dam and wedge, only the stiffness of foundation is considered and density of it is taken as zero. In other words a massless foundation is considered for the dynamic dam analysis.

4. Stability of wedge

The next step for the analysis is to evaluate the wedge stability. For this purpose Londe method for stability of rock slopes is used and some simplifying assumptions are made. The volume of the wedge is limited by intersections of three planes (Planes $Plane_1$, $Plane_2$ and $Plane_3$ in the figure 2). This assumption is conservative as the natural surfaces are generally irregular [2]. The wedge is considered as a rigid body and the geometry of the wedge would not change during application of the forces throughout the investigation. Cohesion and tensile strength are neglected in the contact planes and therefore, it is supposed that the friction between surfaces is the only parameter that can resist sliding. It is supposed that the moments of the forces have negligible influences and can be ignored. The applied forces can be categorized as:

- Weight of the wedge (W_w)
- The thrust force which is the resultant force at the dam wedge interface. This force is time dependent and its magnitude and direction will change by time. So this force can be defined by F_x , F_y and F_z .
- The forces due to uplift pore pressure: U_1 , U_2 and U_3 which are applied to the planes 1, 2 and 3 respectively- these forces do not change during investigation.
- Seismic forces due to applied earthquake: the three components of seismic forces are considered as the ma_x , ma_y and ma_z which m is the mass of the wedge and a_x , a_y and a_z are acceleration time histories which were defined before.
- The reaction of planes: due to applied forces, three reaction forces will develop on the planes (N_1 , N_2 and N_3). As mentioned before these forces can only be compressive. Tensile forces, which mean that the plane is open, are not acceptable and will lead to a different sliding mode respectively exclude sliding in the decoupling plane due to tensile forces.

For wedge stability evaluation at first the three plane reaction forces are to be calculated by solving static equilibrium equations in three direction x , y and z , Figure 5-a. For this wedge geometry and applied forces, due to equilibrium condition and calculated plane reaction forces, eight cases are possible. Table 1 shows all possibilities.

- Case 1: All plane reaction forces are compressive: all planes are in contact and the wedge is perfectly stable.
- Case 2: The reaction force of plane 1 is tensile, but the other two reaction forces are compressive ($N_1 > 0$, $N_2 < 0$ and $N_3 < 0$). In other words plane 1 is open but planes 2 and 3 are in contact yet. In this case to check the movement along the intersection of plane 2 and 3 the force in this direction is calculated. For this purpose the equilibrium equation is solved with these three existing forces, N_2 , N_3 and S_{23} again, Figure 5-b. Then the stability factor can be calculated accordingly:

$$SF = \frac{S_{23}}{N_2 \tan \varphi_2 + N_3 \tan \varphi_3}$$

If the safety factor is less than one the rupture will occur and wedge will move along intersection line of planes 2 and 3.

- Case 3: Sliding along the intersection of plane 1 and 3 ($N_2 > 0$, $N_1 < 0$ and $N_3 < 0$). This case is similar to case 2.

- Case 4: Sliding along the intersection of plane 1 and 3 ($N_3 > 0$, $N_1 < 0$ and $N_2 < 0$). This case is similar to case 2.
- Case 5: Sliding in plane 3 ($N_1 > 0$, $N_2 > 0$ and $N_3 < 0$). In this case the only plane which remains in contact is plane 3. The normal and shear forces of this plane are calculated again by solving the equilibrium equation and ignoring the plane 1 and 2. The Safety factor reads accordingly:

$$SF = \frac{\text{Shear force on plane 3 } (S_3)}{N_3 \tan \varphi_3}$$

- Case 6: Sliding in plane 2 ($N_1 > 0$, $N_3 > 0$ and $N_2 < 0$). This case is similar to case 5.
- Case 7: Sliding in plane 1 ($N_2 > 0$, $N_3 > 0$ and $N_1 < 0$). This case is similar to case 5.
- Case 8: $N_1 > 0$, $N_2 > 0$ and $N_3 < 0$. In this case all planes are open and the wedge is obviously freely moving.

The wedge stability safety factor of the dam during the earthquake is plotted in the figure 6. As shown, the safety factor for a short period of time is less than 1, which means that the wedge would move during this time period. The concept of Newmark's method is used to calculate displacement of the wedge.

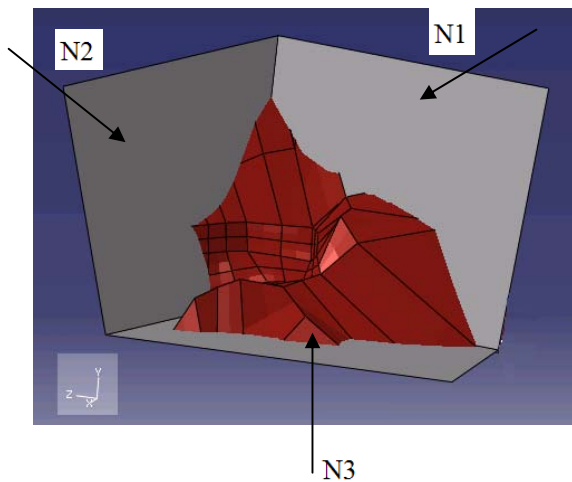


Fig. 5-a: Normal contact forces

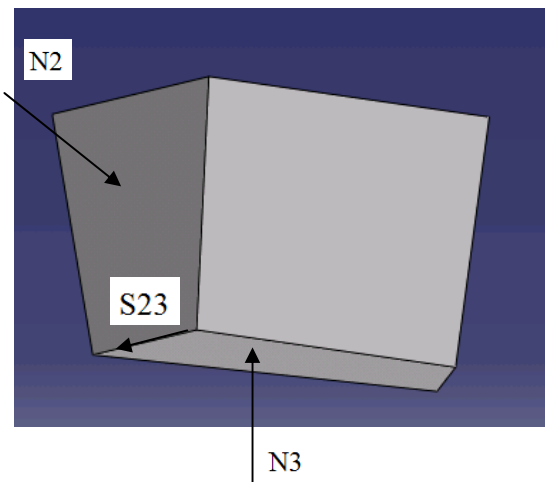


Fig. 5-b: Contact forces for case 2 (sliding along the intersection of planes 2 and 3)

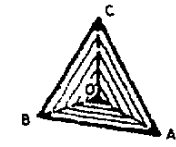
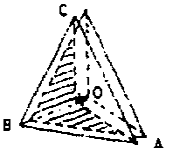

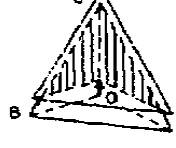
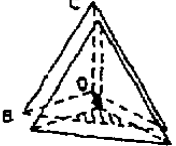

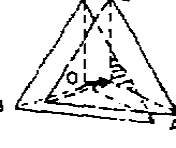

Case	Nature of sliding	Contact faces	Open Faces	Diagram
1	No sliding	1, 2, 3		
2	intersection of Planes 2,3	2, 3	1	
3	intersection of Planes 1,3	1, 3	2	
4	intersection of Planes 1,2	2, 3	3	
5	in plane 3	3	1, 2	
6	in plane 2	2	1, 3	
7	in plane 1	1	2, 3	
8	in space		1, 2, 3	

Table 1: all possible movement cases of the wedge

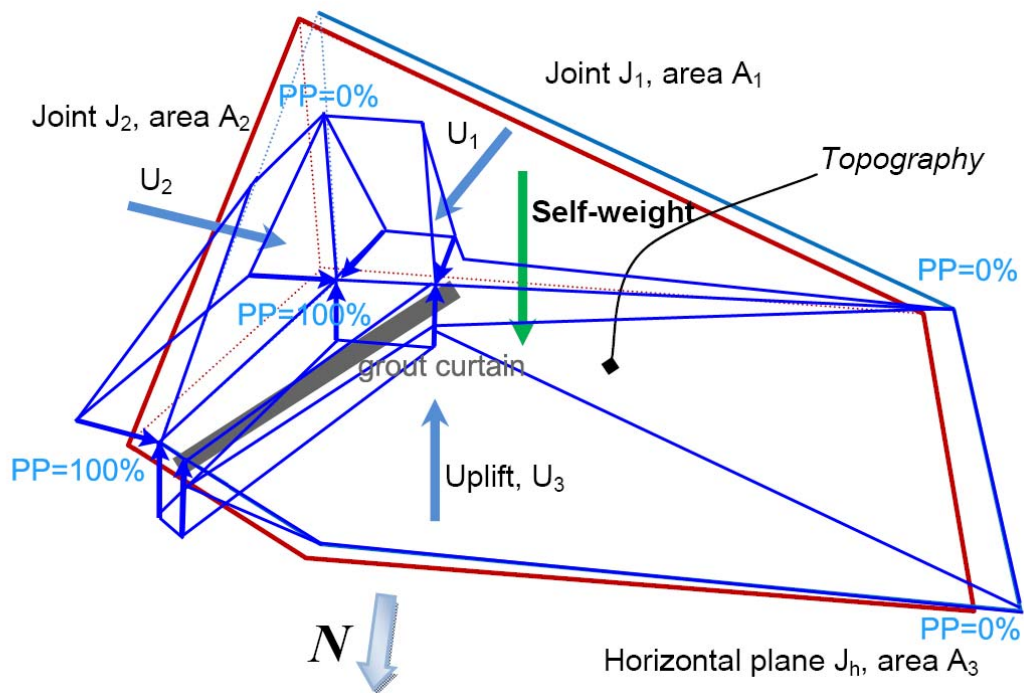


Fig. 6: Sensitivity Analysis - wedge stability uplift assumption

Wedge alone																	
Wet area [m ²]			Wedge														
Jh	J1	J2	Volume [m ³]	Mass [kg]	Weight [MN]	tan 35°											
28650	23300	7200	1,92E+06	4,99E+09	48970	0,70											
Pore pressure [% of full]			Weight of Wedge [MN]			U on Jh [MN]			U on J1 [MN]			U on J2 [MN]			Driving Force [MN]	Stabilizing Force [MN]	SF
Jh	J1	J2	Sw	Gx	Gy	Gz	Uz	Ux	Uy	Uz	Ux	Uy	Uz				
0	0	0	SW	0	0	-48970	0	0	0	0	0	0	0	0	34290	infinite	
100	50	50	SW+hyd	0	0	-48970								11190	10630	0,95	
100	50	50	SW+hyd+dyn	-2960	4330	-44730	28110	900	10320	4830	-3370	600	850	16180	7660	0,47	
50	50	50	SW+hyd	0	0	-48970								11190	20470	1,83	
50	50	50	SW+hyd+dyn	-550	6300	-46370	14050	900	10320	4830	-3370	600	850	17480	18650	1,07	
35	35	50	SW+hyd	0	0	-48970	9840	630	7220	3380	-3370	600	850	8290	24440	2,95	
35	35	50	SW+hyd+dyn	-550	6300	-46370								14500	22620	1,56	
35	35	35	SW+hyd	0	0	-48970	9840	630	7220	3380	-2360	420	600	7830	24620	3,14	
35	35	35	SW+hyd+dyn	-550	6300	-46370								14720	22800	1,61	

Wedge + dam thrust																
Pore pressure [% of full]			Weight of Wedge [MN]			Uplift		Dam Thrust Force [MN]						Driving Force [MN]	Stabilizing Force [MN]	SF
Jh	J1	J2	Sw	Gx	Gy	Gz	Jh, J1, J2	Fx	Fy	Fz	Fres	alpha	beta			
0	0	0	SW	0	0	-48970	0	180	20	-4050	450	87,4	96,5	11	37090	3333
35	35	50	SW+hyd	0	0	-48970	vide supra	-5480	-4680	-4650	8580	32,8	-131	8800	27690	3,15
35	35	50	SW+hyd+dyn	-6740	280	-46930		-9310	-770	-400	12730	18,3	-128	17570	26360	1,41

Fig. 7: Sensitivity Analysis - Wedge stability – Static / Dynamic Loading

5. Displacement of the wedge

To calculate the displacement of the wedge in the first step acceleration of the wedge is calculated in the x , y and z direction. The magnitude of the acceleration is $\frac{\text{Driving Force} - \text{Stabilizing Force}}{\text{mass of the wedge}}$ and its direction

is being defined due to the movement case. (For one plane sliding the resultant acceleration is decomposed due to the applied forces, for example in case 2, $a_x = \frac{F_x - (N_3 \tan \phi)_x}{m}$ and $a_y = \frac{F_y - (N_3 \tan \phi)_y}{m}$, but for two planes sliding the direction is the intersection of corresponding planes which is constant)

Displacement of the wedge is the double integration of this computed acceleration. The integration should continue till the velocity in the considered direction vanishes. For the assumed uplift pressure and failure mechanism of the wedge no sliding during dynamic analysis occurred.

6. Conclusion

Under the assumption of a rigid body wedge the analysis is carried out for dead weight, water loading and uplift. No variation of the earthquake acceleration along the valley is assumed.

The uplift pressure at the wedge interface is varied, and for an engineering assumption of the uplift pressure the factor of sliding safety is 3,15. During dynamic analysis this factor of safety reduces to 1,41.

In a further step, with the help of FEM the wedge is suggested to be analyzed as deforming body and with this the stability of the abutment. In addition, the dynamic analysis of the dam should be carried out with acoustic elements, to better account for the dam reservoir interaction. However, these assumptions are used normally, but were out of scope of this benchmark.

7. Acknowledgement

The support of this work by the research project “Design of Hydraulic Structures” by Pöyry Energy Ltd is gratefully acknowledged.

8. References

1. R. M. Gunn, “Computational aspects of analysis and design of dams”, “Tenth benchmark workshop on numerical analysis of dams”.
2. P. Londe, “Analysis of the stability of rock slopes”, published in “Quarterly Journal of Engineering Geology and Hydrogeology”, vol. 6, issue 1, p. 93-124, 1973.
3. N. M. Newmark, “effect of earthquakes on dams and embankments”, published in Geotechnique, “Milestones in Engineering”, vol. 15, No. 2, p. 109-129, 1965.
4. “Abaqus version 6.7-EF Documentation”.

Stability of the left bank abutment of the Luzzone Arch Dam

*V. B. Glagovsky, A. A. Khrapkov, V. S. Kostylev, M. S. Lamkin, T. O. Sinitsyna,
T. A. Sozinova (JSC “Vedenev VNIIG”, St. Petersburg)*

1. Introduction

This work deals with the arch dam behavior and foundation stability under seismic loads. Software ANSYS was used for calculations. A number of calculations including static and dynamic load ones have been executed. The main goal was to determine impacts from the dam side on a part of embankment abutment situated on the left bank above 1510 m elevation due to earthquake, where according to the data of the test task there is a zone of potentially possible shear.

2. Description of the task and initial data

The initial data of the task were submitted by the conference organizers. Luzzone arch dam (Switzerland) is investigated. This dam built in 1963 and heightened in the end of nineteenth is of 225 m height, 36 m foundation thickness and of crest thickness equal to 10 and 4 m for the old and new parts correspondingly. The arch length is 530 m. Crest elevation is 1609 m. More detailed information is in the task of the formulator [1]. The formulator presented a 3D model of the dam on a rock foundation. The model is in the text format and in the commands of the finite-elements complex TNO Diana, version 9.2. There have been given the parameters of the material and foundation within linear-elastic model as well as the topography of the weakened zones where the detachment of a part of the rock massif is possible. It is also given the reduced internal friction coefficient for the weakened zones accepted in this test task. According to the submitted information some decompressed structures are in the rock foundation on the left bank. For the present task the formulator has chosen the potentially unstable site on the dam left bank formed by the horizontal plane at the 1510 m elevation and also by two planes defined in the task [1]. Stability is estimated assuming that one of these planes has been cracked.

During preparation for evaluations the geometrical model was imported from the text file with the command in the format TNO Diana into the finite-element complex ANSYS. As the direct import from this format is not supported by ANSYS we developed software in program language C++ to import the geometry. At that there have appeared several complications connected with the description of some geometrical primitives inadmissible for the ANSYS complex. Particularly the ANSYS does not support determination of line segments with different numbers but with the same end points forming these segments. It also does not support the surfaces with different numbers but formed by completely coincided lines systems, etc. These incompatibility problems have been partially solved by re-numeration of all primitives of the level lower than the ANSYS “volumes” (i.e. points, lines and surfaces) during import into ANSYS package. After that the 3D model has been divided into finite elements according to the data (a number of line splitting, mesh concentration to the definite points) specified in the file of Diana commands.

The obtained finite-element model is given in Fig.1. The model consists of 14814 serendipity 3D elements of the second order accuracy of “Solid95” type. At that a number of the elements in the dam is 2504, a number of elements in the foundation - 12310. Total number of nodes is 62518. The dynamic loads from the reservoir water are substituted by added masses. The values of the added masses are chosen according to the Russian Rules and Regulations for Building Design (SNiP II-7-81*, Construction in seismic regions). The quantity of the added mass elements in the horizontal direction along the stream is 1783. The added masses in the direction across the stream are not taken into account.

Calculations of the dam-foundation system for the affect of both static and seismic loads have been fulfilled using the linear-elastic model. So the different load cases may be just summed up to obtain the final load case (statics + seismics).

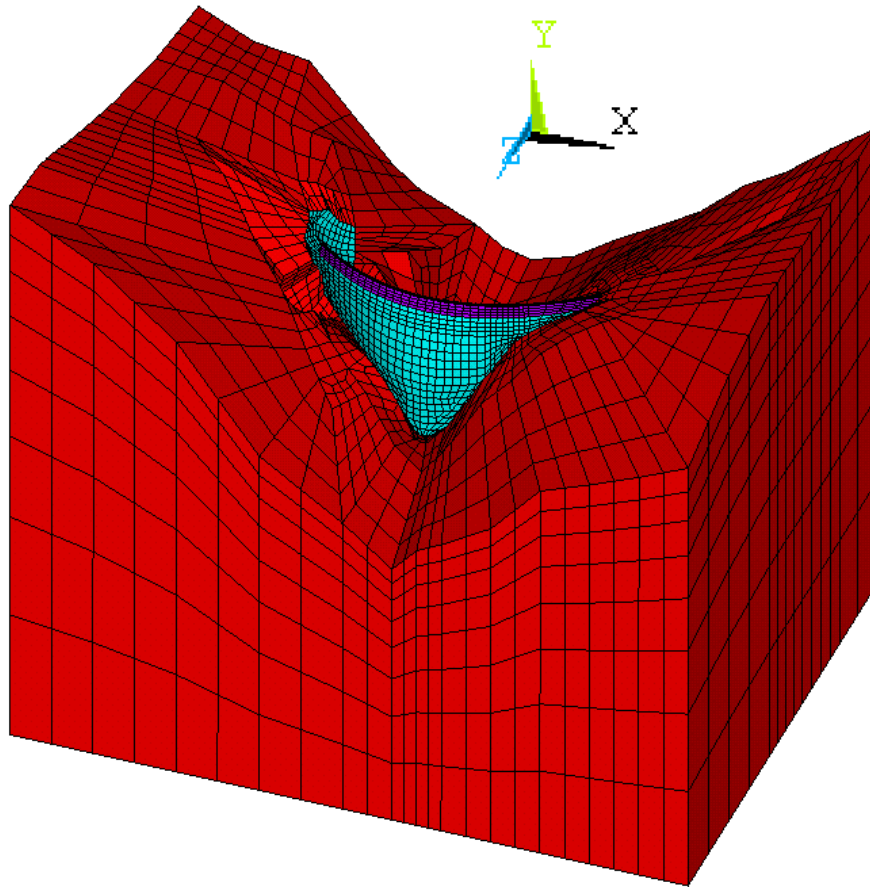


Fig. 1. ANSYS finite element mesh.

3. Calculation for static loading

The dam dead weight loading and hydro-static pressure have been evaluated. According to the formulator task the height of water surface was taken equal to 1610.2 m that corresponds to the overflow over the concrete dam crest with the reservoir overflow. Distribution of the hydro-static pressure by the upstream face obtained in ANSYS is given in Fig. 2. Calculation results are given in Fig. 3. The total load acting from the dam side on the foundation wedge (dam thrust) in the left bank is presented in the Table 3. Dam thrust was calculated by summing up finite element nodal loads acting from the dam elements to wedge elements over the left bank dam nodes located above elevation 1510 m.

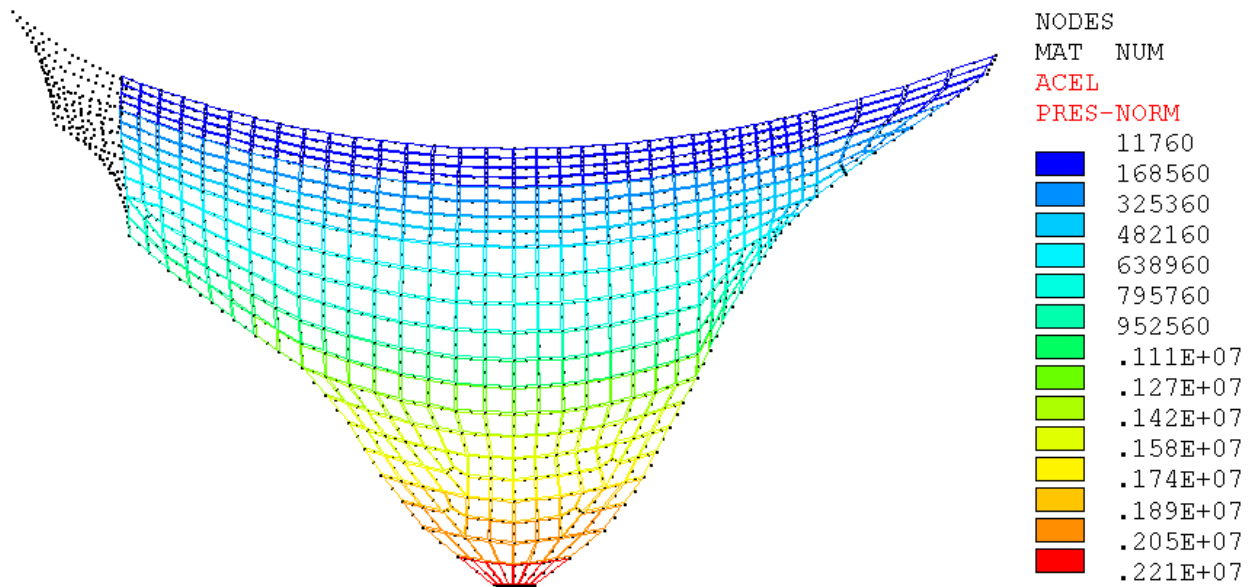


Fig. 2. Distribution of the full hydrostatic pressure, Pa.

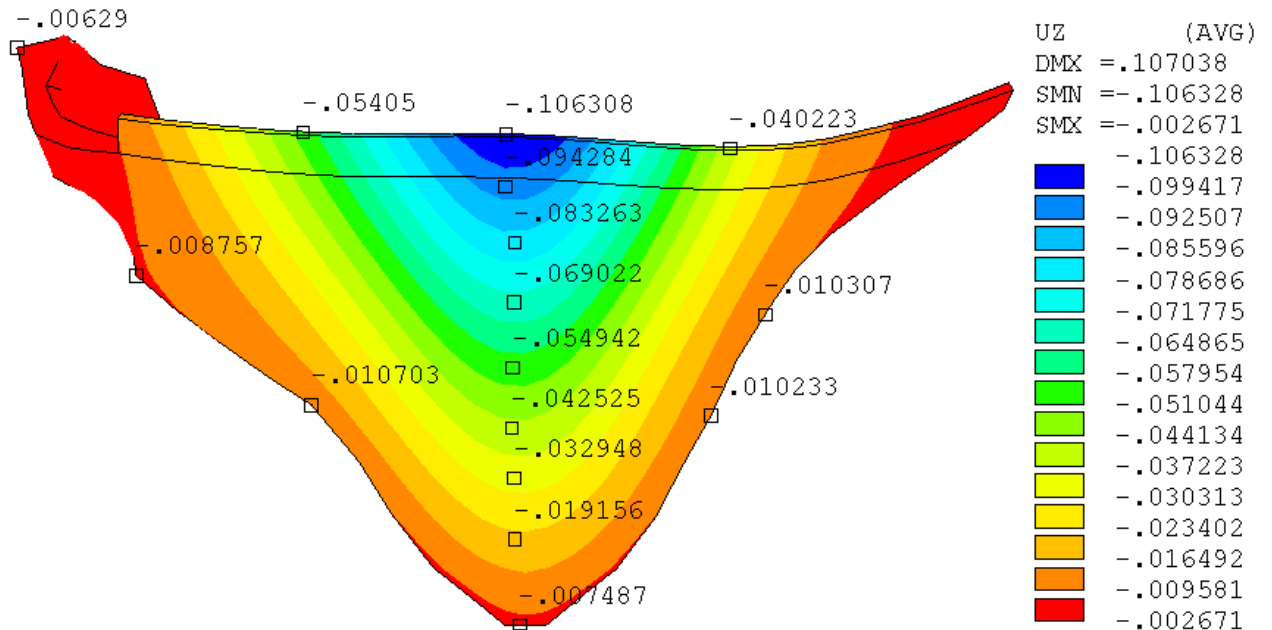


Fig. 3. Upstream displacements on deformed mesh ("Z" direction), m.

4. Calculation for seismic loading

To determine seismic load there have been used the data of free surface acceleration in the dam region (accelerograms) submitted by the formulator of the test task.

In Table 1 are given natural frequencies of the dam without added masses (empty reservoir) as well as with added masses (reservoir elevation 1610.2 m.a.s.l.).

The calculation has been done on inertial base. On the region boundary there have been installed dampers chosen according to [2] (formulas (34), (35)) to reduce the effect of seismic wave reflection from the boundary. The dam calculation on the inertial base is carried out by applying in every time step the inertial seismic forces only to the dam units (by multiplying the seismic accelerations by the dam mass matrix). As mentioned in [3] some commercial finite-

element packages do not have this possibility as built-in, however in ANSYS it can be done either by built in command (“CMACEL”) or manually as it has got an command language that allows us to write macros for applying of the appropriate inertial loads in every time step. The dam calculation on the inertial base has got such benefit that permits to take into account the effect of excited waves attenuation due to presence of damping in the model and, thus, it is not so exacting to the boundary conditions on the foundation boundary (it is quite difficult or even impossible to make a real non-reflecting boundary within the ready finite-element package, dampers reduce wave reflection but doesn’t totally eliminate it). Time histories of total forces affecting on the potentially unstable foundation wedge are given in Fig. 5.

It should be noticed that the seismic load affecting the wedge consists of two components: the dam thrust force and the inertial load caused by the wedge acceleration under the seismic loads. At that the total acceleration is formed of the free field acceleration, given in the initial accelerogram [1], and the additional acceleration caused by the dam presence. The Table 2 contains the maximum and minimum values for the free field accelerations, relative accelerations, averaged by the wedge volume, obtained in the calculation in the corresponding time moments, as well as their sum equal to the absolute wedge acceleration. The table shows that the dam presence does not significantly influence on the foundation acceleration in the wedge area that can be explained by relatively small mass of the arch dam (in comparison, e.g., with gravity ones). Although insignificant reduce of accelerations due to additional dam mass is noticeable but it is so small that in this case it can be ignored during stability calculation. Therefore the inertial forces are evaluated according to the initial accelerogram. Thus, the greatest inertial forces affecting the wedge have been calculated on the basis of the wedge mass ($4.992 \cdot 10^9$ kg) and data by maximum peak ground accelerations (0.16g, 0.1067g, 0.16g by the axes X, Y, Z correspondingly) and were about $8 \cdot 10^3$ MN by the horizontal axes X, Z and $5.3 \cdot 10^3$ MN along the vertical axis Y. Dam thrust time history caused by seismic load only (without the static addition) is shown in Fig. 5. The maximum values of the forces were $1.5 \cdot 10^3$ MN, $1.5 \cdot 10^3$ MN, $3.6 \cdot 10^3$ MN along the axes X, Y, Z respectively. At calculation of the total load (statics + seismics) the direction of the seismic loads was chosen to create the most unfavorable conditions for the wedge (with the sign “+” along the axes X and Y and with the sign “-“ along the axis Z). The Table 3 contains the values of individual summands used in the calculation of the total load. The total load at seismics is given in the resultant Table 4.

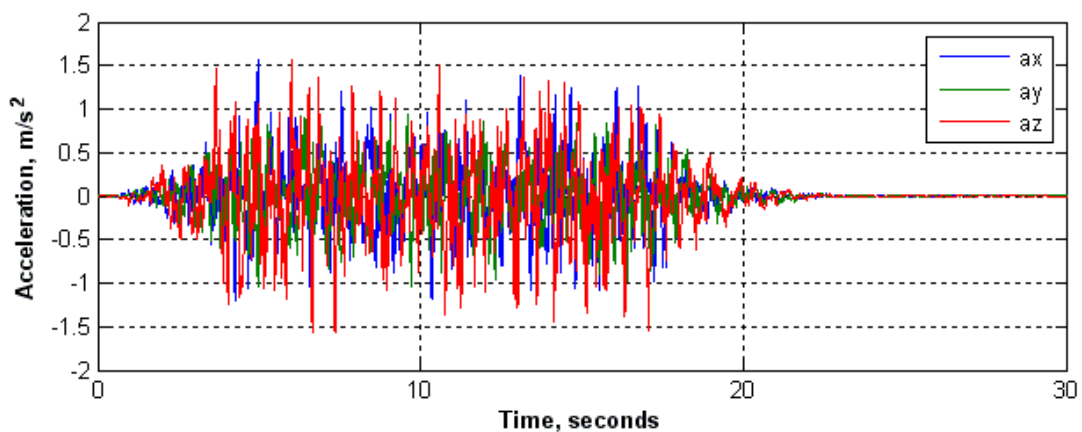


Fig.4. 3-component free-field acceleration time history, [1].

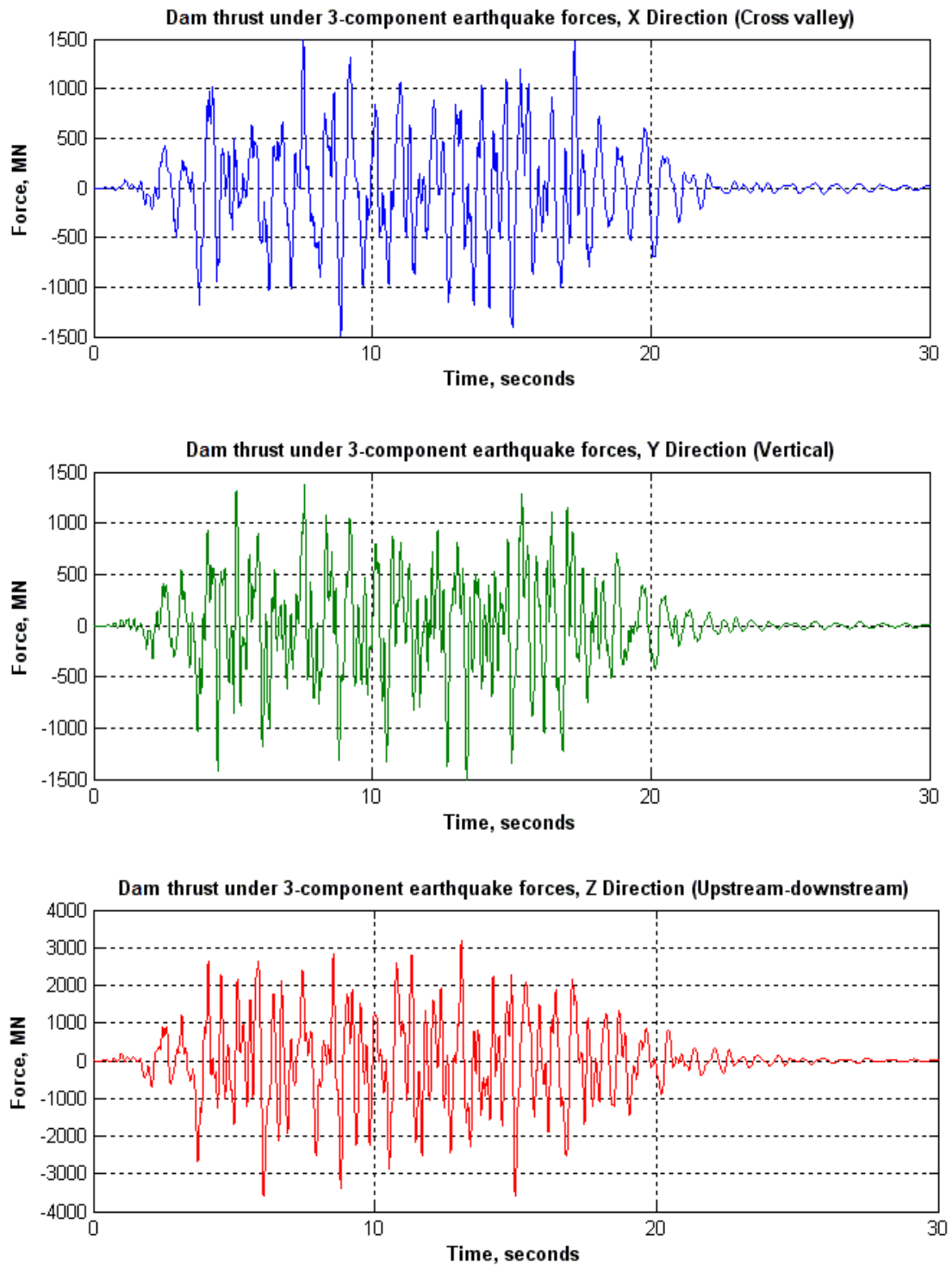


Fig. 5. Dam thrust caused by seismic loading (MN).

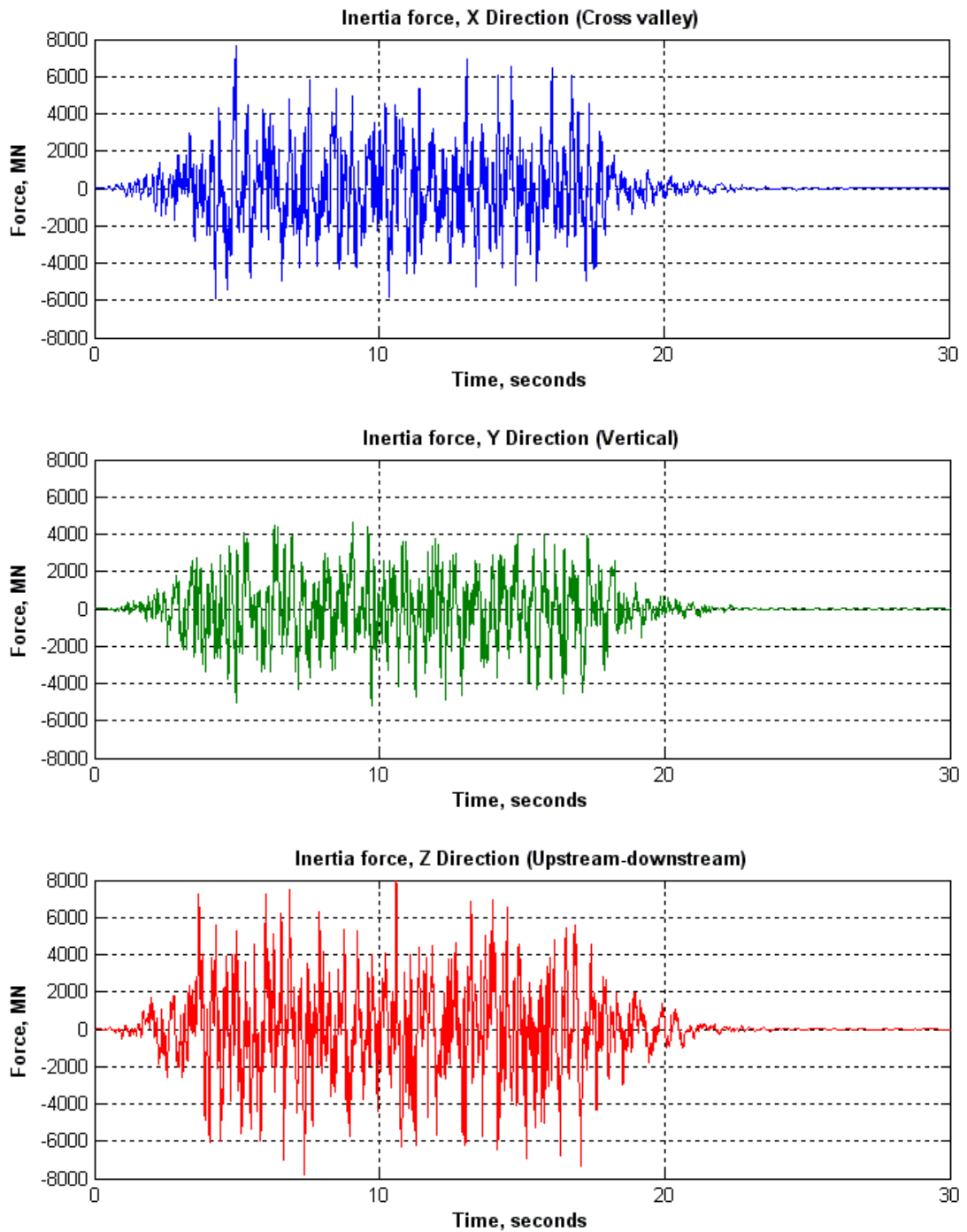


Fig. 6. Inertia force acting on the wedge caused by seismic loading (MN).

5. Determination of hydrostatic uplifts by detachment planes

As it has been stated in [1] there was registered a considerable level of seepage on the left bank of the dam. This circumstance results in forces affecting the wedge by possible detachment planes. The table of the initial parameters from [1] contains areas of the selected shear planes under the upstream level. However, in case of seepage through the foundation groundwater level drop goes by the saturated surface. Precise determination of this surface requires seepage calculation. In this case the task of seepage calculation was more complicated due to the absence of data on the permeability coefficient for the dam foundation and data on drainage measures (drainage holes and galleries) carried out for the left bank of the dam. In the present work the seepage calculation was substituted for the approximate evaluation of possible hydrostatic uplifts

based on the topographic data. To provide illustration on Fig. 7 we show the compositing of the site topography and planes of possible shear taken from the task [1], annex 12.a, on the map with the marked dam (map with dam situation is taken from www.swissdams.ch). Fig. 8 contains views of 3D pattern from [1] for the investigated wedge with headwater decrease marked by lines and taken in this calculation; the contour of the dam support is also marked on the wedge. The hydrostatic uplifts used in the stability calculation were given in the separate columns of the resultant Table 4 to provide greater possibilities for comparison of the results obtained by participants (due to some uncertainty of these forces).

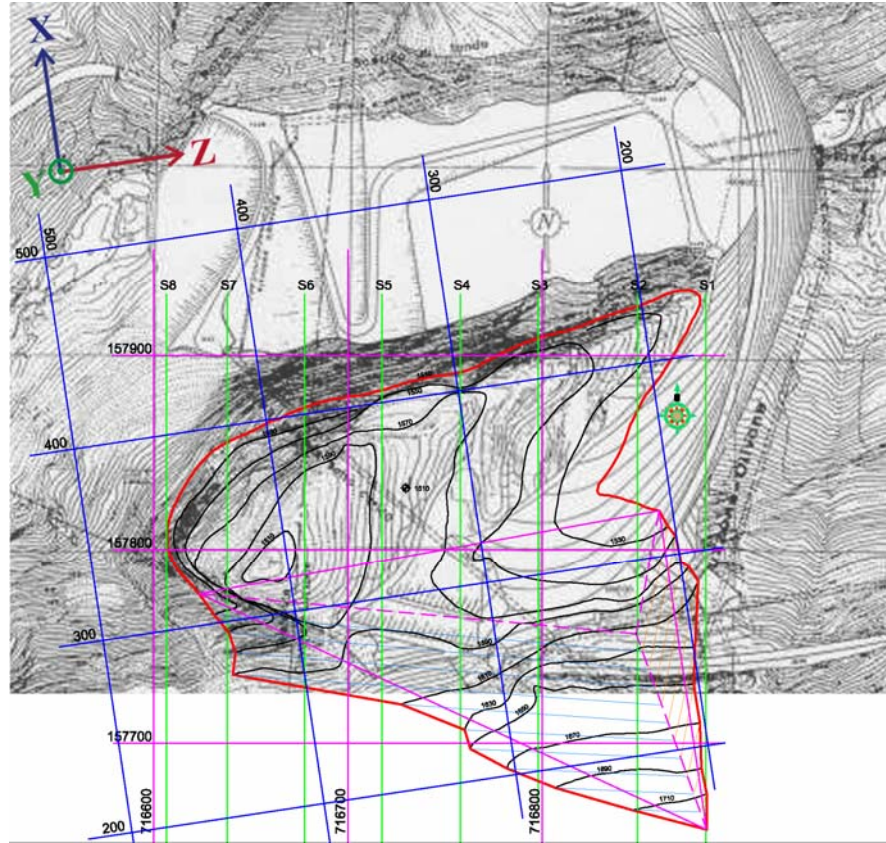


Fig. 7. Foundation wedge ([1], annex 12.a), dam situation (www.swissdams.ch) and finite element model coordinate system combined in single picture.

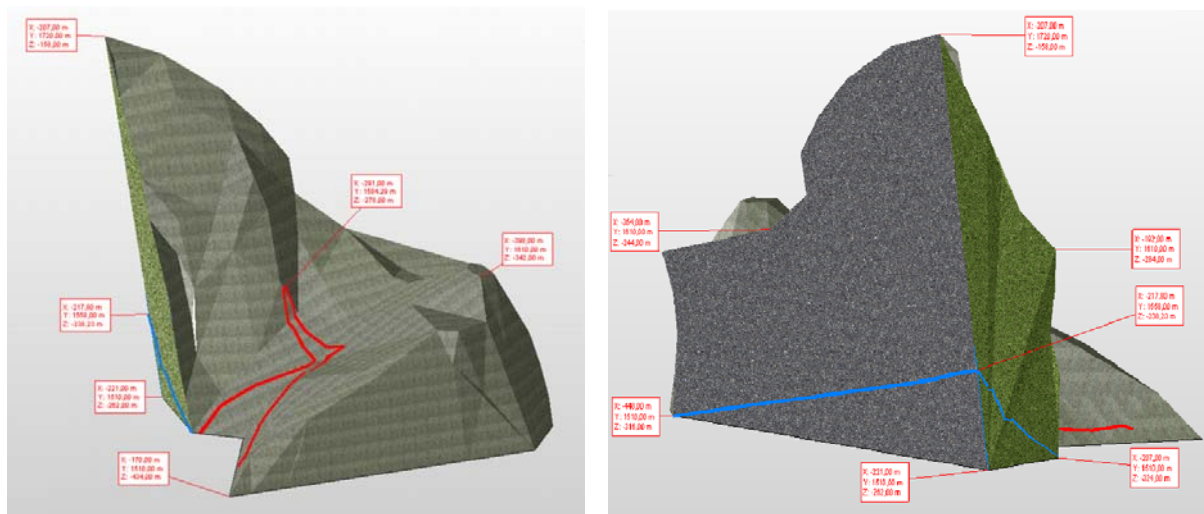


Fig. 8. 3D pattern of the foundation wedge.

6. Calculation of dam foundation stability

Foundation stability was calculated by evaluation of the wedge, given in the task [1], on shear along the edges of the dihedral angle (see [4], [5]). At that the wedge is a solid body and loads affecting it are considered uniformly applied to the whole wedge without taking into account a moment component. The sketch of acting forces on the wedge is presented in Fig. 9.

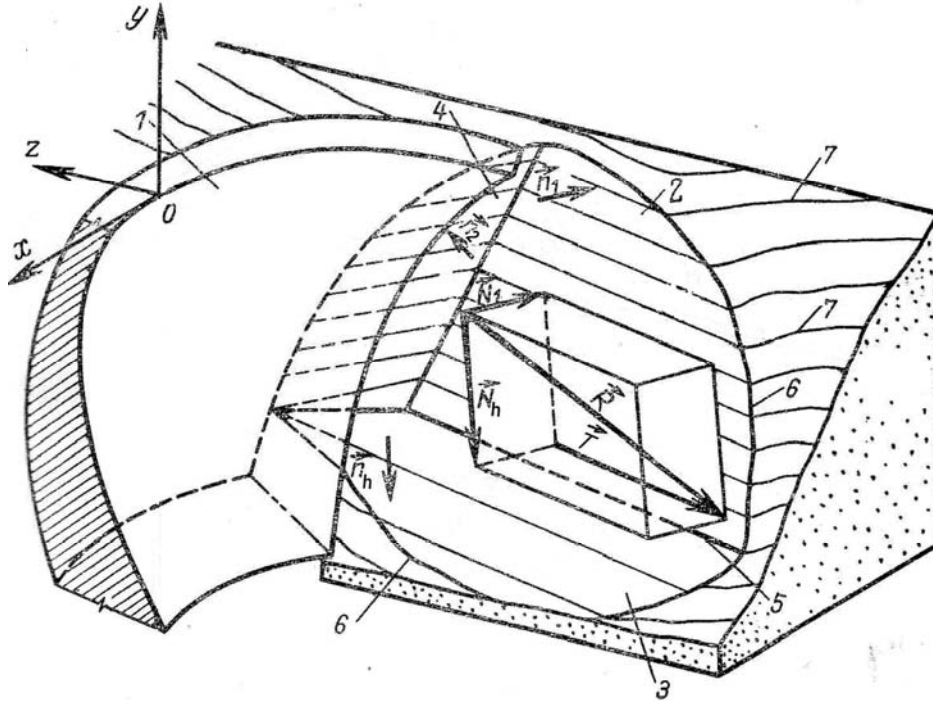


Fig. 9. Foundation wedge and acting forces, picture is taken from [5].

1 – arch dam; 2 – sliding plane J1; 3 – horizontal sliding plane Jh; 4 – plane J2 (crack); 5 – J1 and Jh intersection line; 6 – wedge contour on daylight surface; 7 – topographic contours.

The factor of stability can be calculated by formula:

$$K_s = \frac{N_1 \operatorname{tg} \varphi_1 + N_h \operatorname{tg} \varphi_h + S_1 C_1 + S_h C_h}{T},$$

where \mathbf{R} is vector of total loads acting on the wedge; N_1 and N_h are components of \mathbf{R} normal to planes J_1 , J_h respectively; T is component of \mathbf{R} parallel to the intersection line 5 (see in Fig. 9); φ_1 , φ_h are internal friction angles; S_1 , S_h and C_1 , C_h are J_1 , J_h surface areas and cohesion values.

The results of the stability calculation under static loads are presented in the Table 4. It shows that the stabilizing force is 7.5 times greater than the driving force and so the safety factor in this case is quite large.

It should be noticed that the seismic load given in Table 4 is maximum and is achieved only for a very short time period, so even the exceeding of the forces restraining the wedge due to this load leads only to some accumulation of displacements in time, the total value of which during the accelerogram action permits to make a conclusion of the foundation reliability. Nevertheless the fulfilled stability calculation demonstrated that even at maximum load the restraining forces will not be exceeded and there will not be any displacement. The ratio of the shearing force to restraining force was 1.68. Also it should be remembered that the calculation has been carried out according to the hydrostatic uplifts given and approximately determined in the previous paragraph. More accurate determination of these uplifts can lead either to increase or decrease of the stabilizing forces.

7. Supplementary information

After the completion of this work in the initial version it was recommended by the formulator to determine the factor of stability for the massif under examination assuming that the peak value of acceleration was 0.46g, 0.1067g and 0.16g along the axes Ox, Oy and Oz respectively.

The factor of stability for new initial data was determined with approximation as follows. Seismic load along the axis Ox was increased by the ratio of 0.46/0.16, i.e. 2.875 times in comparison with the values of 1500 MN (seismic load, dam thrust) and 8000 MN (seismic load, inertia), which are presented in the Table 3. The obtained values were 4312.5 MN and 23000 MN, and the corresponding total load value proved to be equal to 25902.5 MN (instead of 8090 MN, as shown in the Table 3). Values Fy and Fz were left without changes. The factor of stability was calculated by the formula (1) and the obtained value is 1.005.

Then another case was examined, where the peak value of acceleration was 0.16g, 0.1067g and 0.48g along the axes Ox, Oy and Oz respectively. The calculations performed by the same method showed that the factor of stability is equal to 0.792.

Tables

Table 1. Natural frequencies of the dam.

№	Eigen frequency	
	No added masses (empty reservoir)	With added masses (reservoir elevation 1610.2 m.a.s.l.)
1	1.891	1.152
2	2.001	1.243
3	2.727	1.787
4	3.256	2.240
5	3.633	2.293

Table 2. Peak values of free field accelerations, corresponding time moments, relative and absolute wedge accelerations.

Parameter	Dimensions	Direction		
		X	Y	Z
Max. Free Field Acceleration	m/s ²	1.57	0.94	1.57
Time moment t ₁	s	4.96	9.59	6.00
Relative Acceleration (t ₁)	m/s ²	-0.02	-0.07	-0.11
Absolute Acceleration (t ₁)	m/s ²	1.55	0.87	1.46
Min. Free Field Acceleration	m/s ²	-1.19	-1.04	-1.55
Time moment t ₂	s	4.25	9.72	6.65
Relative Acceleration (t ₂)	m/s ²	0.02	-0.02	0.06
Absolute Acceleration (t ₂)	m/s ²	-1.17	-1.06	-1.49

Table 3. Static and seismic loads acting on the wedge.

Results Case	Forces Acting on the Foundation Wedge					
	FE model coordinate system			Absolute value, dip angle and dip direction of the force		
	F_x MN	F_y MN	F_z MN	F_R MN	F_α °	F_β °
Static Load $F_{sw}(0)$	590	-4480	640	4564	79,0	38,6
Static Load $F_{hyd}(0)$	-2000	-1710	-5540	6133	16,2	241,4
Static Load $F_{tot}(0)$	-1410	-6190	-4900	8020	50,5	245,2
Seismic load (dam thrust)	1500	1500	3600	4179	-21,0	58,7
Seismic load (inertia)	8000	5300	8000	12494	-25,1	36,3
Total load	8090	610	-16500	18387	-1,9	-72,6

Table 4. Final results.

Result case	Design Interface Forces (Dam thrust) MN			Design Hydrostatic Uplift MN			Active Forces normal to planes MN		Driving Force, MN	Stabilizing Force, MN	Factor of Stability
	F_x	F_y	F_z	U_1	U_h	U_2	N_h	N_1			
Static load	-1410	-6190	-4900	1872	1889	631	52676	870	5028	37493	7,5
Seismic load	8090	610	-16500	1872	1889	631	46487	—	19417	32550	1,68

References

- 1) COMPUTATIONAL ASPECTS OF ANALYSIS AND DESIGN OF DAMS, Tenth Benchmark Workshop on Numerical Analysis of Dams, Theme C “Stability of a dam abutment including seismic loading”, document 9017/4001.
- 2) J. Lysmer, R. L. Kuhlemeyer, “Finite dynamic model for infinite media”, J. of the Engineering Mechanical Division, Proc. of the American Society of Civil Engineers, vol. 95, no. EM4, August 1969, pp 859 – 877, proc. paper 6719.
- 3) SOIL-STRUCTURE INTERACTION, CSI Article, http://www.csiberkeley.com/Tech_Info/16.pdf
- 4) P. Londe, “Une method d’analyse a trios dimensions de la stabilite d’une rive rocheuse”, Annales des Ponts et Chaussées, Vol. 1, pp.37 – 60, 1965.
- 5) S.I. Taicher, U.B. Mgaloblov, “Rascheti Ustoichivosti Skal’nih Beregovih Uporov Arochnih Plotin (Rock Arch Dam Abutment Stability Calculations)”, M, Energia, 1972. (In Russian).